T# 77-26101

NASA CR-145073
BBN Report No. 2797

Some Factors Influencing Radiation of Sound from Flow Interaction with Edges of Finite Surfaces

by
R. E. Hayden
H. L. Fox
R. C. Chanaud

Prepared under Contract No. NAS1-9559-25
by
Bolt Beranek and Newman Inc.
Cambridge, Mass. 02138

for

NASA

National Aeronautics and
Space Administration
Langley Research Center
Hampton, Virginia 23665

1. Report No.	2. Government Accession No.	3. Recipient's Catalog No.
NASA CR-145073		

4. Title and Subtitle	5. Report Date
SOME FACTORS INFLUENCING RADIATION OF SOUND FROM FLOW INTERACTION WITH EDGES OF FINITE SURFACES	1976
	6. Performing Organization Code

7. Author(s)	8. Performing Organization Report No.
R.E. Hayden, H.L. Fox, R.C. Chanaud	2797
	10. Work Unit No.

9. Performing Organization Name and Address	11. Contract or Grant No.
Bolt Beranek and Newman, Inc. 50 Moulton Street Cambridge, Massachusetts 02138	NAS1-9559-25
	13. Type of Report and Period Covered
12. Sponsoring Agency Name and Address	Contractor Report 1973-1976
NASA Langley Research Center Hampton, Virginia 23665	14. Sponsoring Agency Code

15. Supplementary Notes

16. Abstract

This report deals with identifying and characterizing those factors which influence sound generation by, and radiation from, the edges of surfaces which are exposed to unsteady flow. Edges of such surfaces have been shown to cause both strictly acoustic effects and hydrodynamic effects, in the form of generation of new hydrodynamic sources in the immediate vicinity of the edge. An analytical model develops the explicit sound-generation role of the velocity and Mach number of the eddy convection past the edge, and the importance of relative scale lengths of the turbulence, as well as the relative intensity of pressure fluctuations. The Mach number (velocity) effects show that the important parameter is the convection Mach number, M_c, of the eddies; the radiated power from the edge of an acoustically "small" surface varies as M_c^6 at low M_c, to lower powers of M_c as M_c approaches unity — the departure from the familiar M^6 law depending upon the isotropy of the turbulence, and the axial-wise separation between eddies. Thus, the effects of turbulence scale lengths, isotropy, and spatial density (separation) are shown to be very important in determining the level and spectrum of edge sound radiated. For semi-infinite surfaces, the low Mach number limit on velocity exponent is predicted to be M_c^5 for the edge dipole mechanism, the deviation to lower powers at $M_c \geq 0.3 - 0.5$ occurring just as in the case of the acoustically-compact surface. Experimental data is presented which provides support for the dipole edge noise model in terms of Mach number (velocity) scaling, parametric dependence on flow field parameter, directivity, and edge diffraction effects.

17. Key Words (Suggested by Author(s))	18. Distribution Statement
Aerodynamic Noise; Trailing Edge Noise; Leading Edge Noise; Flow/Surface Interaction Noise; Diffraction and Scattering; Airframe Noise	

19. Security Classif. (of this report)	20. Security Classif. (of this page)	21. No. of Pages	22. Price*
Unclassified	Unclassified	94	

* For sale by the National Technical Information Service, Springfield, Virginia 22161

Page
Intentionally
Left Blank

FOREWORD

This report summarizes the findings of a study conducted by Bolt Beranek and Newman, Inc. (BBN) under contract NAS1-9559-25, and under BBN Science Development Program funds, between 1973 and 1976. The subject addressed in this report has received increasing attention by numerous other researchers during that period. Therefore, the findings or views of some of these researchers may not be discussed.

The authors wish to acknowledge helpful discussions and with inputs from several colleagues — Drs. K. Chandiramani, D. Chase, M.S. Howe, and D. Sachs — and Mr. Harvey Hubbard and Dr. Donald Lansing of NASA Langley Research Center.

TABLE OF CONTENTS

TABLE OF CONTENTS (*Continued*)

LIST OF FIGURES

LIST OF FIGURES (*Continued*)

LIST OF FIGURES (*Continued*)

LIST OF FIGURES (*Continued*)

LIST OF SYMBOLS

Symbol	Meaning	Typical Dimensions
a	acceleration	m/s^2 [ft/s^2]
A	area	m^2 [ft^2]
c_0	sound speed	m/s [ft/sec]
C	chord (of an airfoil)	m [ft]
C_{xy}	cross-covariance coefficient	- None -
D	diameter	m [ft]
D_ω	dipole strength	m^2/s^2 [ft^2/s^2]
f	frequency	sec^{-1}
F	force	N [lb_f]
h	height (or separation distance)	m [ft]
i	$\sqrt{-1}$; or a direction	- None -
I	acoustic intensity	[N-s/m] [lb_f-sec/ft]
k	acoustic wavenumber	$(m)^{-1}$ $[ft]^{-1}$
ℓ	length scale of turbulence	m [ft]
L	chord lengths of surface	m [ft]
m	effective number of sources	-
M	Mach number	-
p (or P)	pressure	N/m^2 [lb_f/ft^2]
q	dynamic pressure	N/m^2 [lb_f/ft^2]
r (also R)	radius or radial distance	m [ft]

LIST OF SYMBOLS (*Continued*)

Symbol	Meaning	Typical Dimensions
S	Strouhal number	- None -
t	time	sec
T	Lighthill stress tensor	m/s [ft/sec]
U	mean velocity	m/s [ft/sec]
v	local fluid velocity component	m/s [ft/sec]
W	span of a surface or flow field	m [ft]
x	dimension in streamwise direction	m [ft]
y	dimension in spanwise direction	m [ft]
z	dimension in normal direction	m [ft]

Subscripts	Meaning	Typical Dimensions
a	acoustic	
c	convection	
d	dipole	
FF	free field	(No Dimensions)
HP	half-plane	
ℓ	length scale	
o	ambient or mean value	
max	maximum value	

LIST OF SYMBOLS (*Continued*)

Subscripts	Meaning	Typical Dimensions
n	in the direction normal to a surface	
r	in the radial direction	
SE	source-to-edge distance or path	(No Dimensions)
s	having to do with, or measured at, the surface	
x,y,z	in the x, y, or z direction	

Greek Symbols	Meaning	Typical Dimensions
γ	relative axial spacing between eddies: $\gamma = U_c/f\ell_x$ also, ratio of specific heats for ideal gas	None
δ	shear layer thickness	m [ft]
η	ratio of axial scale to mean scale ($\ell_x/\overline{\ell}$)	None
θ	angle in polar coordinates	[degrees, or radians]
λ	acoustic wavelength	m [ft]
ξ	relative spanwise spacing between eddies of spanwise scale	None
Π	sound power	N-m/s [ft-lb_f/sec]
ρ	fluid density	Kg_m/m^3 [16 lb_m/ft^3]
τ	time delay	[seconds]
ψ	angle in polar coordinates	[degrees, or radians]
ω	frequency	[radians/sec]

SECTION 1

INTRODUCTION

1.1 Effects of Surface Discontinuities

It is well known in acoustics that radiation of sound is strongly influenced by boundary discontinuities. The effect arises both in the sense that moving but non-propagating (evanescent) fields, associated with non-radiating surface motions, become radiative at points of discontinuity, in the same sense that an acoustic plane wave is scattered at points of discontinuity. It is equally well-known that fluid flow past a body of given compressibility is generally disturbed where the compressibility or shear stress changes. This effect arises both in the sense that the flow may undergo a transition from a laminar to turbulent state, and in the sense that the structure of an already-turbulent flow may change as a result of the compressibility or shear discontinuity.

Given these well-established effects, it is not surprising that the relative motion between a surface (wing, flap, plate, etc.) and the surrounding fluid medium is likely to result in acoustic radiation from the region around the trailing (and/or leading) edge, as has been verified by many experimental measurements. In fact, trailing edge noise can be, for many configurations, the dominant source of received noise below an aircraft, and at other receiver points. Since the prediction and control of edge noise are important, it is important to understand its character (spectral density and directivity) and its relationship to the flow-field characteristics, surface geometry, edge configuration, and surface impedance.

To obtain the relationship between flow field characteristics and sound radiated from the edge region, it is necessary to determine which mechanism is primarily responsible for the radiation. Each postulated mechanism leads to a particular characterization of the sound field and of its relationship to the flow field characteristics. Empirical measurements and similarity arguments can then be used to establish *a posteriori* verification of the choice of mechanism.

1.2 Types of Radiation Mechanisms from Turbulent Flow Interaction with Edges of Surfaces

All the mechanisms of acoustic radiation that have been grouped and described as *edge noise* fall into two categories — those which describe basically acoustic effects, taking the turbulence above the edge as given, and those which attribute the predominant radiation to hydrodynamic effects. In the second category are included the theories which describe wake-related tones (often called "vortex shedding" noise) which acknowledge that the edge has a strong hydrodynamic effect in terms of sound generation. However, in the "hydrodynamic" theories, it is also acknowledged that there can be acoustic diffraction of the edge-generated sound by other edges of the surface.

In the acoustic theories (Ffowcs-Williams and Hall, 1970; Chase, 1972, 1975; Goldstein, 1974; and Chandiramani, 1974), the existence of non-propagating (evanescent) waves — i.e., those which have an exponential decay leaving the region of turbulence — is assumed, and presence of the edge is shown to enable these waves to propagate due to the combination of phases (scattering) as these waves encounter the edge.

In the work of Curle (1955; 1968) and Goldstein (1974), who take Lighthill's (1952) equation (but point out that his solution only contains volume integrals) and add surface integrals, the most developed form has three terms, which correspond to the generation of sound by the volume quadrupole sources (T_{ij}) (Lighthill's original solution), pressures exerted by these volume sources on fixed boundaries (P_i) momentum imparted to the fluid by moving boundaries ($\rho v_i v_n$), and volume displacement $\partial(\rho v_n)/\partial t$

$$4\pi\gamma(p-p_o) = \frac{\partial^2}{\partial x_i \partial x_j} \int_{\text{volume}} \frac{T_{ij}}{r} \, d\tau(\hat{y}) \qquad \text{(quadrupoles)}$$

$$- \frac{\partial}{\partial x_i} \int_{\text{surface}} \frac{P_i - \rho v_i v_n}{r} \, d\tau \, S(\hat{y}) - \int_{\text{surface}} \frac{\partial}{\partial t} (\rho v_n) \frac{d\tau(\hat{y})}{r}$$

(pressures on rigid boundary; moving boundary momentum effects; volume displacement)

The strength of Goldstein's work is that he has shown how the work of several authors actually correspond to different limiting conditions of the general solution, whose applicability to the edge noise problem is limited because it begins with Lighthill's differential equation and includes boundary (and therefore edge) effects only insofar as they affect acoustic radiation, but not the turbulence itself. Goldstein acknowledges these limitations by stating: "The crucial step in Lighthill's analysis is to regard the source term as known *a priori*."

Thus, the essence of the Lighthill approach is to regard the turbulence terms as given. One cannot expect, from such an analysis, anything else but an explanation of the acoustic effect of an edge on the turbulent field. Since it is possible to have momentum exchange across the plane of the surface downstream of the edge, it is clear that such a mechanism should also give rise to dipole-like fields.

Ribner's fluid diliation theory of aerodynamic sound (1962) presented the perspective that all sources of flow disturbances — e.g., velocity, thermal, and mass fluctuations — can be replaced by an equivalent source *pressure*. This view has stimulated investigations — including this one — in which the readily-measured pressure fluctuations are taken as the principal input to a source formulation. (See also, for example, Chase [1975].)

The hydrodynamic mechanism of edge noise generation was first proposed by Powell (1959) who performed some similarity analyses to identify the dependence of sound generation on gross parameters of the flow.

The edge effect proposed by Hayden (1969) involves both hydrodynamic and acoustic effects. First, it postulates a localized disturbance which occurs just behind the edge, corresponding to a sudden acceleration of the elements of turbulence (flow disturbances) upstream of the edge. The source region is assumed to be acoustically compact (at least in the streamwise direction). The strictly acoustic effect of this model is that these compact dipole sources are diffracted strongly because they are closer than an acoustic wavelength to the surface. This model is extended in the present study to include more detailed description of flow field parameters and surface finiteness effects.

1.3 General Features of the Dipole Theory of Edge Noise

The important features of the present description of edge noise source generation are:

(1) *Compactness:* The "generators" corresponding to a certain scale ℓ are in a zone of length ℓ_x (turbulence scale) within the edge. Even though these generators may be related to the subsequent wake hydrodynamically, the phenomenon responsible for the sound radiation is a transient acceleration of the medium immediately behind the edge, which is an acoustically-distinct phenomenon from the spatially-extended radiation from the free shear layer of the wake itself, or from the upstream surface.

(2) *The source is intrinsically dipole because it results from an imbalance of hydrodynamic forces normal to the plane of the surface.* Since unsteady forces normal to the surface exist elsewhere, the acoustically-important feature is that the pertinent ones are localized in the region of the edge, and are accompanied by an almost discontinuous acceleration.

(3) *Mach Number Effect:* The interrelationship between turbulence parameters and the Mach number at which the turbulence is convected past the edge has a definite effect on radiation efficiency of the dipole edge noise source. The implications of this effect are that the often-examined velocity dependence of radiated sound from a particular flow field/edge interaction varies throughout the Mach number range, and as a function of frequency (or Strouhal number).

1.4 Applicability to Trailing and Leading Edge Sources

The model developed in this study is equally applicable to trailing edge or leading edge noise generation, where the surface dimensions are on the order of, or larger than, an acoustic wavelength. The differences between trailing edge noise radiation, and leading edge relate to the source of the unsteady flow. Broadband trailing edge noise is to be expected whenever flow over the surface is turbulent. Narrowband noise also originates hydrodynamically at the trailing edge due to vortex shedding caused by a laminar flow instability, and/or the hydrodynamic

instability produced by a blunt trailing edge. A typical trailing edge sound field illustrating these effects is shown in Fig. 1, for the case of two identical turbulent wall jets flowing over a thin rigid plate. The vortex shedding peak occurs at about 2000 Hz, with lower sidebands resulting from low velocity regions away from the center line of the finite-width jet.

The principal difference between trailing edge and leading edge sources is that the flow field causing leading edge noise is not intimately related to the surface, as with the trailing edge, but rather a consequence of the particular environment in which the surface is placed.

The remainder of this report includes first a section (2) in which the analytical model of dipole edge noise is developed, followed by a section (3) in which strictly-acoustic effects of the surface are treated. The subsequent section (4) summarizes experiments which provide a base of empirical data on both trailing and leading edge noise parametric effects, followed by a section in which the analytical model is tested on specified trailing edge and leading edge experimental configurations, and compared with measured data. Appendices supply additional details of the diffraction calculations, and experimental data.

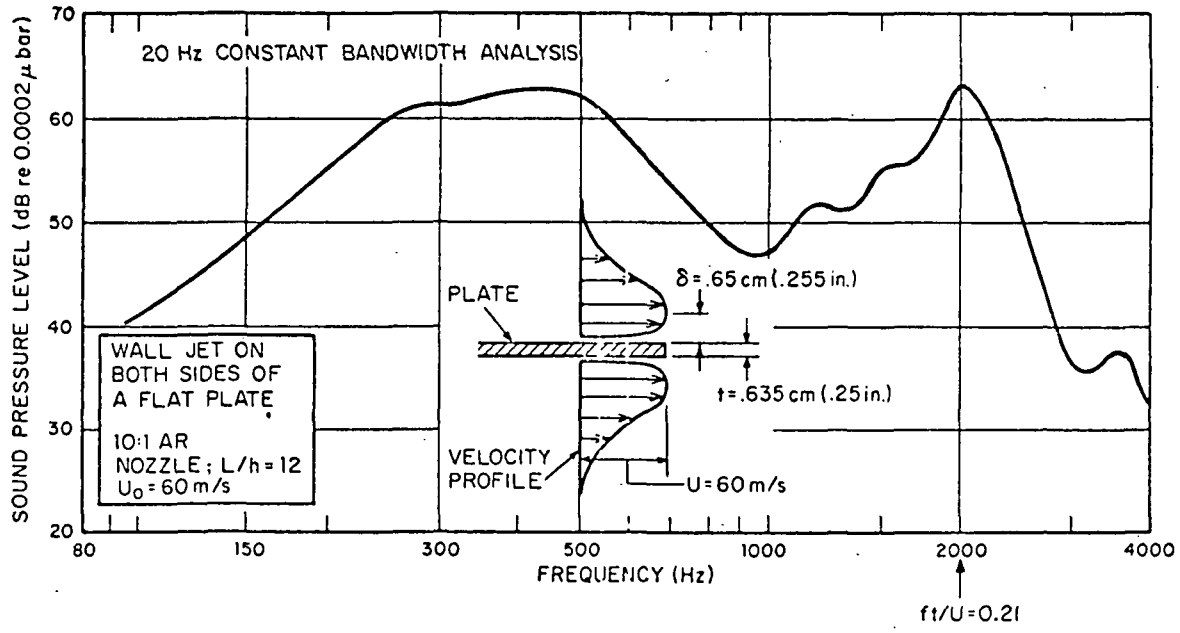

FIG. 1. TYPICAL SPECTRAL CHARACTERISTICS OF A TRAILING EDGE SOUND FIELD.

SECTION 2

FORMULATION OF THE SOURCE DESCRIPTION

It has already been pointed out in Sec. 1 that it is necessary to distinguish among the various contributions to the sound field, which are usually all described as edge noise mechanisms. In this section, we extend in detail the acoustically-compact edge noise model reported by Hayden (1969). This requires a description of the hydrodynamic generators of the sound at the edge, and then an analysis of the edge (and the entire surface) as diffractor of the sound generated in the immediate region behind the trailing edge.

Some previous studies of trailing edge noise (Powell, 1959; Hayden, 1969 and 1972; Hayden and Chanaud, 1970) have postulated a dipole distribution at the trailing edge, and made assumptions regarding the similarity behavior of the fluid mechanical parameters responsible for the sound generation, and thus predicted trends in the radiated sound level and spectrum. One result was a set of limited, although useful, semi-empirical noise prediction "curves," as summarized by Hayden (1972) for wall jets. It was contended that the data, which led to the normalized curves, bore out the premise that the role of the trailing edge was to act as a dipole source generator by virtue of its pressure-release effect on incoming flow disturbances, and its typical destabilizing effect of the sheared flow field encountering the edge. This premise has been justifiably questioned by some who regard the edge as strictly a "scatterer" of evanescent waves already present in the flow; i.e., the edge does not produce any additional fluid dynamic sources of unsteady pressure (Ffowcs-Williams and Hall, 1970; Chase, 1971 and 1975; Chandiramani, 1974). Except for highly idealized cases, in which the surface impedance discontinuity at the edge would not be accompanied by a surface shear discontinuity, it is the common experience that a substantial hydrodynamic instability exists at the trailing edge due to the high curvature of the surface there. It is thus contended that the edge generates new hydrodynamic sources as well as "scattering" those already present in the upstream flow. Following Ribner's view, the fluid dynamic sources can arise from any fundamental type of physical disturbance, and can be represented by pressure fluctuations.

To provide more direct evidence as to the validity of the dipole hydrodynamic theory of edge noise, the problem is now reformulated in terms of a more detailed specification of the

structure of the local flow field, i.e., in terms of actual measurable unsteady flow parameters, rather than more ambiguous mean flow parameters. An attempt will be made to retain the connection between the final resultant sound field and mean flow parameters, but we will attempt to derive spectral details from a knowledge of the structural parameters of the flow.

2.1 The Generation Mechanism Near the Edge of a Rigid Surface

In the region *immediately* upstream from the trailing edge, there appear elements of turbulence (vortices) which retain their identity as they convect to the trailing edge, (see Fig. 2). Upstream of the edge, they experience no net motion normal to the rigid surface, although they may fluctuate and thereby produce a weak quadrupole field — "weak" because they constitute a non-compact incoherent distribution resulting in no volume momentum transfer, and "quadrupole" because the dipole corresponding to normal fluctuation is reflected by the rigid boundary. The lack of net normal motion is a result of the lack of a net force on each element. On one side of an eddy, the fluid exerts a fluctuating force; on the other side is the rigid surface which exerts an equal and opposite reaction force. This, of course, follows from the usual assumption of incompressibility. To the extent that the elements of turbulence are compressible, there would be a deformation leading also to weak radiation of an octapole character (reflected quadrupoles).

As an element of turbulence of mean scale $\overline{\ell}$ leaves the surface, it accelerates, since it no longer encounters the reaction force of the rigid surface, and it encounters a change in the shear stress which had been excited at the surface. This acceleration, due to pressure release, may be written as (from Newton's law)

$$a = \frac{P_\varepsilon}{\rho \cdot \overline{\ell}} = (U_c^2/2\overline{\ell}) \quad (\overline{p/q_0}) \qquad (2.1)$$

in which P_ε is a measure of the fluid pressure above and ρ is the fluid density. The equivalent expression $(U_c^2/2\overline{\ell})$ $(\overline{p/q_0})$ expresses the rms acceleration of this typical element of mean scale $\overline{\ell}$ in terms of the commonly measured quantities U_c, the convection velocity, and $\overline{p/q_0}$, the ratio of fluctuating pressure to mean dynamic pressure (turbulent pressure intensity). Examples of

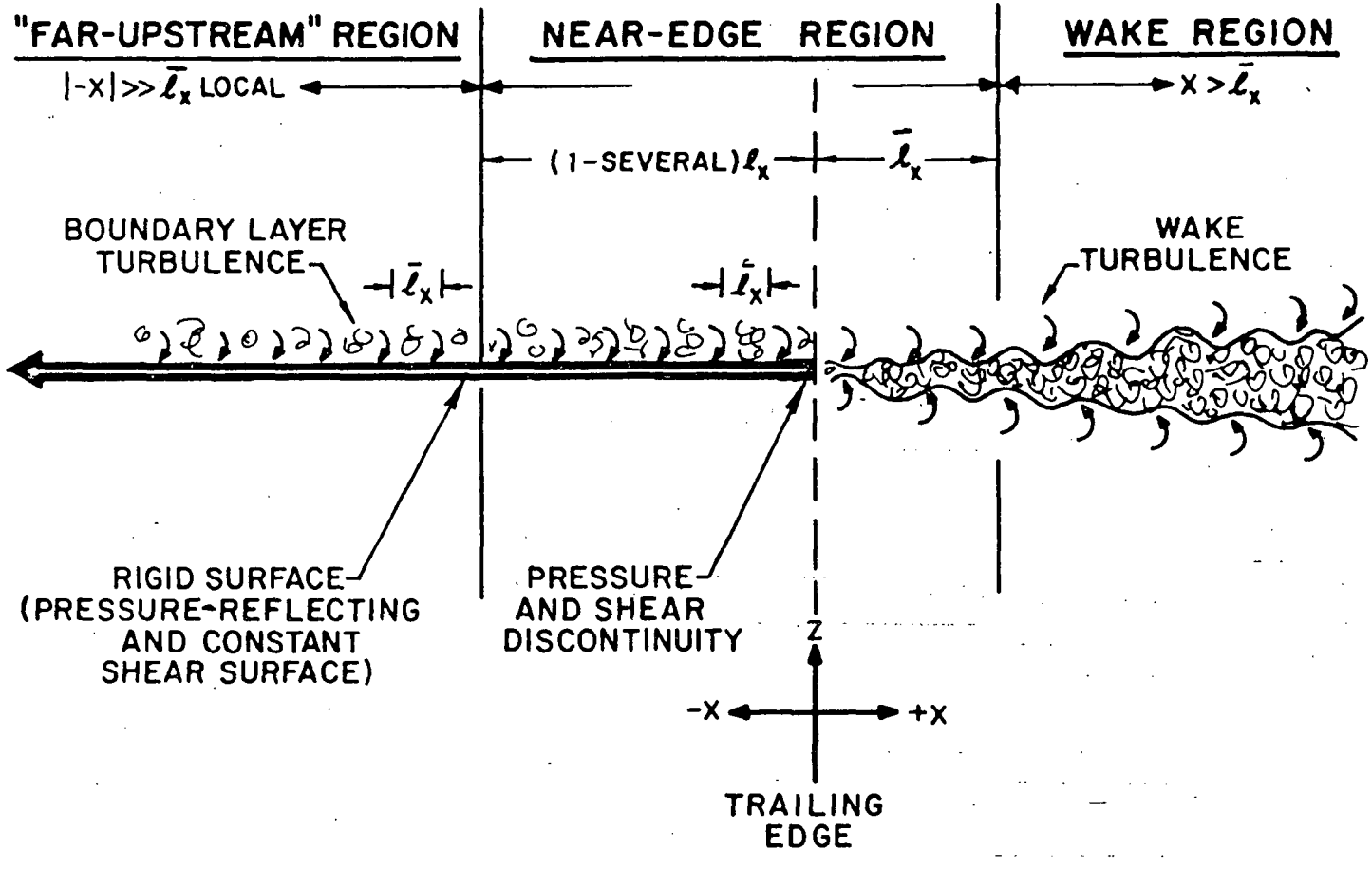

FIG. 2. SCHEMATIC OF FLOW REGIONS AND DISCONTINUITIES IN THE VICINITY OF A TRAILING EDGE.

measured values of scale dependence of $\overline{p/q_0}$ are illustrated in Fig. 3. The characteristics of $\overline{p/q_0}$ of particular importance are (1) constancy for lengths larger than some characteristic dimension (~6δ, or 4D); (2) its proportionality $A(\bar{\ell})^{-3}$ for lengths smaller than the characteristic value (~6δ, or 4D); and (3) its rapid decrement for lengths larger than some maximum (the last is not illustrated in the figure due to lack of data).

The acceleration, a, of the element of scale $\bar{\ell}$ occurs in the region just behind the surface, and being directional (normal to the plane of the surface), corresponds to a dipole radiator occupying a volume $\sim\bar{\ell}^3$ ($\bar{\ell}^3 = \ell_x \ell_y \ell_z$). We now examine this resulting fluid motion more carefully. The quantity "a" is a mean measure (say, rms) of acceleration, associated with scale $\bar{\ell}$. Any given element of turbulence of scale $\bar{\ell}$ will accelerate according to an unspecified detailed time history; but all elements of scale $\bar{\ell}$ produce, on the average, the value a. Furthermore, the element of scale $\bar{\ell}$ passes into the compact edge-noise zone in the time Λ/U_c — the time required for it to convect off the edge — in which Λ is the mean streamwise distance between elements of scale $\bar{\ell}$. Immediately following its passage, another element is accelerated. In general, its scale is different and, correspondingly, its acceleration history is different. The average measure of acceleration of all such scales will, however, also follow Eq. (2.1). One can envision the typical normal acceleration behind the edge which would be generated by this process (Fig. 4).

If one were to measure the rms acceleration of all events of duration Λ/U_c the value $a(\bar{\ell})$ would be obtained. Furthermore, such a random function can be represented by an infinite series of infinitely dense periodic functions. The acceleration $a(\bar{\ell})$ would be the weight for the function of period Λ/U_c in the series. Since the radiation motion is of a dipole character, the acceleration measure $a(\bar{\ell})$ is the weight to assign to a periodic function of frequency $f = U_c/\Lambda$, and the local acoustic source is effectively an ensemble of dipole radiators of definite frequency and random phase and amplitude. We now develop the functional relationships for radiated sound in terms of a dipole model.

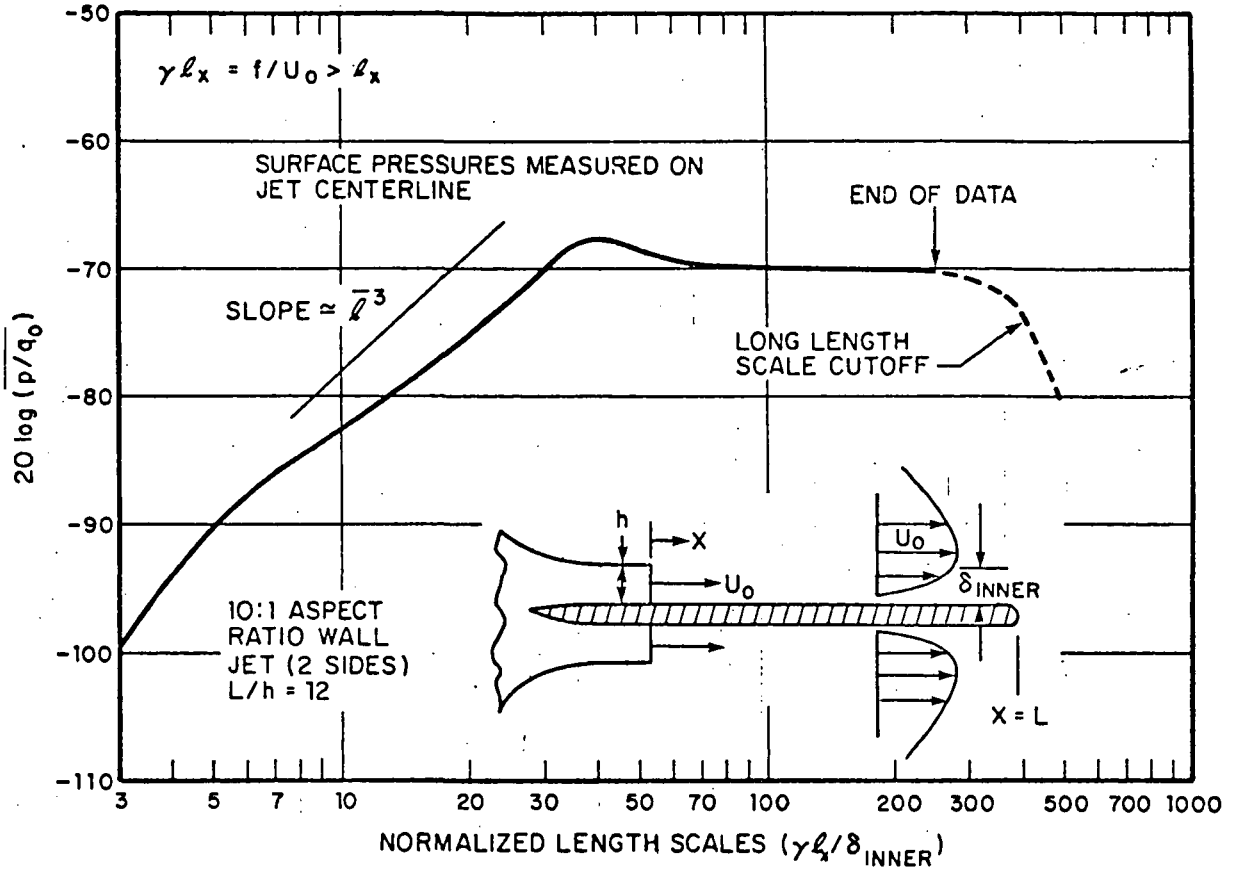

FIG. 3a. SURFACE PRESSURE INTENSITY FOR VARIOUS EDDY LENGTH SCALES: WALL JET TRAILING EDGE.

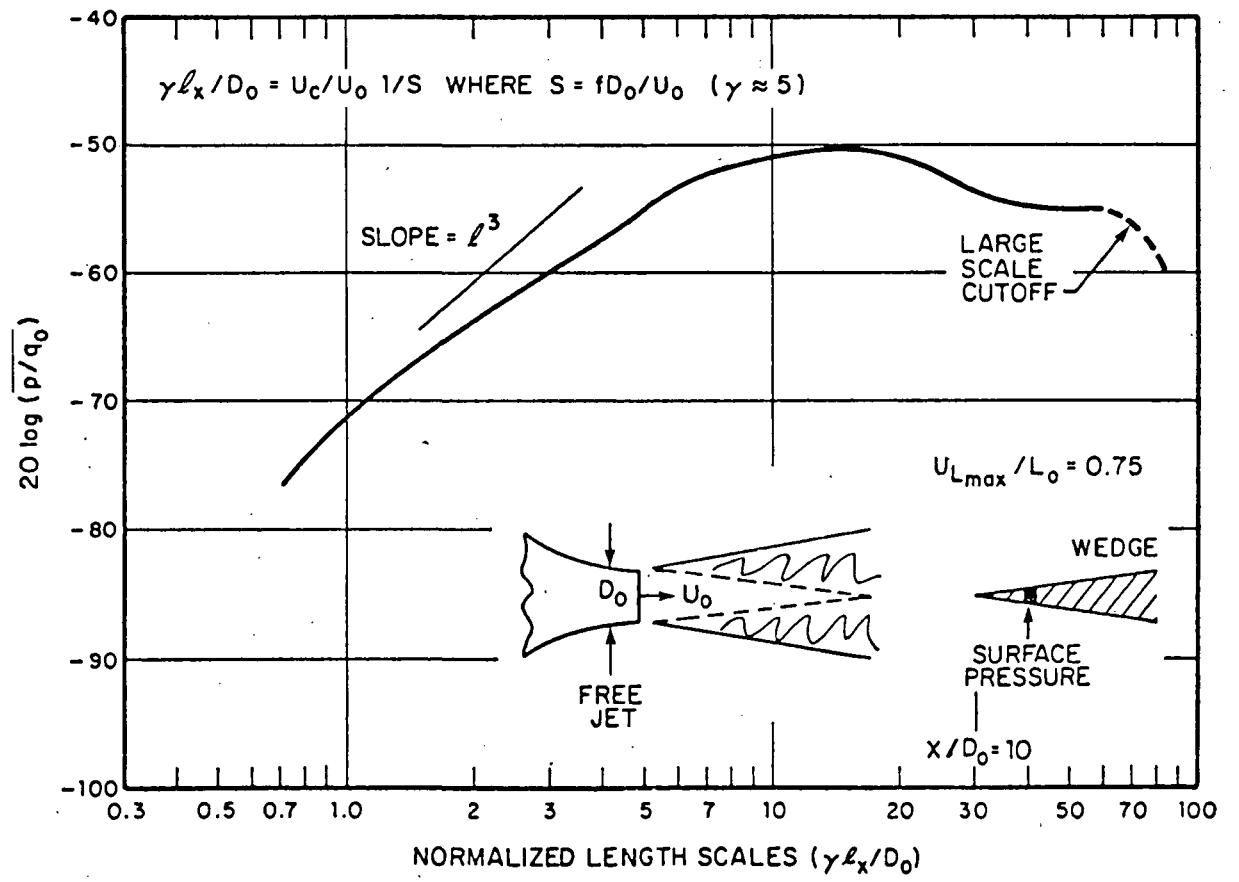

FIG. 3b. SURFACE PRESSURE INTENSITY FOR VARIOUS EDDY LENGTH SCALES: LEADING EDGE IN A FREE JET.

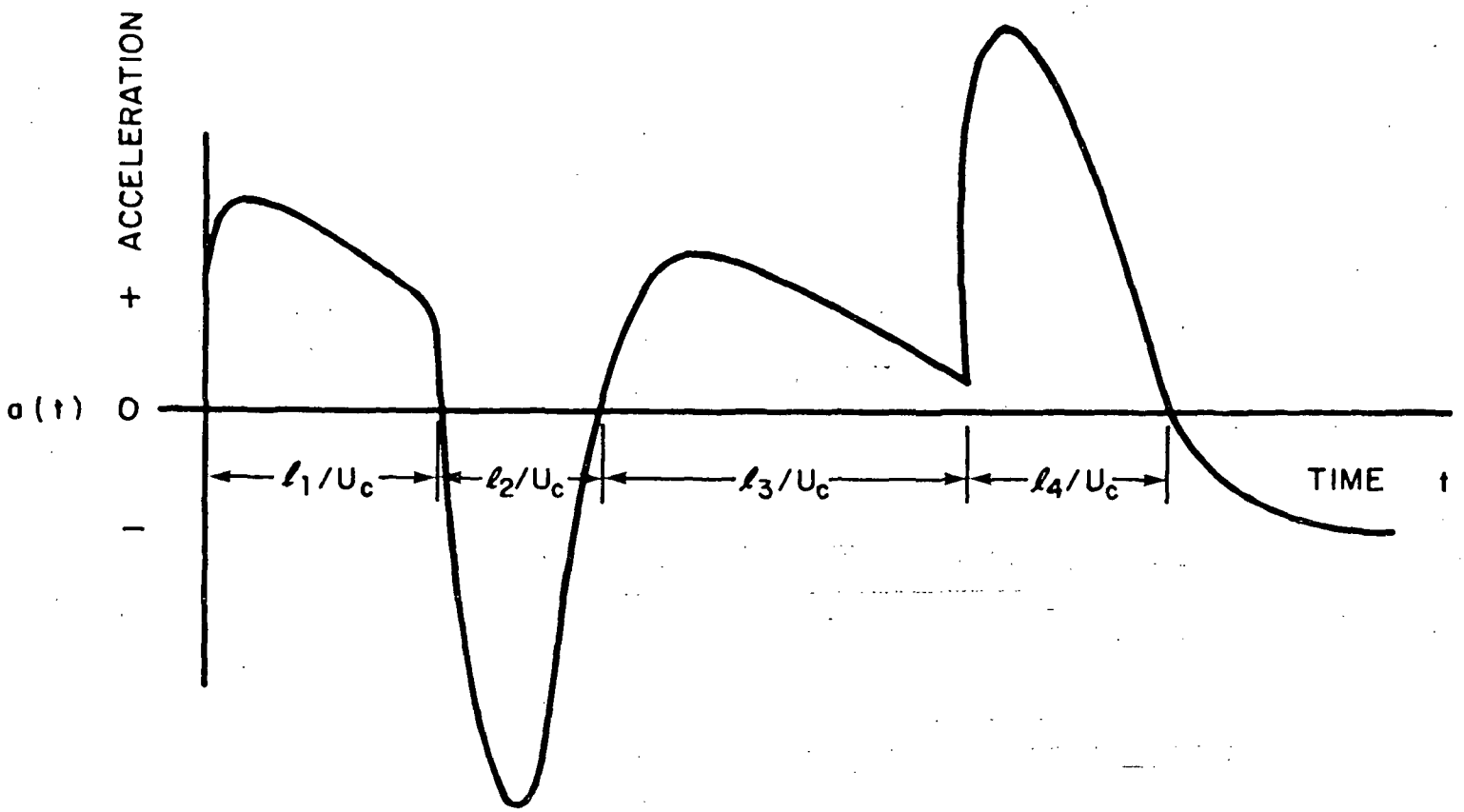

FIG. 4. TYPICAL TIME HISTORY OF NORMAL FLOW ACCELERATION IMMEDIATELY DOWNSTREAM OF A TRAILING EDGE.

2.2 Dipole Model for a Single Source Near an Edge

Morse and Ingard (1968) give the relationship for the radial velocity of point dipole source of frequency ω as

$$U_r = \frac{-k^2 D_\omega}{4\pi r} \left(1 + \frac{2i}{kr} - \frac{2}{k^2 r^2}\right) e^{i(kr-\omega t)} \sin\theta \qquad (2.2)$$

and the total power at that frequency as

$$\Pi = \frac{\rho \omega^4}{12\pi c^3} |D_\omega|^2 \qquad (2.3)$$

Note that these expressions are for free field sources in which the wavelength is much larger than the surface dimensions; the presence of the surface upstream of the edge will modify both the angular dependence of U_r and the total power radiated. The derivation of the parametric dependence of total is now developed for the finite surface in which the chordwise dimension is not large with respect to a wavelength, and the observer is well into the far field ($kr >> 1$).

The effects of a semi-infinite chordwise dimension will be examined later, and the kC range between these two limits will be discussed.

We wish to derive the dipole strength D_ω in terms of the acceleration, a, caused by turbulence encountering the edge as expressed in Eq. (2.1)

Differentiating Eq. (2.2) gives

$$a_d = \frac{i\omega k^2 D_\omega}{4\pi r} \left(1 + 2i\,\frac{1}{kr} - \frac{2}{(kr)^2}\right)(\sin\theta) \qquad (2.4)$$

The mean square acceleration $a_d a_d^*$ is thus

$$|a|^2 = \frac{\omega^2 k^4 D_\omega^2}{(4\pi)^2 r^2} \left(1 + \frac{4}{(kr)^4}\right) (\sin^2\theta) \qquad (2.5)$$

From Eq. (2.1), the mean square acceleration of the medium caused by an eddy of scale $\bar{\ell}$ is

$$|a_\ell|^2 = \frac{U_c^4}{(2\bar{\ell})^2} \quad (\overline{p/q_0})^2 \tag{2.6}$$

Equating (2.5) and (2.6) and solving for D_ω^2 gives

$$D_\omega^2 = \frac{U_c^4}{(2\bar{\ell})^2} \quad \frac{(4\pi)^2 r^2}{\omega^2 k^4} \quad \overline{\left(\frac{p}{q_0}\right)^2} \quad \left[1 + \frac{4}{(kr)^4}\right]^{-1} \tag{2.7}$$

Now, a simple set of substitutions is made to derive the dipole strength D_ω in terms of flow parameters.

The wavenumber k is

$$k = \frac{2\pi f}{c_o}, \text{ and since } f = \frac{U_c}{\Lambda}, \text{ can be written}$$

$$k = \frac{2\pi \frac{U_c}{\Lambda}}{c_o}, \text{ or } k = \frac{2\pi M_c}{\Lambda} \tag{2.8a}$$

where $\Lambda = \gamma \ell_x$, the axial spacing between eddies of scale ℓ_x.

Thus, k could be finally written as

$$k = \frac{2\pi M_c}{\gamma \ell_x} \quad . \tag{2.8b}$$

The final step before substitution is to let $r \approx \bar{\ell}$, since we are postulating that the important impulsive acceleration takes place within one scale length. Note that $\bar{\ell}$ typically decreases with increasing frequency.

We thus have

$$|D_\omega|^2 = \frac{U_c^4 (4\pi)^2 (\bar{\ell})^2}{(2\bar{\ell})^2 \left(\frac{2\pi U_c}{\gamma \ell_x}\right)^2 \left(\frac{2\pi M_c}{\gamma \ell_x}\right)^4} \overline{\left(\frac{p}{q_0}\right)^2} \left[1 + \frac{4\gamma^4 \ell_x^4}{(2\pi M_c \bar{\ell})^4}\right]^{-1} \tag{2.9}$$

Equation (2.9) reduces to

$$|D_\omega|^2 = \frac{c_o^2}{M_c^2} \frac{\gamma^6 \ell_x^6}{(2\pi)^4} \overline{\left(\frac{p}{q_0}\right)^2} \left[1 + \frac{4\gamma^4 \eta^4}{(2\pi)^4 M_c^4}\right]^{-1} \tag{2.10}$$

where $(\ell_x/\bar{\ell})$ has been replaced by η in the right hand term. This could be regarded as an axial anisotropy factor for the turbulence near the edge, which reflects the typical stretching of eddies in the axial direction. The values of η vary substantially from one type of flow field to another, ranging from 1 to 10 typically.

We now substitute Eq. (2.10) into Eq. (2.3), recalling that $\omega = 2\pi U_c/\gamma \ell_x$, and arrive at an expression for the radiated power.

$$\Pi = \frac{\rho M_c^2 c_o^3}{12\pi} \gamma^2 \ell_x^2 \overline{\left(\frac{p}{q_0}\right)^2} \left[1 + \frac{4\gamma^4 \eta^4}{(2\pi)^4 M_c^4}\right]^{-1} \tag{2.11}$$

This expression contains a number of interesting parametric dependences. First, we see that, in the $M_c^2 [\ ]^{-1}$ terms, the hydrodynamic dipole model of edge noise allows for more than a single unique velocity dependence of radiated power. Secondly, a strong influence of both the scale of turbulence (ℓ_x) and non-isotropy (η) of turbulence, is evident. Finally, the turbulent pressure intensity factor ($\overline{p/q_0}$) ("gustiness") is present, as one would expect.

Since a most intriguing result given in Eq. (2.11) is the non-unique velocity dependence, let us examine some limits. For $M < 0.1$, and $\gamma\eta \gtrsim 1$, the right-hand bracketed term in Eq. (2.11) reduces to

$$[\ ]^{-1} = \frac{M_c^4 (2\pi)^4}{4\gamma^4\eta^4}$$

which gives the following parametric dependence:

$$\Pi = \frac{\rho M_c^6 c_o^3 \ell_x^2 \pi^3}{3\gamma^2\eta^4} \overline{\left(\frac{p}{q_0}\right)^2} \qquad (2.12a)$$

or

$$= \frac{\rho U_c^6 \pi^2 \ell_x^2}{3\gamma^2\eta^4 c_o^3} \overline{\left(\frac{p}{q_0}\right)^2} \qquad (2.12b)$$

This shows a U^6 dependence and will be referred to as the *low Mach number limit.*

The Mach number dependence of the exponent of radiated power is examined below for various values of $\gamma\eta$. Figure 5(a) shows that, as the turbulence becomes more isotropic, ($\eta \to 1$), and the axial separation between eddies is reduced ($\gamma \to 1$), the rate of power generation is reduced even at relatively low convective Mach numbers. For $\gamma\eta$ products near 10, which are more typical of boundary layer and wall jet flow fields, the sound generation efficiency does not fall off until one reaches high subsonic Mach numbers.

Another way to view these effects is to examine regimes where deviations occur from the U^6 power law, which has been shown to be the low Mach number limit for the hydrodynamic dipole edge noise mechanism. Figure 5(b) plots the power law as a function of Mach number for various combinations of $\gamma\eta$. The plot speaks for itself — *a variation in velocity exponent of radiated power from the edge source may occur over a range of Mach numbers, depending on details of the turbulence structure.* The velocity dependence of sound generation from a particular

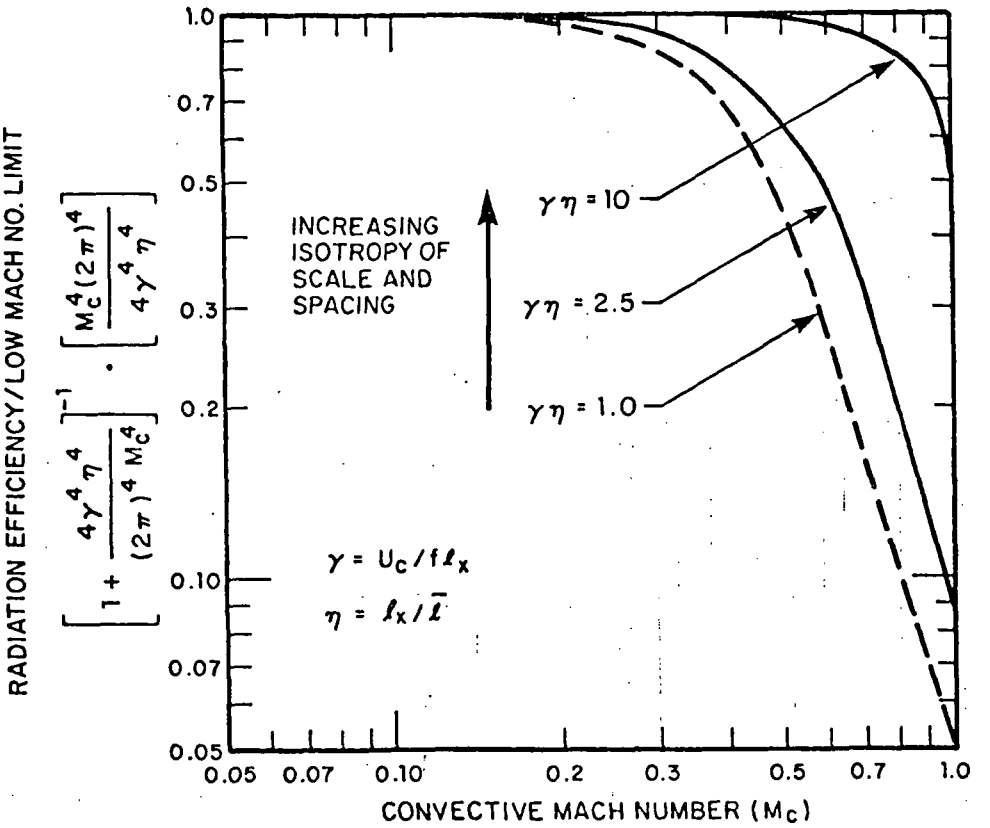

FIG. 5a. EFFECT OF TURBULENCE ISOTROPY, STREAMWISE SEPARATION AND CONVECTIVE MACH NUMBER ON EDGE DIPOLE RADIATION EFFICIENCY.

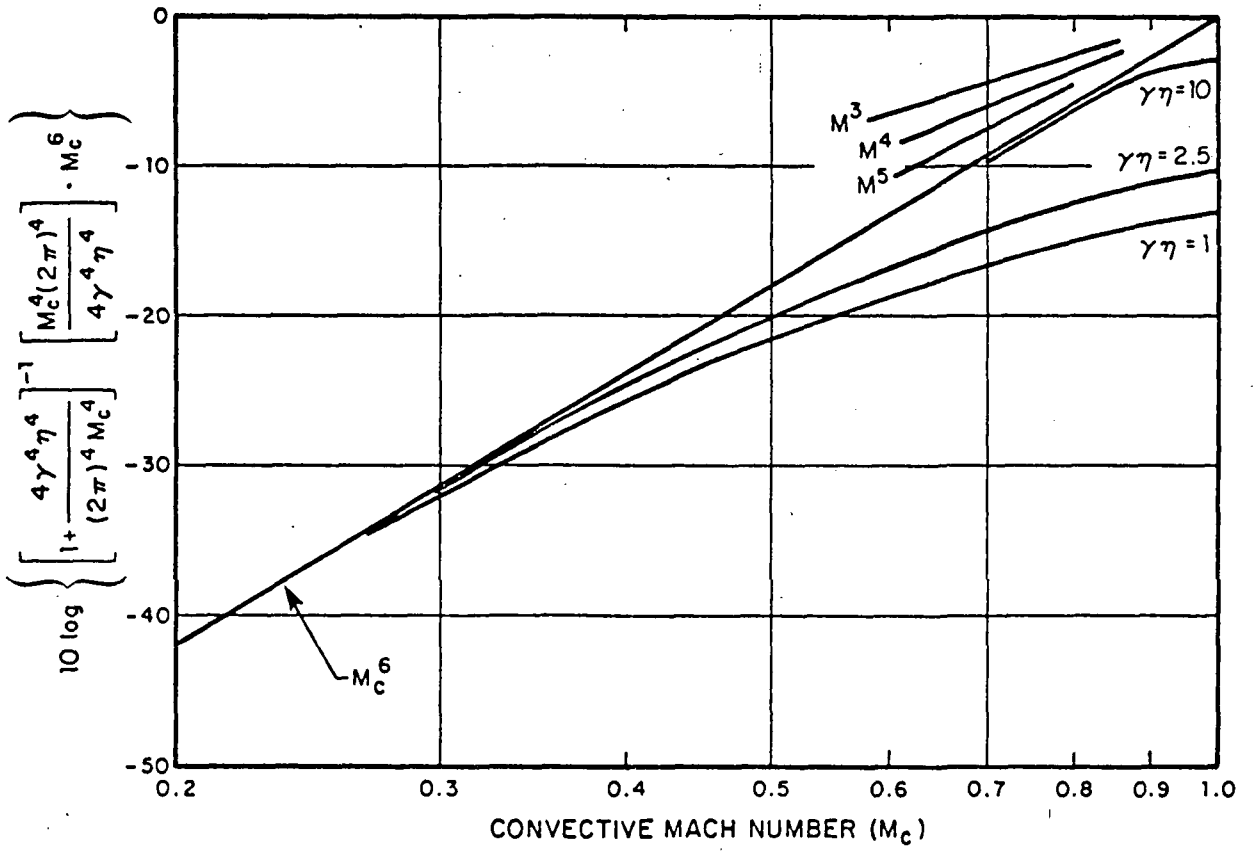

FIG. 5b. EFFECT OF TURBULENCE PARAMETERS AND MACH NUMBER ON VELOCITY SCALING OF EDGE DIPOLE SOUND SOURCE.

flow field/surface configuration will vary as a function of Mach number, even if the flow parameters M_c, ℓ_x, ℓ_y, γ, η, and $(\overline{p/q_o})$ obey similarity at all Mach numbers (which, in general, cannot be expected to be rigorously true). Likewise, it is suggested that the power *vs* M_c law is likely to be different from one flow field to another, and may vary with frequency for a given flow field.

2.3 Radiation from Incoherent Sources Along a Span

The foregoing expressions have been developed for a single source region of span ℓ_y. It is desirable to extend the relationships to the more realistic case of a finite wetted span W of an edge which is "excited" by turbulent flow with statistically homogeneous properties across the span. If the localized sources are incoherent along the span, then the sound power will increase by a multiple m equal to the effective number of *incoherent sources.** This can be represented by $m = W/\xi\ell_y$, where ξ is the relative spacing between eddies of spanwise scale ℓ_y. This multiple will be a function of frequency, typically increasing monotonically with increasing frequency. However, it will be shown later from examination of actual length scale data that this function can be a complicated function of frequency. We thus can now write the expression for total power from turbulent flow interaction with a span of edge over which mean flow and unsteady flow parameters are statistically similar

$$\Pi = \frac{\rho M_c^2 c_o^2}{12\pi} \gamma^2 \ell_x^2 \left(\frac{W}{\xi\ell_y}\right) \left(\frac{\overline{p}}{q_o}\right)^2 \left[1 + \frac{4\gamma^4\eta^4}{(2\pi)^4 M_c^4}\right]^{-1} \qquad (2.13a)$$

Which reduces to

$$\Pi = \pi^3 \frac{\rho U_c^6 \ell_x^2}{3\gamma^2\eta^4 c_o^3} \left(\frac{W}{\xi\ell_y}\right) \left(\frac{\overline{p}}{q_o}\right)^2 , \quad \text{for } M_c < 0.3 \qquad (2.13b)$$

*The effects of partial coherence are treated in Sec. 2.5.

2.4 Alternate Forms of the Source Equation

Equation (2.13) may be manipulated into a free field formulation, which may be useful in analyzing experimental data.

Another manipulation would be to replace U_c^6 by $U_o^6\ (U_c/U_o)^6$ which allows one to simply use the relative convection speed and maximum free stream velocity separately.

Another manipulation is to take the ratio of far field sound pressure-to-surface pressure, thus forming an "edge transform" or transfer function between these two other measured quantities. Such a transform is written below for the low Mach number case, where η has been replaced by $\ell_x/\sqrt[3]{\ell_x \ell_y \ell_z}$:

$$\frac{\overline{p_a^2(r,\theta,\psi)}}{\overline{p_s^2}} = \left(\frac{W}{\xi \ell_y}\right) \frac{\pi}{2r^2 c_o^2} \left(\frac{U_c^2}{\gamma^2 \ell_x^2}\right) \left(\overline{\ell_x \ell_y \ell_z}\right)^{4/3} \left(\frac{U_c}{U_o}\right)^4 \sin^2\theta \qquad (2.14)$$

Equation (2.15) may be rewritten in terms of radian frequency ω as

$$\frac{\overline{p_a^2(r,\theta,\psi)}}{\overline{p_s^2}} = \omega^2 \left(\frac{U_c}{U_o}\right)^4 \left(\frac{W}{\xi \ell_y}\right) \frac{\left(\overline{\ell_x \ell_y \ell_z}\right)^{4/3} \sin^2\theta}{8\pi r^2 c_o^2} \qquad (2.15)$$

In the subsequent sections, we will compute this transform for several edge noise experiments for which sufficient data exists.

2.5 Radiation from Partially Coherent Sources

In Sec. 2.3, the model for radiation from a single source region of spanwise dimension ℓ_y was extended to a span W over which the unsteady flow field characteristics $(\overline{p/q_o})^2$, η, γ were statistically similar, and over which there was no phase coherence

between sources. In practice, there may be situations where hydrodynamic source regions are not completely incoherent. These cases may involve trailing edge flow fields where the eddy scales are large, and only a small part of the span (compared to eddy scales, and a typical acoustic wavelength) is immersed in flow, such as a low aspect ratio wall jet. In such a case, the eddy structure of the free shear layer may be partially coherent on each side of the core region, or the edge sources associated with the large-scale eddy structure may be in each others acoustic near field. Another case of fundamental and practical importance is the case of similar (or dissimilar) flow fields on opposite sides of a trailing edge. In this case, there may be partial cancellation of the acceleration of an eddy leaving say the upper surface by one of a similar scale leaving the lower surface, thus reducing the unsteady acceleration and the resultant total sound power output of the edge source. The effects of partial coherence, although hydrodynamic in origin, can be examined on a strictly acoustic basis, omitting the flow field details which were developed earlier in this section.

To model the sound radiated from an entire edge, we will form an array of dipoles, which for the moment will be assumed to be aligned either along the same axis, or along parallel axes along the edge. Equation (2.15) is rewritten as

$$\overline{p_a^2}\,(r,\theta,\psi) \propto \omega^2\, \overline{p_s^2}\, \left(\overline{\ell_x \ell_y \ell_z}\right)^{4/3} \left(\frac{W}{\xi \ell_y}\right) .$$

The terms $\overline{p_s^2}\, \left(\overline{\ell_x \ell_y \ell_z}\right)^{4/3}$ can be replaced by a dipole force $\overline{F^2}$ (where $F = p \times A$ = pressure × area), and (W/ξ_y) replaced by m, which was taken earlier to be the number of uncorrelated sources along the span. Since it is now to be assumed that the sources are not necessarily uncorrelated along the span, or from upper to lower surface, the following analysis will essentially be deriving an alternate term m' to replace m.

Thus, we are now dealing with a familiar relationship between radiated sound pressure $\overline{p_a}$, and dipole force F; i.e.,

$$\overline{p_a^2} \propto \frac{m' \omega^2 \overline{F^2}}{r^2}$$

Let us first consider two sources described by strength F_1 and F_2, separated by a distance h. We will then extend the model to a more general distribution.

The mathematical model chosen is that of *two* free field dipoles acting in each others hydrodynamic field. Since we are dealing here with an otherwise plane surface and since pressure dipoles are the only important sources, the axes of the dipole force are directed away from the surfaces.

The potential field for a point dipole with a given force spectral density $F(\omega)$ is

$$\Phi_D = \frac{3F(\omega)}{4\pi k\rho_0 c_0} \quad \frac{(kr-i)}{r^2} \quad \cos\theta \; e^{-ikr} \qquad (2.16)$$

To obtain the potential of two such sources, we simply add the potentials:

$$\Phi_{total} = \Phi_1 + \Phi_2$$

In summing the two potentials, we make the following approximations (all of which are physically and practically realizable):

1. The observer is in the geoemtric far field.
2. The observer is in the acoustic far field.
3. The sources are in each other's acoustic near field.

This potential then simplifies to

$$D = \frac{3\cos\theta \; e^{-ikr}}{4\pi\rho_0 c_0 r} \left[F_1(\omega) \; e^{ikh\cos\theta} - F_2(\omega) \; e^{-ikh\cos\theta} \right] \qquad (2.17)$$

so the sound pressure spectral density is

$$|p|^2 = \frac{9k^2\cos^2\theta}{16\pi^2 r^2} \left[F_1F_1^* + F_2F_2^* - \left(F_1F_2^* \; e^{i2kh\cos\theta} + F_1^*F_2 \; e^{-i2kh\cos\theta} \right) \right]$$

(2.18a)

$$\overline{|p|^2} = \frac{9k^2\cos^2\theta}{16\pi^2 r^2} \left[|F_1|^2 + |F_2|^2 - 2\mathrm{Re}\left(F_1 F_2^* \, e^{2ikh\cos\theta} \right) \right] \quad (2.18b)$$

The first two terms represent the force spectral densities of each source and the third (bracketed) term shows the effect that phase relationships may have on the sources. The third term need not be small, for if the forces are highly positive in correlation, the source degenerates into a quadrupole. For instance, if $F_1 \equiv F_2$,

$$|p|^2 = \frac{9k^2 F_1^2 \cos^2\theta}{2\pi^2 r^2} \sin^2(kh\cos\theta)$$

which, for dipoles separated by a small fraction of an acoustic wavelength (i.e., $kh << 1$) reduces to

$$|p|^2 = \frac{9k^4 F_1^2 h^2 \cos^4\theta}{2\pi^2 r^2}$$

The model thus indicates that the noise radiated from an edge region by collinear but opposed dipole forces ($F_1 \equiv -F_2$) would increase up to a factor of 4 (6 dB), while, for parallel but not necessarily collinear forces of the same sense (e.g., $F_1 = F_2$), a quadrupole field could be observed, with the dipole field being comparatively reduced in strength.

The relative strength of these effects in practical cases may be determined by correlation measurements near the edge of a surface, both along the span, and from upper to lower surfaces.

In general, the force (or surface pressure) cross-spectral density will have a "co" component and a "quadrature" component. The "co" component may be represented by positive cross-covariances which reduce the sound output. The "quad" component may be represented by negative cross-covariances which give increased sound pressure and introduce some asymmetry into the sound field. A limited set of cross-covariance measurements have been made near a trailing edge, and the results strongly suggest the applicability of this concept. These measurements are summarized in Sec. 4.

If the sources F_1 and F_2 are equal but completely uncorrelated, then Eq. (2.18) gives a simple addition of the two strengths (+3 dB).

To look at a general distribution of dipole sources, we may examine the effects of coherence between hydrodynamic source regions by extending Eq. (2.18) to a more general distribution of m sources.

The radiation sound from such a source distribution is proportional to:

$$\overline{p_a^2} \propto \omega^2 \left[F_1 F_1^* + F_2 F_2^* - 2\mathrm{Re}\left(2F_1 F_2^* e^{i\chi} + F_1^* F_2 e^{-i\chi} \right.\right.$$

$$\left.\left. + \text{---} + F_1 F_m^* e^{i\chi} + F_m F_1^* e^{i\chi} + \text{---} \text{ etc.} \right) \right]$$

where χ is $kh\cos\theta$.

From two adjacent source regions, 1 and 2, the radiated intensity from the pair then simplifies to

$$\overline{p_a^2} \propto \omega^2 \left(\overline{F_1^2} + \overline{F_2^2} - 2F_1 F_2 \right)$$

The term $F_1 F_2$ accounts for the coherence between source regions and, if positive, reduces the sound radiation below that which would be suggested by a simple addition of the mean square values of the independent sources. The term $F_1 F_2$ may be written in terms of an easily measured normalized weighting function, the cross-covariance coefficient, which will be called C_{12}:

$$F_1 F_2 = C_{12} \sqrt{\overline{F_1^2}\ \overline{F_2^2}}$$

For the case of sources F_1 and F_2 with similar characteristics (i.e., $\overline{F_1^2}(\omega) = \overline{F_2^2}(\omega)$, the radiation is

$$\overline{p_a^2} \propto \omega^2\ 2F_1^2\ (1 - C_{12}) \quad .$$

For m sources with similar characteristics $\left| \text{i.e., } \overline{F_1^2(\omega)} = \overline{F_m^2(\omega)} \right|$, the radiated sound becomes

$$p^2 \propto m\omega^2 \overline{F_1^2} \left(1 - C_{12}(\omega) - C_{13}(\omega) \text{ --- } - C_{im}(\omega) \text{ etc.}\right)$$

Thus, in the formulation of the dipole edge noise radiation from a generalized situation, we could redefine the "source number" term, m (= $W/\xi \ell_y$), in Eq. (2.15) as

$$m' = m \left(1 - C_{12}(\omega) - C_{13}(\omega) - \cdots - C_{im}(\omega) \text{ etc.}\right) \qquad (2.19)$$

To utilize this refinement, one must either measure or estimate the cross-covariances between various points along the span of an edge, and between upper and lower surfaces.

It has thus been shown that viewing the trailing (or leading) edge source with the physical perspective taken in this study — i.e., that the hydrodynamic acceleration of turbulence near the edge created localized dipole sources — gives rise to parametric relationships which can account for strengthening or weakening of the sound field from an array of such sources along or across an edge, and the degeneration of the dipole behavior into quadrupole behavior, as well as the earlier-described reduction of dipole radiation efficiency at high convective Mach numbers. The analysis thus far has beem limited to surfaces which have a dimension (say, chord) which is smaller (or at least not much larger) than an acoustic wavelength. This case represents one "limit" in the acoustic sense. In practice, surfaces which may generate "edge noise" are not always small with respect to an acoustic wavelength. Thus, it is of interest to look at the other limit — a semi-infinite chord surface.

2.6 Effect of Semi-Infinite Surface on Field Radiated by a Near-Edge Dipole

The semi-infinite surface (or half-plane), although physically unrealizable, provides a means for analyzing the limiting case of radiation of edge-generated sound by a surface very long with respect to the wavelength of sound generated by flow past the edge. It has already been postulated that turbulent

flow past an edge of a rigid surface will cause sound to be generated within a turbulent length scale of the edge. Other analyses of the rigid half-plane edge noise phenomenon (e.g., Ffowcs-Williams and Hall, 1970; Chase, 1972, 1975; Chandiramani, 1974), which have been based upon the premise that the edge plays an acoustic role but not a hydrodynamic one, have shown directivity pattern of edge-generated sound which varies like $\cos^2\phi/2$ in the plane normal to the surface and as velocity to the fifth power in intensity, regardless of the Mach number range. Hayden (1969) attempted to adapt the generalized dipole diffraction solution of Yildiz and Mawardi (1960) to the trailing edge dipole perpendicular to and near (in terms of wavelength) the edge of a semi-infinite thin rigid plate and, in doing so predicted the same directivity pattern ($\cos^2\psi/2$) in the plane normal to the surface passing through the point dipole axis as the above investigators, and a $\sin^2\theta$ directivity with respect to the edge itself (see Hayden, 1972, 1973 for details). However, the model used did not predict a U^5 dependence but rather a U^6 dependence. It has been suggested to the authors that the Green's function developed by Yildiz and Mawardi (1960) contains an error and thus the adaptation is incorrect in terms of velocity effect. Therefore, an alternate, but straightforward, analysis has been performed using well-accepted diffraction solutions published by Bowman *et al.*, (1969). The results are summarized below.

The pressure from a point dipole of source strength D (= Qd, where Q is the monopole strength of two antiphase monopoles separated by a distance d, which is very small with respect to a wavelength; (i.e., kd <<< 1) is:

$$p_{FF}(r,\psi) = - \frac{\omega\rho Dk}{2\pi r} \sin\theta \, e^{ikr} \qquad (2.20)$$

If the same dipole (or pair of anti-phase monopoles separated by d <<< λ) is moved close to and perpendicular to the edge of a semi-infinite rigid half-plane, at a distance r' which is << λ (i.e., kr' << 1), and the observer is well into the far field $\left(r >> \sqrt{(r')^2 + (d^2)}\right)$, then the pressure field becomes

$$p_{HP}(r,\psi,\theta) = - \sqrt{\frac{1}{\pi}} \quad \frac{\rho\omega D}{2\pi r} \quad \frac{k \cos(\psi/2) \sin\theta \, e^{i(kr + \pi/4)}}{\sqrt{k\left[(r')^2 + (d/4)^2\right]^{1/2} + kr'}} \qquad (2.21)$$

We have already indicated that the appearance of d is a result of the formation of the dipole field by two monopoles, and is very small compared to λ. We also assume now that it is small with respect to r'.

It is thus obvious that the proximity of the dipole to the surface is important in determining the strength of the field, and that there is a $1/\sqrt{k}$ difference between the half-plane pressure and the free field pressure. The differences in radiated mean square pressure (or intensity) can be found by forming a ratio

$$\frac{\overline{p^2_{HP}}}{\overline{p^2_{FF}}} = \frac{1}{\pi} \left[\frac{1}{2kr'}\right] \frac{\cos^2\psi/2 \sin^2\theta}{\sin^2\psi} \tag{2.22}$$

The difference in radiated power is:

$$\frac{\Pi_{HP}}{\Pi_{FF}} = \frac{1}{2kr'} \tag{2.23}$$

Using previously-developed concepts for relating source parameters to flow field parameters, k can be rewritten as

$$k = \frac{\omega_o}{c_o} = \frac{2\pi U_c}{\gamma \ell_x} \left(\frac{1}{c_o}\right) ;$$

and $$r' = \frac{\ell_x}{2}$$

Thus

$$\frac{1}{2kr'} = \frac{\gamma}{2\pi M_c} \tag{2.24}$$

We thus have the following expressions for a spanwise m distribution of hydrodynamic dipoles near the edge of a rigid semi-infinite half-plane (where $m = W/\xi\ell_y$, as before)

$$\Pi_{HP} = \frac{\rho M_c c_o^2}{24\pi^2} \gamma^3 \ell_x^2 \left(\frac{W}{\xi \ell_y}\right) \left(\frac{\overline{p}}{q_o}\right)^2 \left[1 + \frac{4\gamma^4\eta^4}{(2\pi)^4 M_c^4}\right]^{-1} \quad (2.25)$$

which reduces to

$$\Pi_{HP} = \frac{\pi^2 \rho U_c^5 \ell_x^2}{6\gamma\eta^4 c_o^2} \left(\frac{W}{\xi \ell_y}\right) \left(\frac{\overline{p}}{q_o}\right)^2 \quad \text{for } M_c < .3 \quad (2.26)$$

The corresponding free field mean square pressure

$$\overline{p_{a_{HP}}^2}(r,\theta,\psi) = \frac{\rho^2 U_c^5 \ell_x^2}{16 r^2 c_o \gamma \eta^4} \left(\frac{\overline{p}}{q_o}\right)^2 \sin^2\psi \cos^2\theta/2 \left[\quad\right]^{-1} \quad (2.27)$$

Thus, it is immediately obvious that the hydrodynamic dipole located immediately downstream of the edge of, normal to, and diffracted by, a semi-infinite rigid plane radiates as M_c^5, as a low Mach number limit, not U_o^6 as previously published. However, for finite surfaces, the radiated sound power (or intensity) will depend on a power of velocity greater than 5 — rapidly approaching 6 due to diffraction contributions (re-radiation) by the edges away from the hydrodynamic source. The "middle ground" (i.e., chord lengths which are neither semi-infinite, nor small with respect to a wavelength) involves very complex diffraction solutions which are beyond the scope of the present analysis. However, for an observer in the geometric far field of a *finite* surface of chord C (i.e., r >> C), the radiated intensity will *always* have a null in both the upstream and downstream directions in the plane of the surface and will always radiate with an M_c exponent >5, assuming flow field similarity and that one is at an M_c below the value at which the previously-described downward deviations from a simple velocity-exponent based power law begin. The Mach number and turbulent field dependent modifications of the "radiation efficiency" of a hydrodynamic dipole source near the edge of a semi-infinite plane would be expected to take place in precisely the same manner as for the "small surface" case, since those deviations are source effects, only the low Mach number asymptote would be M_c^5 instead of M_c^6

As a final note on the semi-infinite surface case, it is of interest to speculate on the M_c at which the semi-infinite surface radiates more (or less) power than the "small" surface for the same source strength, distance from the edge, etc. Returning to Eq. (2.23),

$$\frac{\Pi_{HP}}{\Pi_{FF}} = \frac{\gamma}{2\pi M_c}$$

As shown by data in Sec. 5, γ typically ranges from 2-6, depending on the flow field. For an attached wall flow (e.g., wall jet), $\gamma \approx 3$ is a reasonable average value. Using that,

$$\frac{\Pi_{HP}}{\Pi_{FF}} \approx \frac{1}{2M_c} \quad , \quad \text{which means that for } M_c \lesssim 0.5,$$

$$\Pi_{HP} > \Pi_{FF}$$

but for $M_c \gtrsim 0.5$, $\Pi_{HP} < \Pi_{FF}$.

This simple dimensional argument merely points out a possible trend which can be verified by acquiring very detailed flow field and simultaneous acoustic measurements.

In summary, it is seen for the first time that several of the postulated source mechanisms for trailing edge noise can produce the same velocity dependence of radiated power (U_o^5 or M_c^5) for a semi-infinite plane if the convective Mach number is below the value at which the radiation efficiency changes (in the case of the hydrodynamic dipole source.

Extension of the two limiting cases to formulations for "real" surfaces have not been made; however, it is clear that the radiated field will depend on Mach number to a power >5 and that the directivity will have nulls in both the upstream and downstream directions. The effects of finite surfaces are examined in more detail in Sec. 3.

Convective amplification effects such as discussed by Crighton (1975) have not been included in the current formulations. His results show an increase in free field pressures convection factors of $(1-M\cos\theta)^{-3/2}$ for edge diffraction of propagating acoustic waves, and $(1-M\cos\theta)^{-5/2}$ for near field scattering.

SECTION 3

ACOUSTIC EFFECTS OF SURFACE GEOMETRY

The surface of a plate, airfoil, wing, etc., plays a role in the generation of the turbulence which is radiated at the trailing edge by acceleration of the eddies, in the manner described in the preceding section. The surface is believed to play a less significant role in modifying the flow field *incident* upon the leading edge of a plate, airfoil, wing, etc., although the flow is modified in those cases once the surface has been encountered. However, in both the cases of leading edge and trailing edge sound radiation, the surface may play a significant acoustic role in determining the structure of the far field sound — both in the structure of the frequency spectrum, and in the directivity pattern. These strictly acoustic consequences of the surface geometry are usually interlocked (i.e., at a particular observation angle, the surface geometry may add structure to the frequency spectrum; or, conversely, in a particular frequency band, the surface geometry may modify the directivity pattern).

In the ensuing discussion, two of the most significant acoustic effects of surface geometry are treated.

3.1 Deviation from Point Dipole Directivity

3.1.1 Finiteness correction for coherent "whole body" dipole radiation

When an airfoil-like surface of finite extent (chordwise) is much smaller than an acoustic wavelength of the sound generated by unsteady flow interaction with its edges, the surface may radiate like a point dipole, or a spanwise array of point dipoles. In such a case, the radiation efficiency is $\propto k^2$; i.e., sound power output increases with the square of the frequency of the forces, and the directivity resulting from such forces is a symmetric figure-of-8 pattern, with an intensity variation following a $\sin^2\theta$ relationship, where θ is measured from the plane normal to the axis of the fluctuating forces.

When the dimensions of the surface increase (in the chordwise direction) to the point where the wavelength is no longer much larger than the chord, acoustic cancellation effects reduce the radiation efficiency, and the surface no longer behaves

like a point dipole. The radiation efficiency changes from $I \propto k^2$ to

$$I \propto \frac{k^2C^2}{1 + k^2C^2} \quad ,$$

where C is the chord (see, for example, Hayden, 1972; 1973).

When $kC >> 1$, then the edge regions radiate independently, and the contribution from the coherent whole body forces is overwhelmed by the edge regions, which radiate in the manner described in Sec. 2.

3.1.2 Modified directivity of edge sources by surfaces which are large with respect to an acoustic wavelength

A point source near a surface will experience a change in radiation directivity due to the presence of the surface. A dipole near the edge of, and oriented normal to, a large plane surface experiences a directivity change and change in radiation efficiency. Hayden (1969) modeled this as a semi-infinite surface and showed that for near-edge dipoles, the intensity was modified from a free-field dipole to a cardiod-shaped baffled dipole whose directivity can be described by $\sin^2\theta \cos^2\psi/2$. The directivity of such a source is shown in Fig. 6. If the surface is semi-infinite, the directivity change is simply that shown in Fig. 6 and given in Eq. 2.14 – namely, the radiation pattern changes from the axisymmetric free field point dipole source figure-8-shaped $\sin^2\theta$ directivity (θ measured from a plane normal to the axis of the force in spherical coordinates) to $\sin^2\theta \cos^2\psi/2$ cardioid-shaped directivity pattern with a maximum along the plane of surface, instead of the usual minima found in a free field dipole source (Fig. 7).

If the surface is of finite extent (chordwise or spanwise), then an additional factor must be taken into account; namely scattering (diffraction) from those edges not associated with the source generation (e.g., a leading edge will diffract trailing edge-generated noise, etc.). As shown schematically in Fig. 7, the diffracted field will add structure to the far field directivity pattern (at a given frequency) and will cause fluctuations in the frequency spectrum at a given point. The strength of the diffracted field is a function of the distance of the diffracting edge from the source edge, as well as of the spanwise extent of the source. The diffraction problem is discussed below.

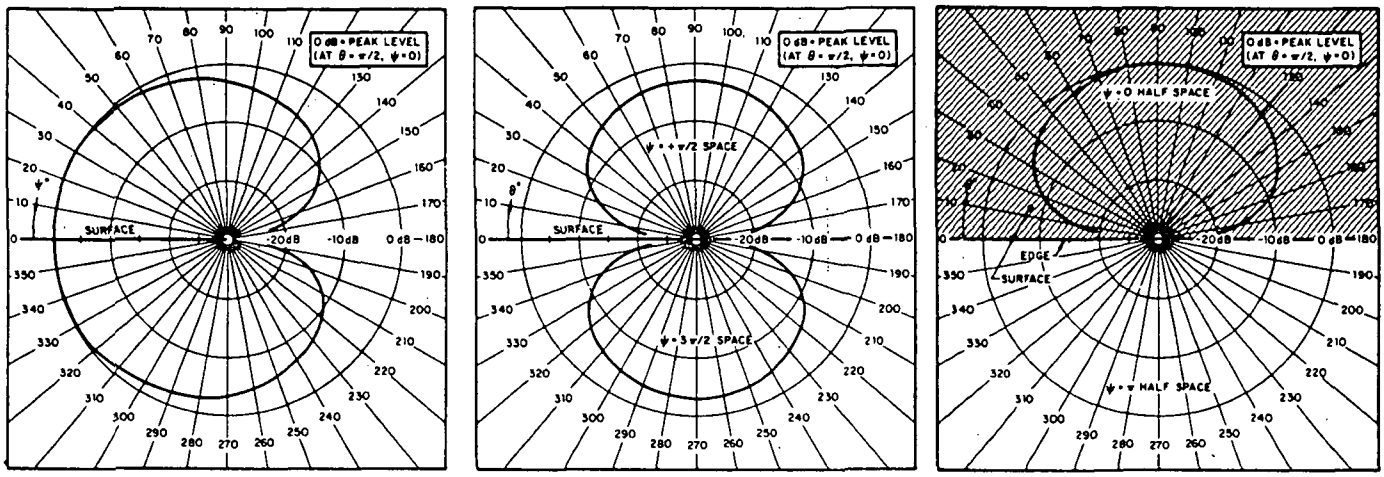

(a) In plane normal to surface and to span

(b) In plane normal to surface and parallel to span

(c) In plane of surface

FIG. 6. DIRECTIVITY OF POINT DIPOLE SOURCE AT THE EDGE OF A SEMI-INFINITE PLANE SURFACE.

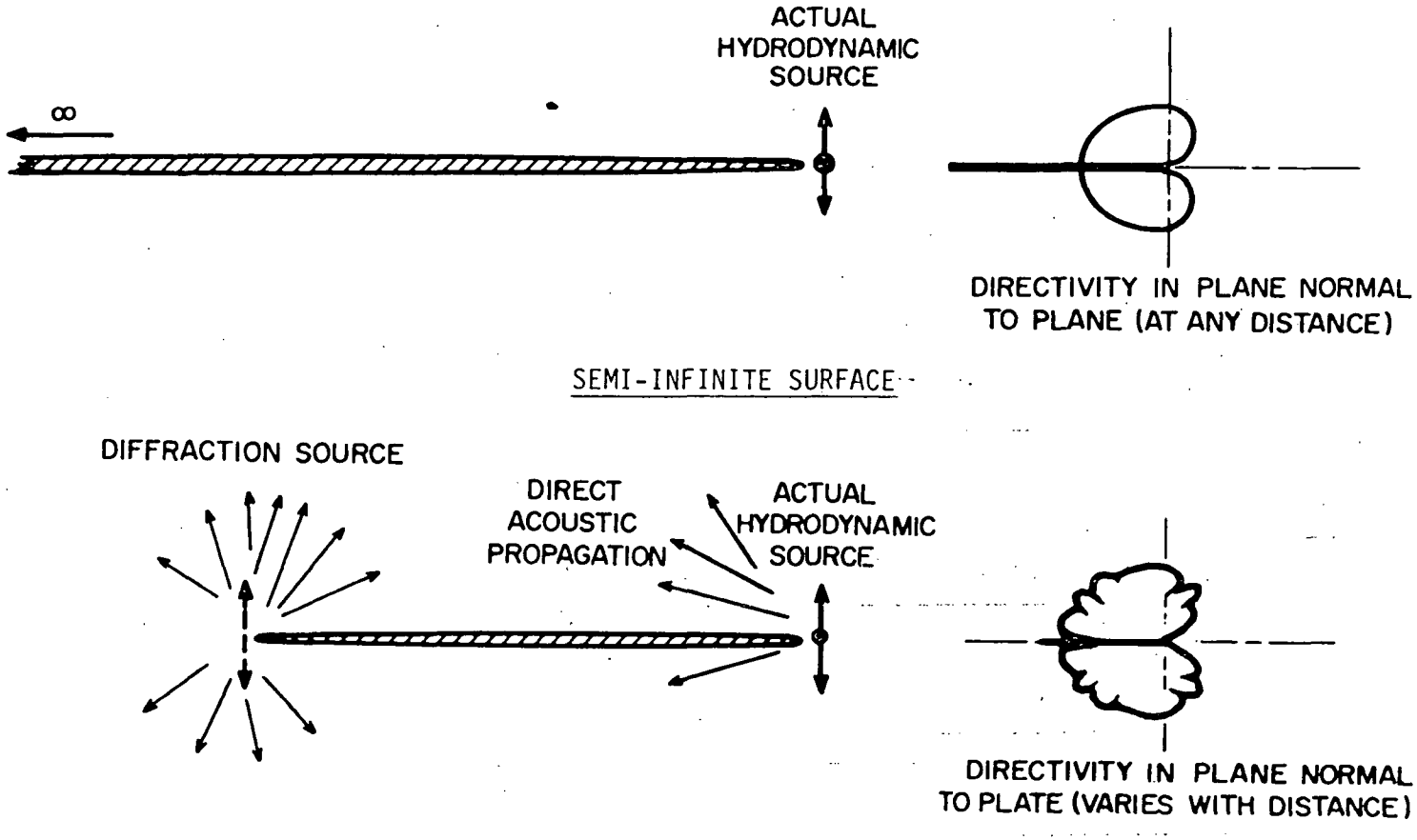

FIG. 7. SCHEMATIC OF MAJOR EFFECTS OF A SURFACE ON RADIATION FROM TRAILING EDGE DIPOLE SOURCES.

Whether or not diffraction from a non-source-generating edge takes place, the presence of the surface will always modify the directivity of an edge source, and the cardioid-shaped pattern will always be observed near the source (i.e., well away from the diffracting edge) as long as the surface is not small with respect to an acoustic wavelength.

3.2 Diffraction by Edges of Finite Surfaces with Localized Sources Along One Edge

It has been shown that the source of edge noise radiation can be represented by a distribution of dipoles at the edge or much less than an acoustic wavelength downstream of an airfoil or plate. The sound field, which has strong radiation intensity along the surface of the foil, is diffracted at the non-source edge. The strength of the far field diffraction depends upon the phase of the diffraction source compared to the hydrodynamic source, Fig. 8a shows schematically that for a localized source S_1 at the edge of an airfoil, the path lengths x_{ij} to the diffracting edge vary. Thus, unless the hydrodynamic source is highly coherent along the span, in which case the path lengths to the diffracting edge would be similar, or the directivity effects of the edge sources (which are strong toward the leading edge) reduce the importance of paths not aligned with the chord, the diffraction contribution in the far field may be relatively weak.

To assess the relative strength of diffraction effects for practical edge noise situations, and to provide further evidence that the principal edge noise source is a localized dipole immediately downstream of the trailing edge, a series of experiments were conducted in which the source area was confined in the spanwise direction to a small percentage of the surface dimension; the surface geometry was then varied. Figure 8b shows the various plate shapes tested. The flow field was a wall jet provided by a pair of 10:1 aspect nozzles (1.27 cm height × 12.7 cm span) on opposite sides of a rigid plate (thickness 0.635 cm). The distance from the nozzle to the trailing edge was held constant at 60 nozzle heights. Thus, the source characteristics can be assumed to be identical regardless of the geometry of the plate outside the flow field. Therefore, the only differences in far field spectra would be caused by diffraction effects of the different surfaces.

The plate shapes included two rectangular plates, over which the phase and amplitude of the diffraction sources would vary strongly, and a circular plate with center located 30

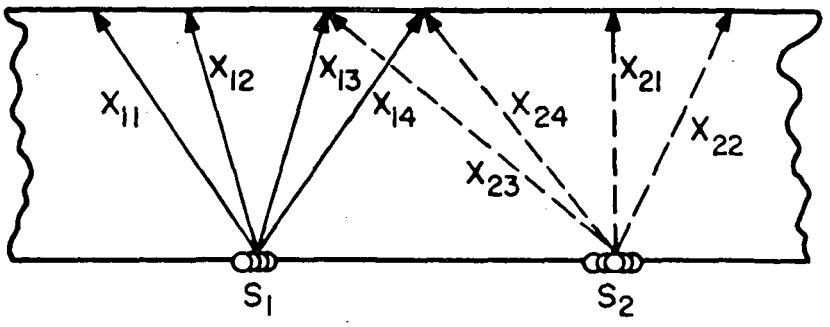

PLAN VIEW OF AIRFOIL

(a) DIFFRACTION GEOMETRY FOR LOCALIZED SOURCES AT THE EDGE OF A CONSTANT CHORD AIRFOIL.

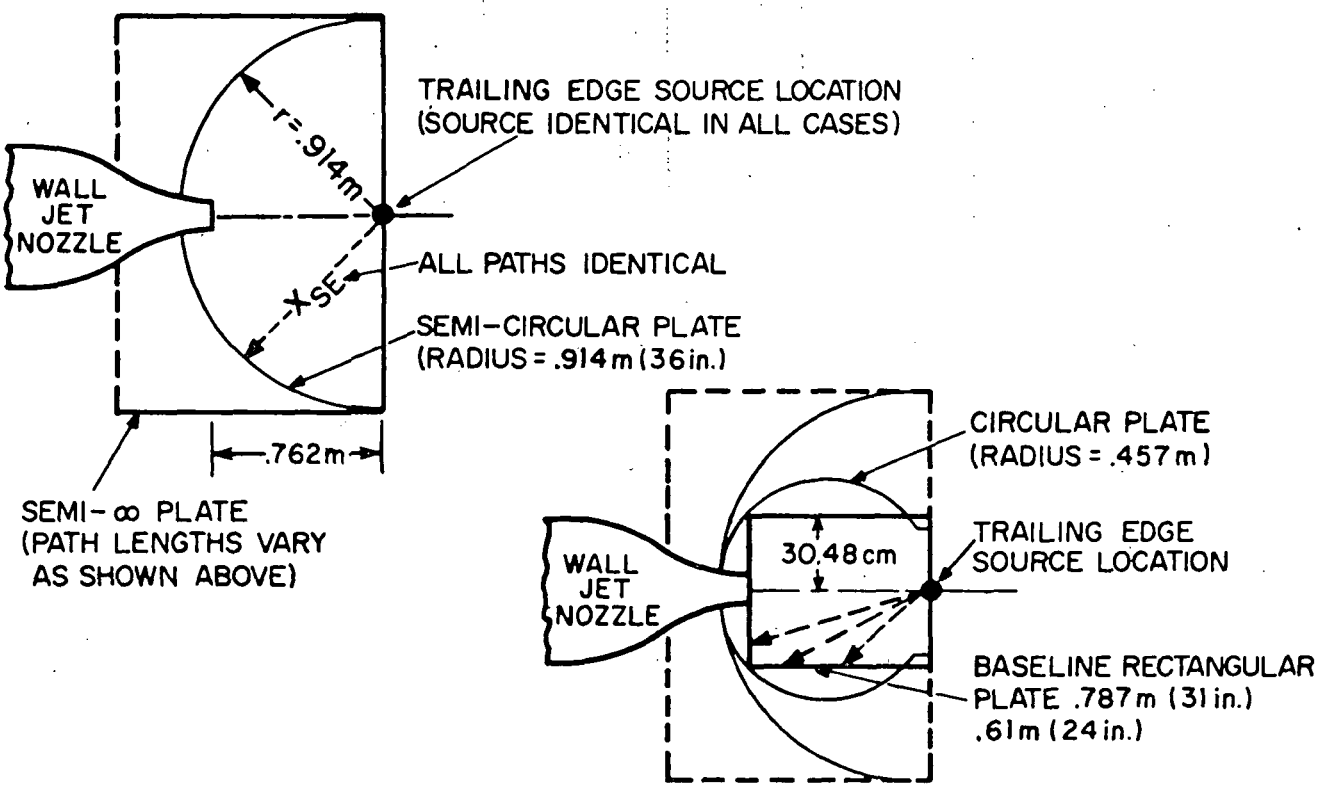

(b) PLATE GEOMETRY FOR SIMULATION OF FINITENESS EFFECTS WITH WALL JET TRAILING EDGE SOURCE

FIG. 8. PRACTICAL AND IDEALIZED GEOMETRIES FOR STUDYING DIFFRACTION EFFECTS OF EDGE NOISE.

nozzle heights upstream from the trailing edge which would also cause substantial phase variations of a localized dipole located immediately downstream of the trailing edge. Finally, a semi-circular plate geometry was devised to intentionally create a fully in-phase diffraction source along the edge of the plate, thus maximizing the contribution of the edge scattering to the total far field sound.

A survey of results of far field measurements is shown in Fig. 9. The effect of surface geometry on the spectrum details is quite dramatic. The most notable geometry is the semi-circular plate which produced strong interference effects in the spectrum. This result indicates that the assumption of a localized dipole source near the trailing edge is apparently valid, and gives an indication of typical relative strength of diffraction effects.

To provide more conclusive arguments on the question of a localized dipole source, an analysis was made of the diffraction effects from the particular semi-circular plate described above, and for the observation position measured. The details of the analysis are presented in Appendix A. The pertinent results are presented below.

A dipole source of strength D_1 was assumed to be immediately downstream (much less than an acoustic wavelength) from the trailing edge. The directivity of that source within the boundaries of the plate was assumed to be $\sin^2\theta \cos^2\psi/2$ (and alternately, omni-directional along the plate, for comparison). The effective size of the source region r_o was taken to be half width of the three dimensional wall jet at that trailing edge, and the dipole strength was assumed to fall as of $(r_o/r)^2$ from that point. The edge diffraction source was also assumed to be an edge dipole with the cardioid-shaped directivity of strength D_2 with the usual phase reversal due to the impedance discontinuity.

To calculate the perturbations on the "undiffracted" sound field, a baseline spectrum was derived by a curve fit through experimental data from the rectangular plate case (Fig. 10). The measured total direct-plus-diffracted field for the semi-plate is shown in Fig. 11.

The comparison of the predicted diffracted fields for the assumed conditions is made in Fig. 12. Two cases are shown, one assuming omni-directionality of the source in the plane of the plate, and the other assuming the theoretical directivity of an edge dipole located at the origin of the circular arc which forms the plate boundary.

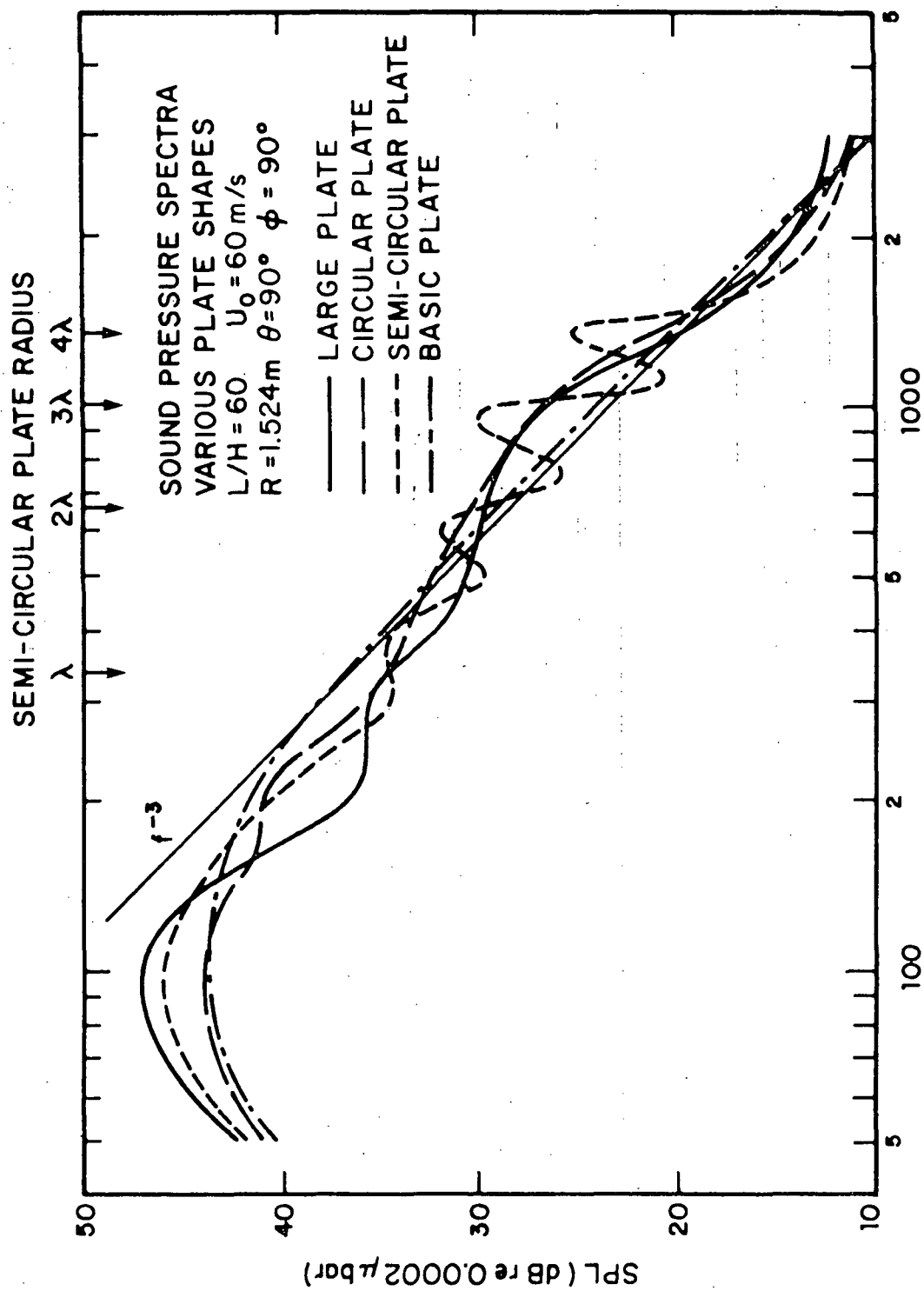

FIG. 9. EDGE NOISE SPECTRUM SHAPE AS A FUNCTION OF SURFACE PLANFORM GEOMETRY.

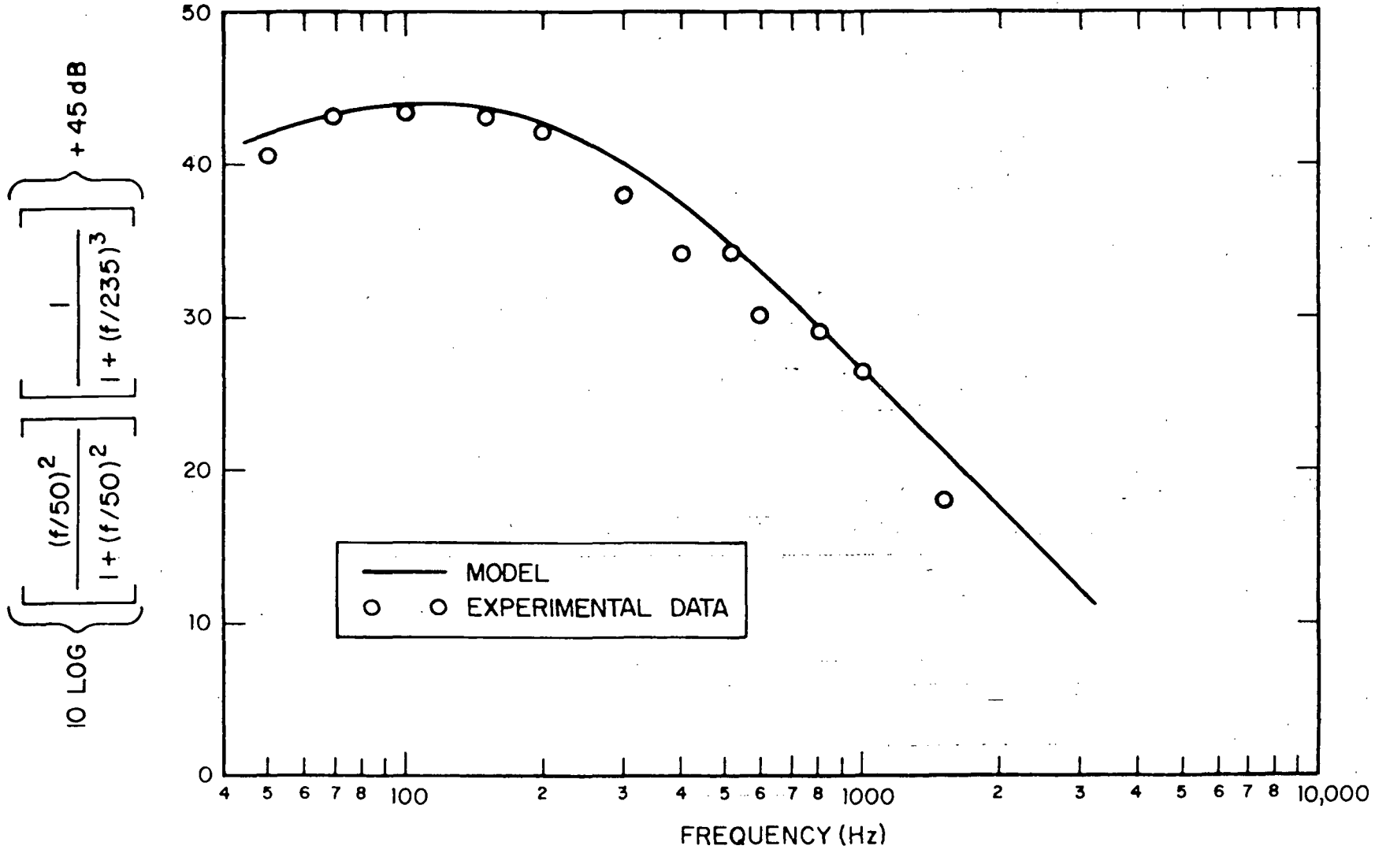

FIG. 10. BASELINE FAR FIELD SPECTRUM USED IN DIFFRACTION CALCULATION.

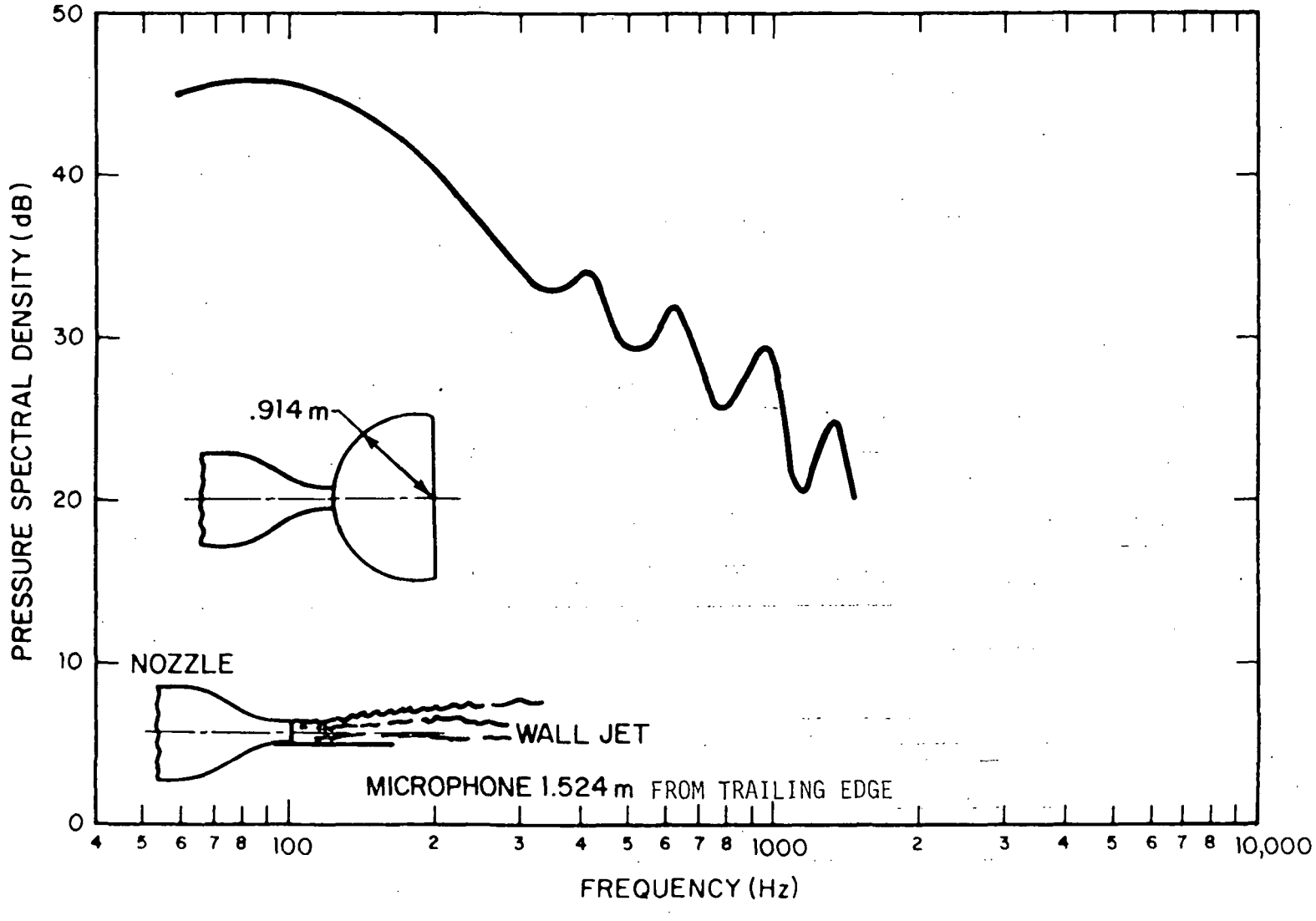

FIG. 11. MEASURED SOUND FIELD FROM SEMI-CIRCULAR PLATE.

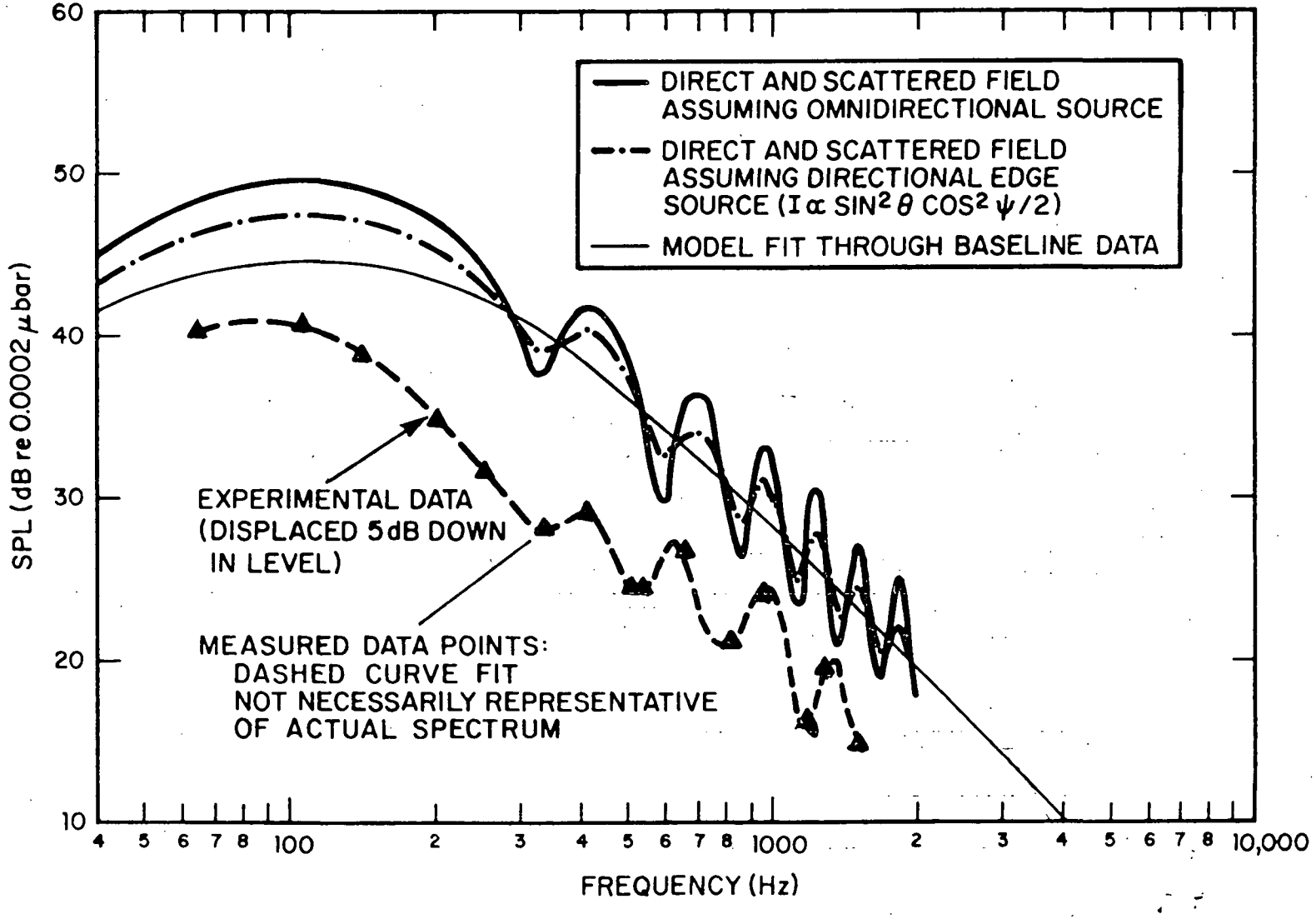

FIG. 12. PREDICTED DIFFRACTED FIELD OF EDGE DIPOLE FOR SEMI-CIRCULAR PLATE.

The measured data are plotted on Fig. 12 (displaced in level for clarity) and are seen to agree well with the prediction of the dipole source model in terms of amplitude of fluctuation of the spectrum and frequency of peaks and nulls in the oscillating spectrum. The disagreement in frequency of the measured peak at 1300 Hz with the prediction is presently unexplained, but may be due to errors in replotting experimental data.

SECTION 4

REVIEW OF SIGNIFICANT RESULTS OF EXPERIMENTS ON SOME ELEMENTARY CONFIGURATIONS

A number of experiments have been performed to isolate both the trailing edge noise source and the leading edge noise source, and to provide evidence of the parametric behavior of these sources, as well as physical phenomena important in the generation and radiation of edge sound. This section summarizes some of the key results from a number of definitive experiments.

4.1 Trailing Edge

The trailing edge experiments which are described below were conducted on a configuration first used by Hayden (1969), which consisted of a rectangular wall jet blowing tangentially over a flat plate which could be varied in length. The basic configuration is shown in Fig. 13. This apparatus was later modified to produce identical flow fields on both sides of the edge by adding a second nozzle to the lower side of the plate (Chanaud and Hayden, 1970). Also, the previously-discussed studies of diffraction effects were carried out on a two-sided configuration.

4.1.1 Effect of the edge on hydrodynamic pressure fluctuations

The model for edge sound radiation proposed in Sec. 2 is based upon the premise that hydrodynamic pressure fluctuations cause unsteady acceleration of the medium immediately downstream of the trailing edge. It also has been suggested that the hydrodynamic discontinuity (which is also an acoustic discontinuity) at the trailing edge may enhance the hydrodynamic pressure fluctuations.

An experiment on the wall jet apparatus was conducted to assess the order of magnitude of this effect. First, surface pressure transducers were located at a distance of 13 nozzle heights downstream of the nozzle ($x/H = 13$), at various spanwise positions relative to the flow centerline (y/H from 0 to 8). The plate was extended to the wall of the anechoic room at least 300 nozzle heights away. The pressure spectra, shown in Fig. 14, were similar in shape and level at all spanwise positions which were in the high velocity flow field ($y/H \lesssim 6$), the highest levels corresponding to positions under the intense side shear layers.

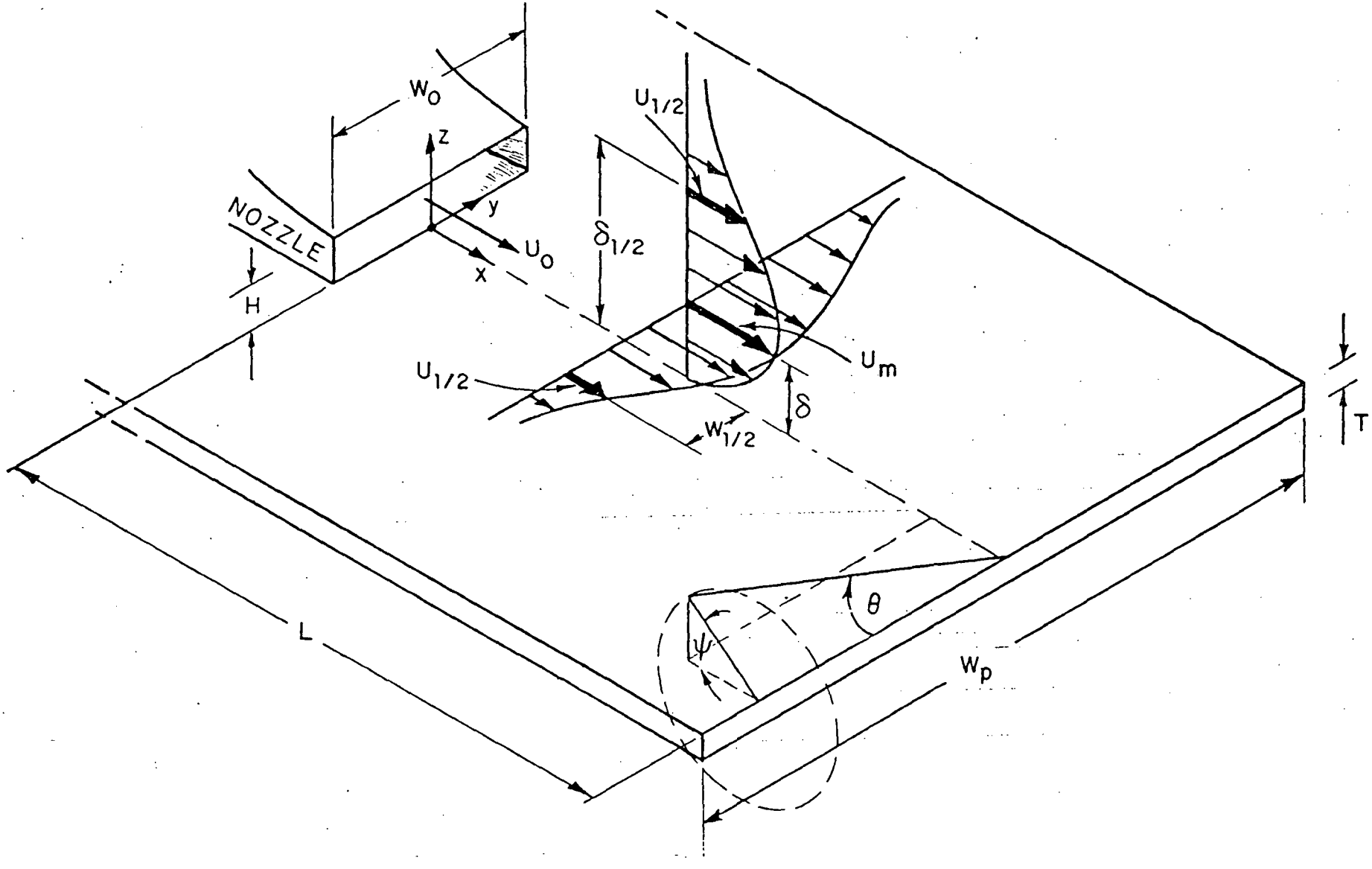

FIG. 13. COORDINATE SYSTEM AND TERMINOLOGY FOR WALL JET TRAILING EDGE EXPERIMENTS.

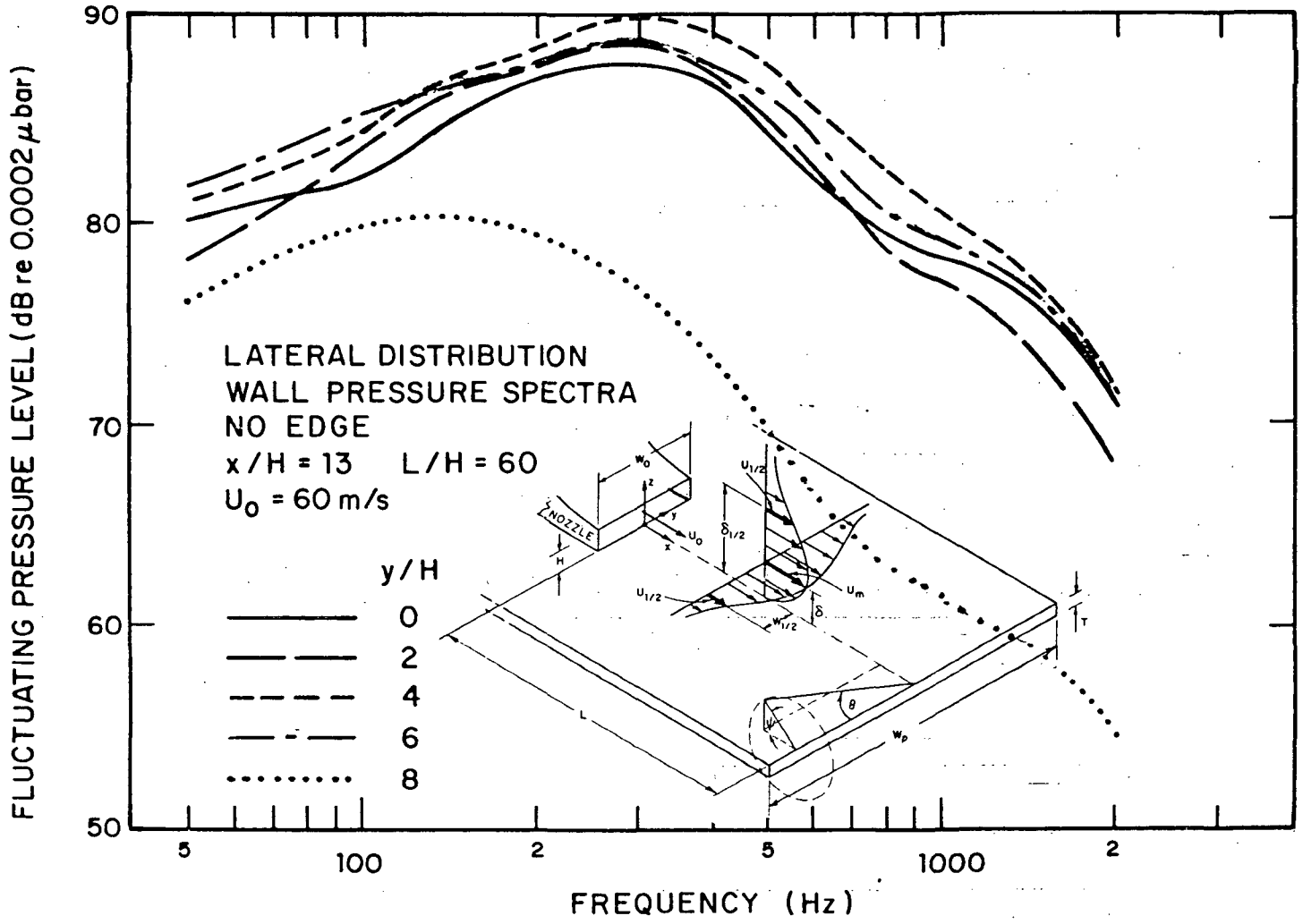

FIG. 14. SPANWISE DISTRIBUTION OF SURFACE PRESSURE WITH NO EDGE PRESENT.

The plate was then cut off at x/H = 12, and the sensors moved slightly upstream. The results showed a significant increase in low frequency levels and the appearance of a narrowband peak associated with vortex shedding from the plate, as shown in Fig. 15. Figure 16 compares the spectra at selected spanwise locations, from which it is evident that a 5-10 dB increase in hydrodynamic pressures is caused by the presence of a trailing edge.

From these experiments, it is concluded that the sheared flow field encountering a trailing edge is significantly influenced by the discontinuity, and new hydrodynamic sources of edge noise are generated at the edge.

4.1.2 Dependence of trailing edge-radiated sound on mean velocity for large but finite surfaces

The analysis of Sec. 2 (Eqs. 2.12, 2.13) indicates that dipole-generated edge sound may vary with flow velocity (U_o) from U_o^6 at low Mach numbers, to lower powers of velocity at high Mach numbers. The analysis also shows that the turbulence parameters intensity, length scales, and convection Mach numbers, affect the velocity scaling relationship. Recently there has been some controversy over the speed scaling laws for edge noise, and some of the conclusions presented by Hayden (1972) based on his original wall jet data (1969) have been challenged (e.g., Fink, 1975).

Figure 17(a) presents spectral data replotted from Hayden's wall jet experiments (1969), the original plots of which are reproduced in Appendix B for reference. The speed range covers over a factor of 3, from 28.35 m/s (93 fps) to 90.22 m/s (296 fps). The flow field regime is the so-called characteristic decay region in which the trailing edge is located 16 nozzle heights downstream of the nozzle. The spectra are seen to increase in level with velocity and shift toward higher frequencies, as would be expected from the usual similarity considerations. However, some features of the spectra, particularly a null in the 1000 Hz 1/3-octave band and a peak in the 1250 Hz band, do not shift with frequency. These features are undoubtedly due to diffraction of the trailing edge sound by the edges of the plate side, or leading edge (the plate protruded .3m to either side of the nozzle) at about .3m upstream of the nozzle. As shown in Sec. 3, enhancement of lower frequencies should also be expected due to diffraction effects.

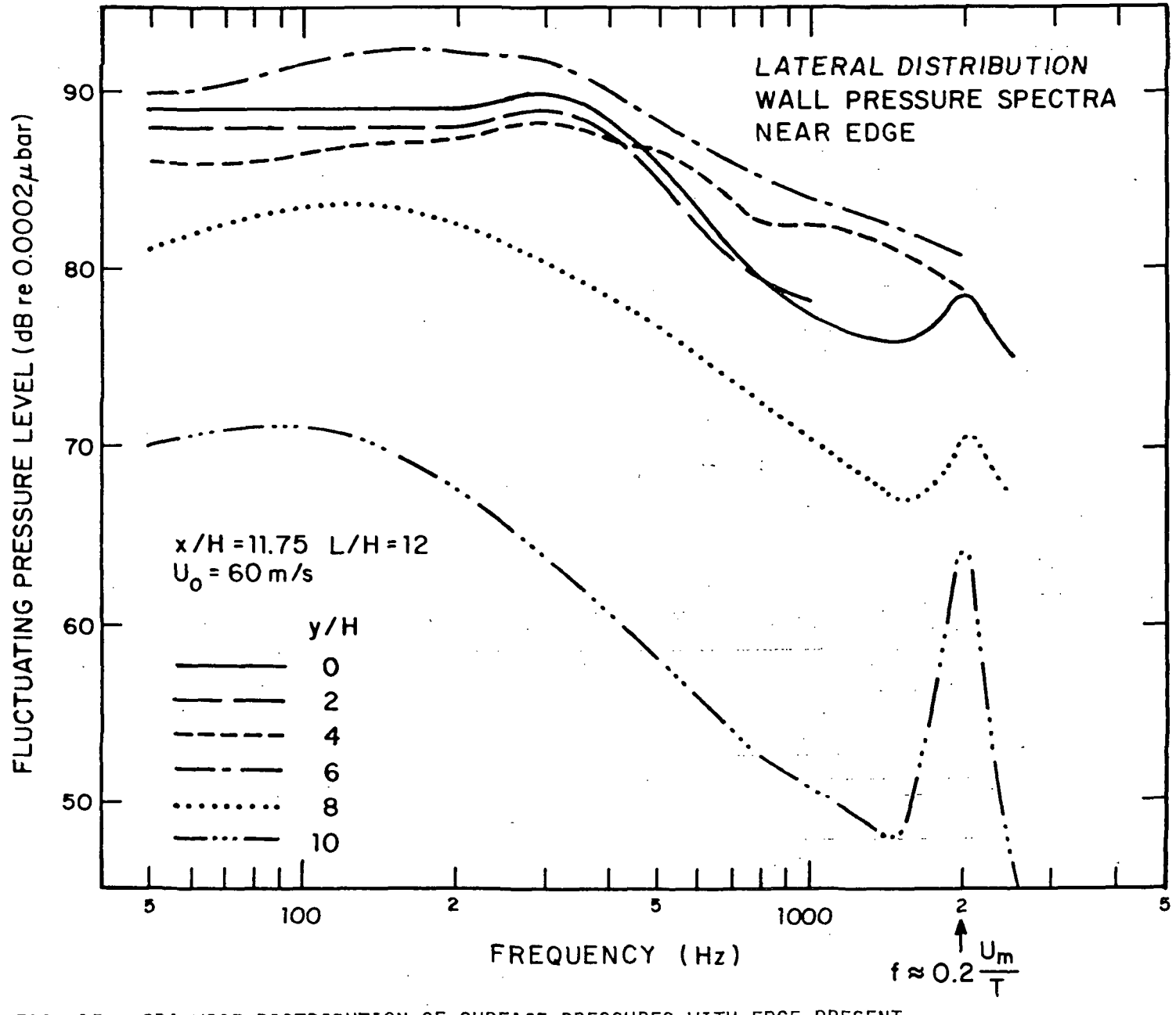

FIG. 15. SPANWISE DISTRIBUTION OF SURFACE PRESSURES WITH EDGE PRESENT (NOTE WAKE PEAK AT 2 kHZ).

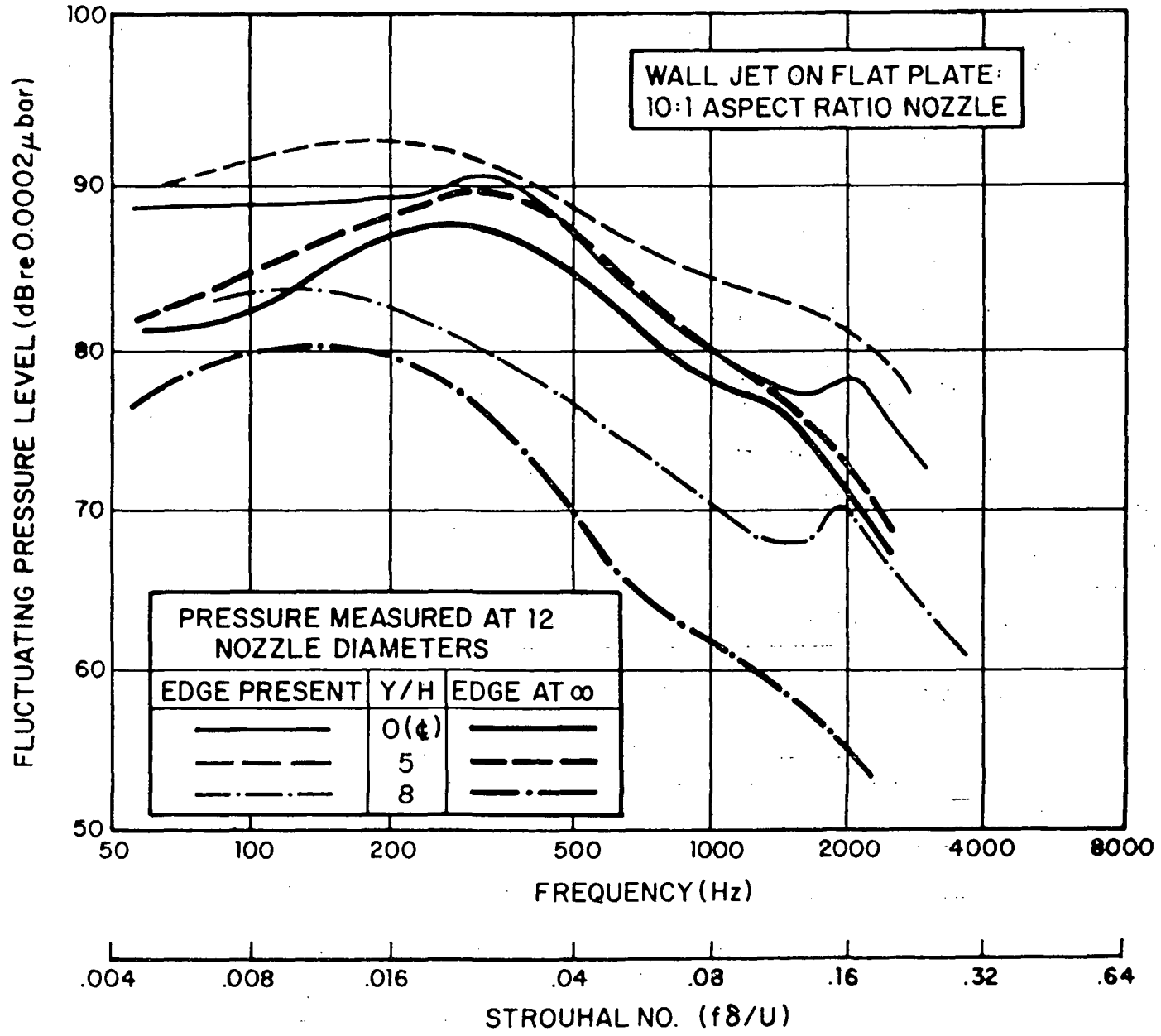

FIG. 16. SURVEY COMPARISON OF INCREASED HYDRODYNAMIC PRESSURES CAUSED BY A TRAILING EDGE.

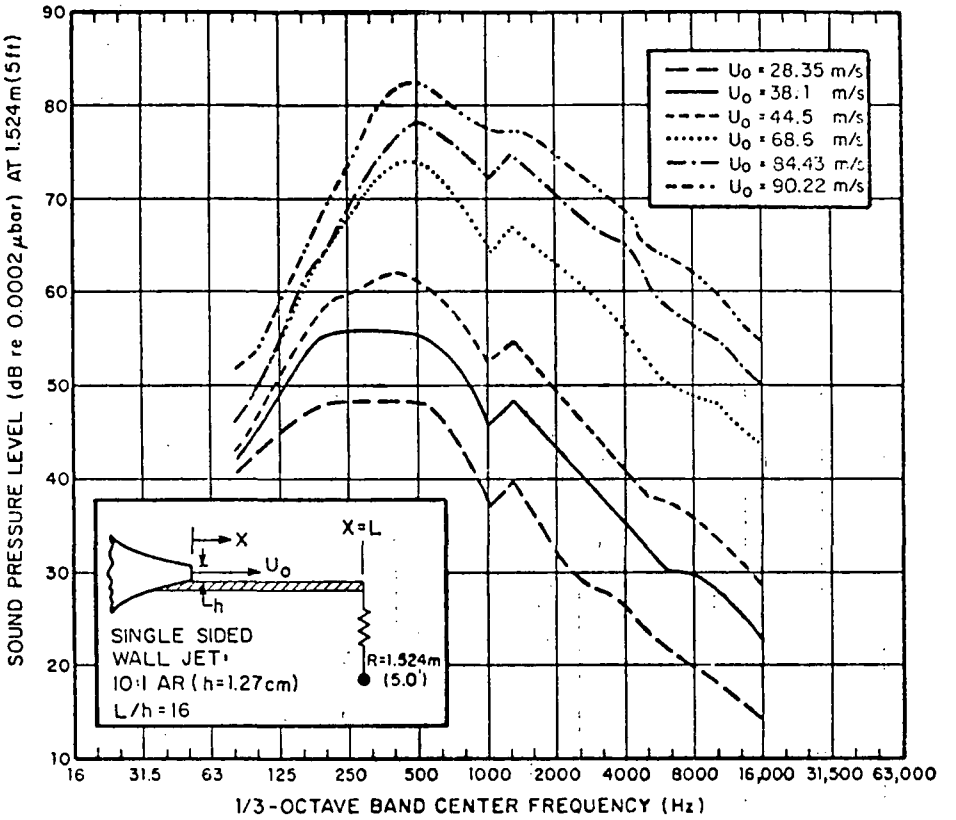

FIG. 17a. REPLOTTED TRAILING EDGE NOISE SPECTRA AS FUNCTION OF VELOCITY (FROM HAYDEN, 1969).

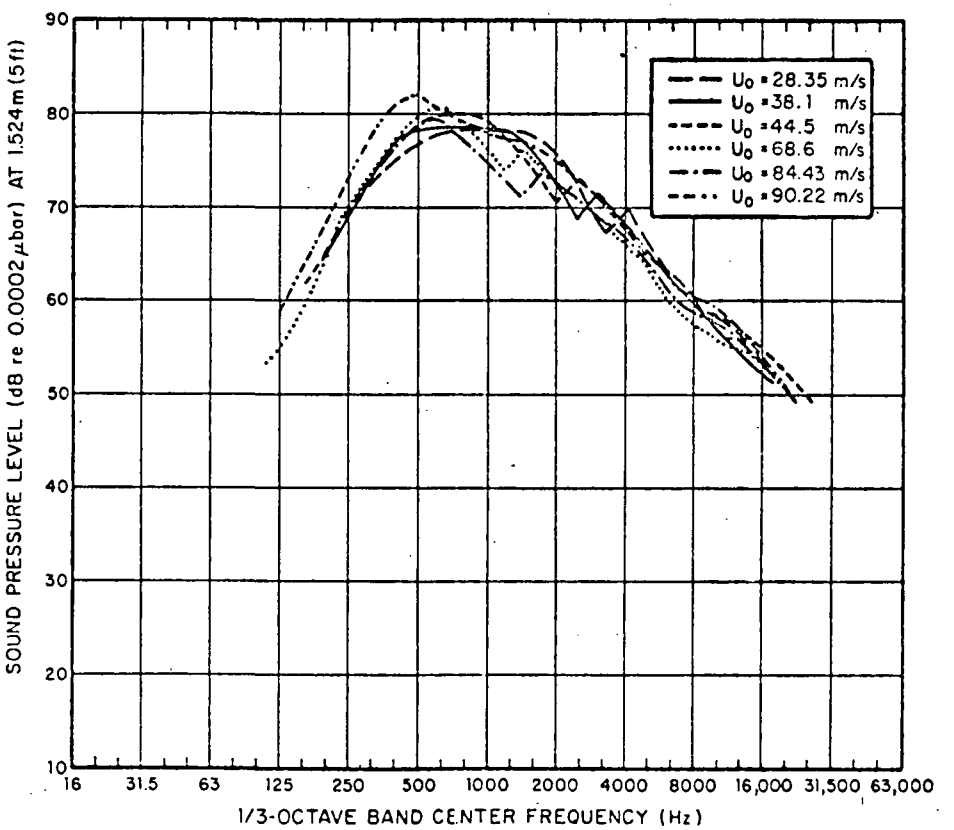

FIG. 17b. TRAILING EDGE NOISE DATA SCALED TO 90.22 m/s (296 fps) BY U^6.

The raw spectra were scaled to a velocity of 84.4 m/s (277 fps) by increasing the level according to a U^6 law, and shifting frequency linearly with velocity. The results are shown in Fig. 17(b), which indicates good collapse using the U^6 law, and the scatter caused by the apparent diffraction effects. To attempt to clarify the issue further, the raw data was smoothed to qualitatively remove the diffraction-related peaks and nulls (Fig. 17(c)), and re-plotted after scaling according to U^6, as shown in Fig. 17(d). The scatter in Fig. 17(d) is much reduced from that in Fig. 17(b). Both scaling exercises support the low Mach number limit M_c^6 scaling laws outlined in Sec. 2.

A similar scaling exercise for data from the so-called radial decay flow regime of the wall jet ($x/h = 60$) (Fig. 18a) shows the same good collapse and U^6 basis (Fig. 18b), although the velocity range is more limited. However, in this regime, the plate is larger with respect to a wavelength from the plate used in the characteristic decay region experiments. Original data curves are also provided in Appendix B for these data.

These data support the edge dipole model presented in Sec. 2, although, since Mach numbers were below 0.3 in all cases, the higher Mach number effects (change in velocity dependence) predicted by the model have not been tested. The above scaling exercise also reaffirms the conclusions reached by Hayden (1972) as to the appropriate velocity scaling for the low Mach number wall jet data, although the leading edge diffraction effects in the spectra were overlooked in the 1972 report. The transition regime between finite surfaces which obey acoustically "small" scaling laws and those exhibiting quasi-semi-infinite behavior thus, remains to be defined.

4.1.3 Directivity

In Sec. 2, the model for directivity from an edge dipole near a large surface was given as $\sin^2\theta \cos^2\psi/2$ factor when the observer is not well into the geometric far field.

Experimental data supporting that model were presented by Hayden (1969) for wall jet flow over one side of a trailing edge, and by Chanaud and Hayden (1970) for flow over both sides of an edge of a large plate whose chordwise dimension was approximately 1.2m (4 ft). The data from the latter case are presented in Fig. 19 for various frequency bands. Good agreement with the predicted cardiod-shaped pattern is seen, thus supporting such a model for the semi-infinite surface case, although the surface was anything but large with respect to a wavelength at low frequencies (e.g., at 200 Hz, $kL \approx 6$; at 100 Hz $kL \approx 3$).

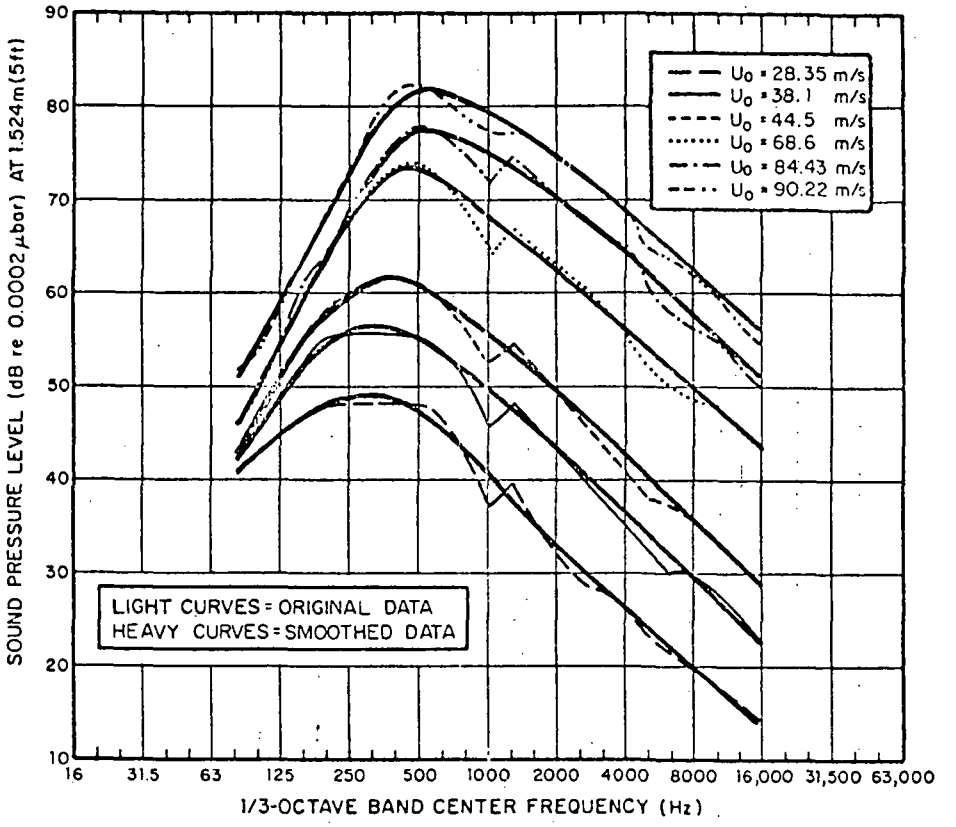

FIG. 17c. TRAILING EDGE SPECTRA SMOOTHED TO REMOVE DIFFRACTION EFFECTS.

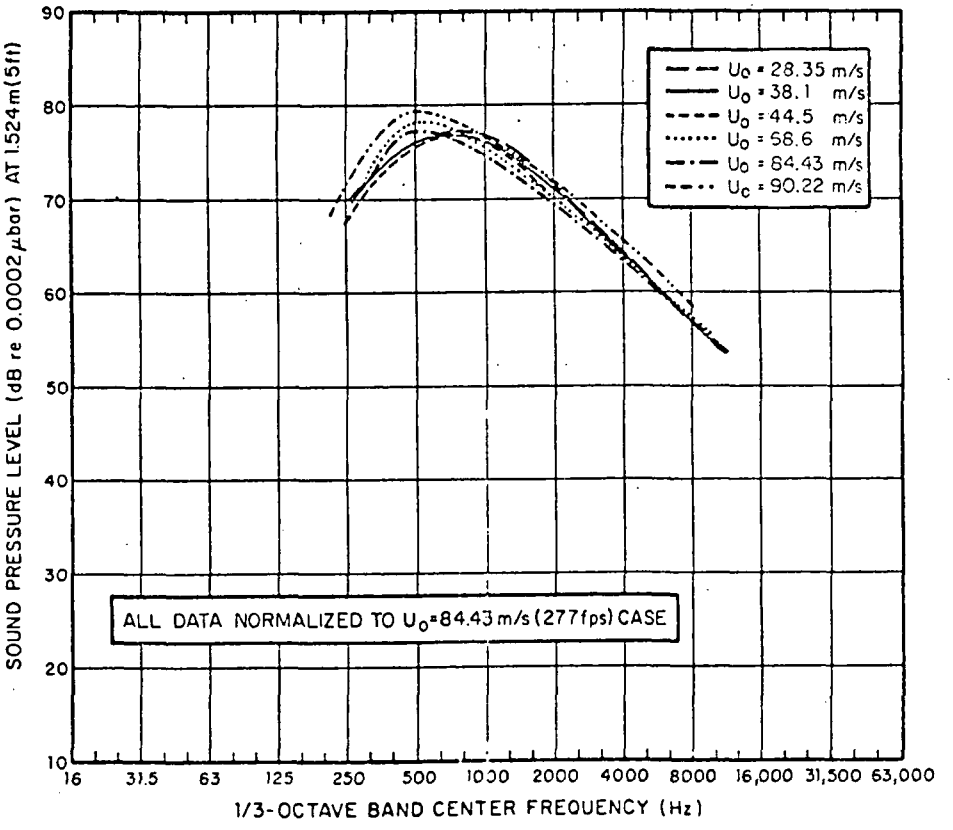

FIG. 17d. SMOOTHED SPECTRA SCALED BY U^6 to 84 m/s (277 fps).

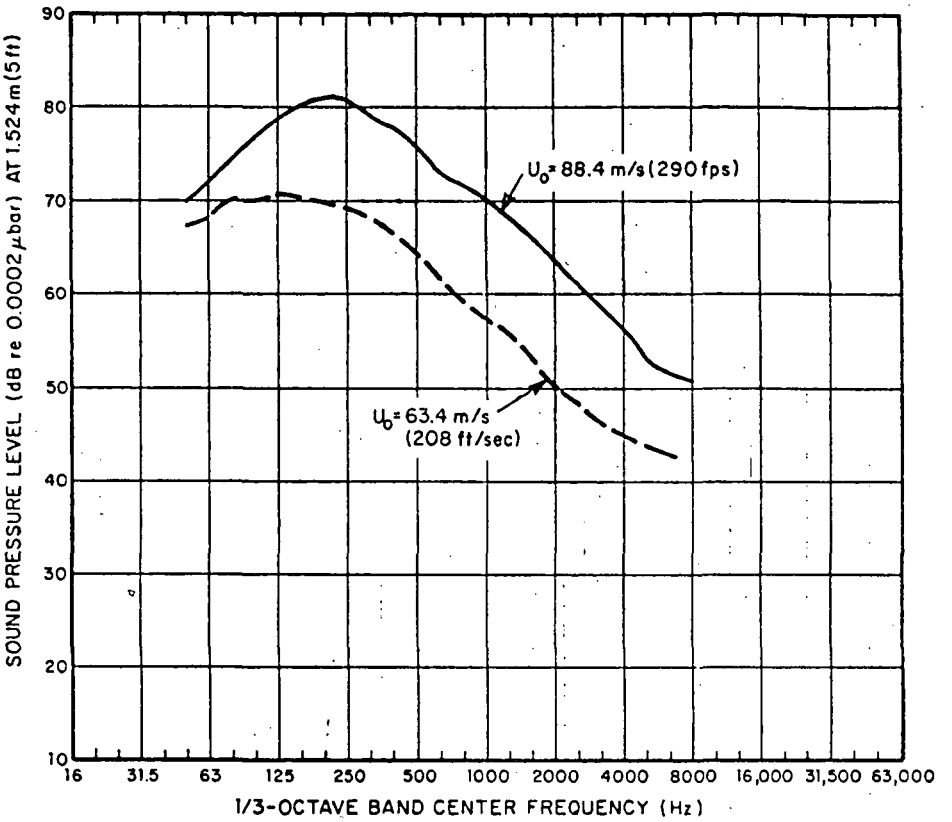

FIG. 18a. WALL JET TRAILING EDGE SPECTRA FROM PLATE (L/h = 60).

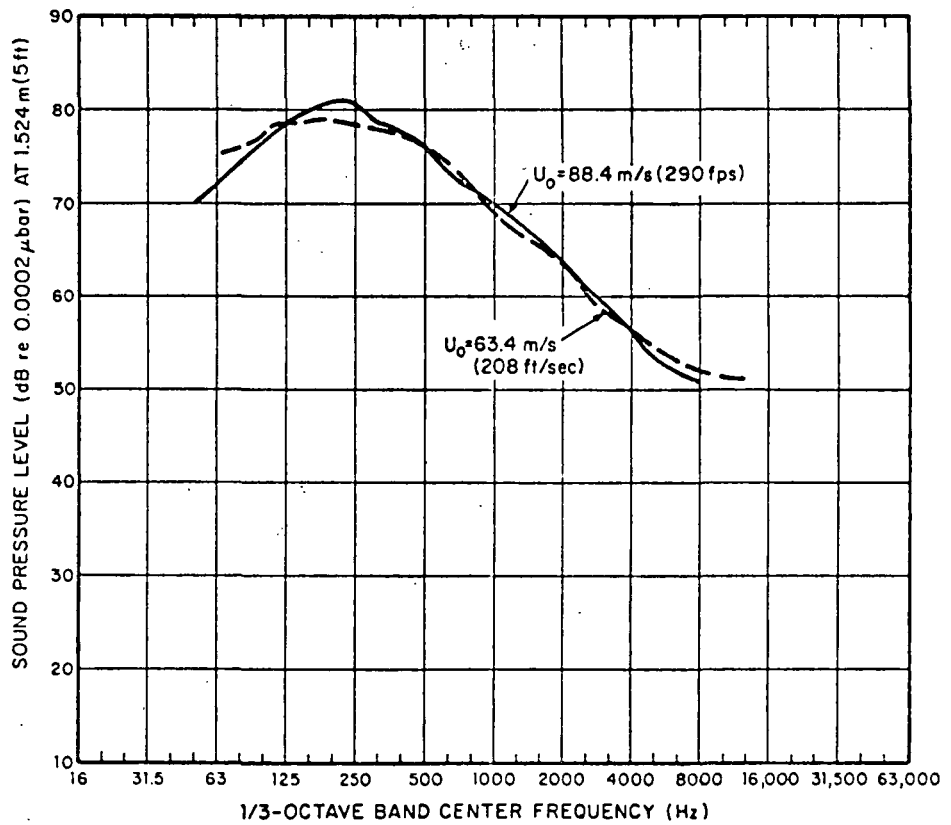

FIG. 18b. WALL JET TRAILING EDGE SPECTRA SCALED BY U_o^6 to U_o = 88.4 m/s (290 fps) (L/h = 60 plate).

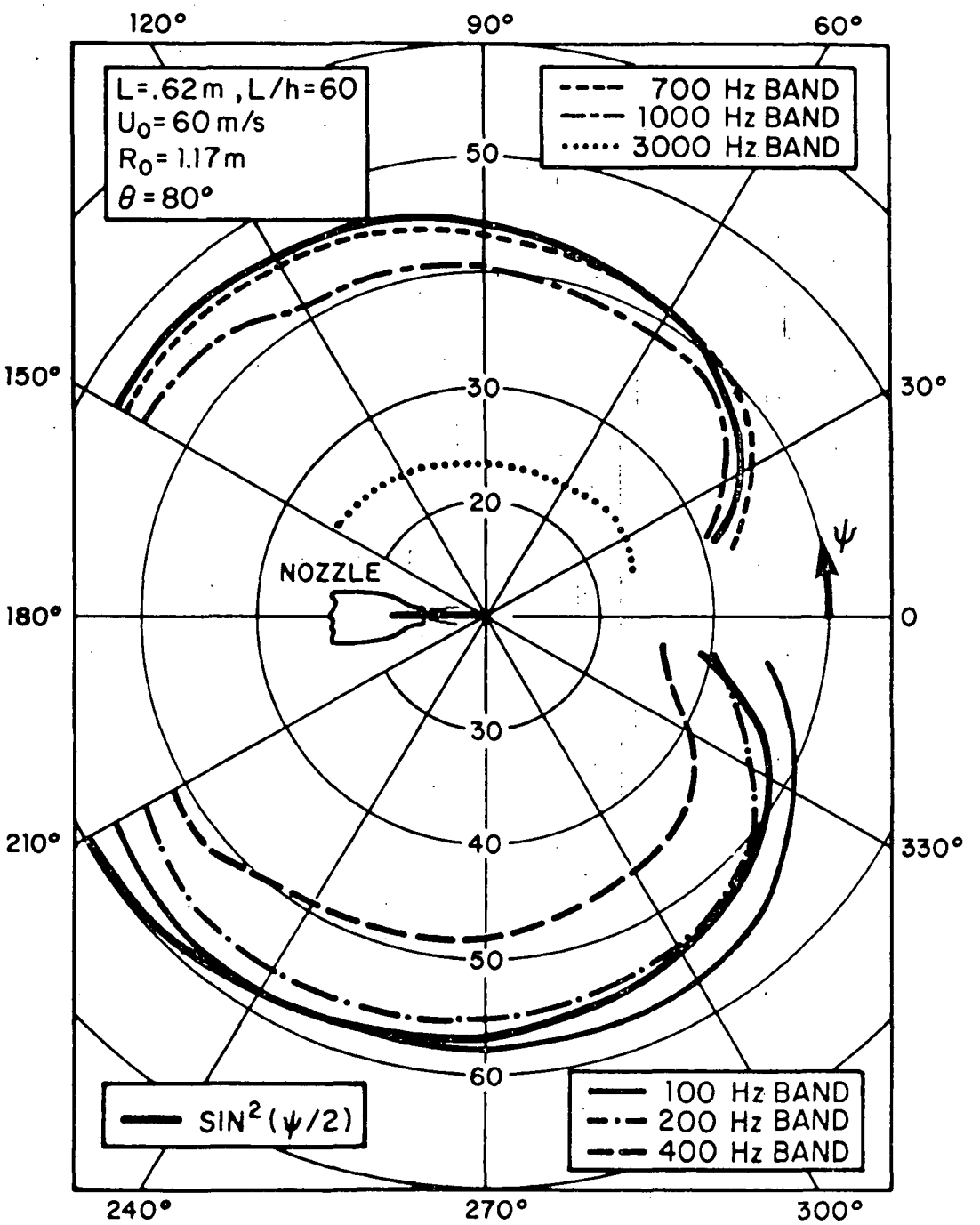

FIG. 19. MEASURED DIRECTIVITY FROM TRAILING EDGE SOURCE.

4.1.4 Effect of trailing edge thickness

Two measurements of the effect of edge thickness on edge sound radiated from flow on one side of a surface have been made, and are shown in Figs. 20 and 21. The first, from Hayden (1969), shows reduction in free field sound pressure level at a position normal to the trailing edge of the plate. It was not established whether or not the directivity of the sound field was changed by the thicker edge, thus no conclusion on the principal effect of the thicker edge could be drawn. However, the second experiment, conducted by Bender, *et al* (1972) in a reverberant room, indicates that increased edge thickness reduces the power output of the edge source, as shown in Fig. 21.

Although the explanation for this phenomenon is not clear, and diagnostic measurements have not been carried out to date, it is clear that the edge thickness controls the local flow streamlines and may thus influence the stability of the near-edge flowfield.

4.1.5 Effect of flow on both sides of an edge

A very important practical case of interest is the effect of flow on both sides of an edge. The analysis in Sec. 2.5 indicated that sound output could be either reduced or increased, depending upon the correlation between the upper and lower surfaces. The data in Sec. 4.1.4 also suggest that the thickness of the edge might play a role in the correlation between upper and lower surfaces.

An experiment has been conducted on the two-sided wall jet configuration described above, for a plate length of 60 nozzle heights (L/h = 60). Pressure sensors were placed simultaneously on the upper and lower surface near the edge and the pressures were cross-correlated at zero time delay, thus deriving a cross covariance coefficient C_{AB} between the upper and lower surface

$$\left(\text{i.e., } C_{AB} = \frac{(\overline{p_A \cdot p_B})_{\tau=0}}{\sqrt{\overline{p_A^2} \cdot \overline{p_B^2}}} \right)$$

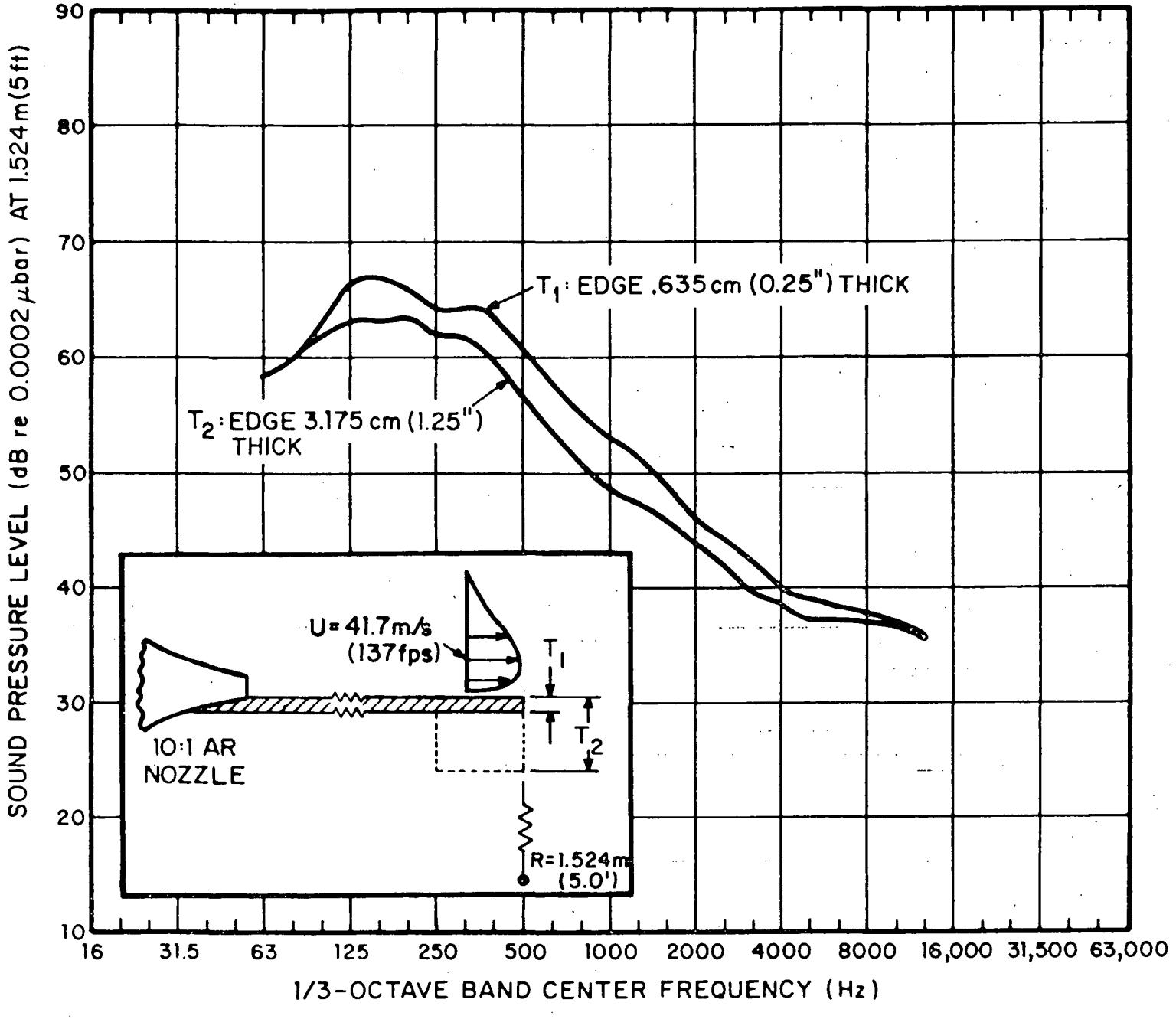

FIG. 20. MEASURED REDUCTION OF TRAILING EDGE SOUND BY THICK EDGE.

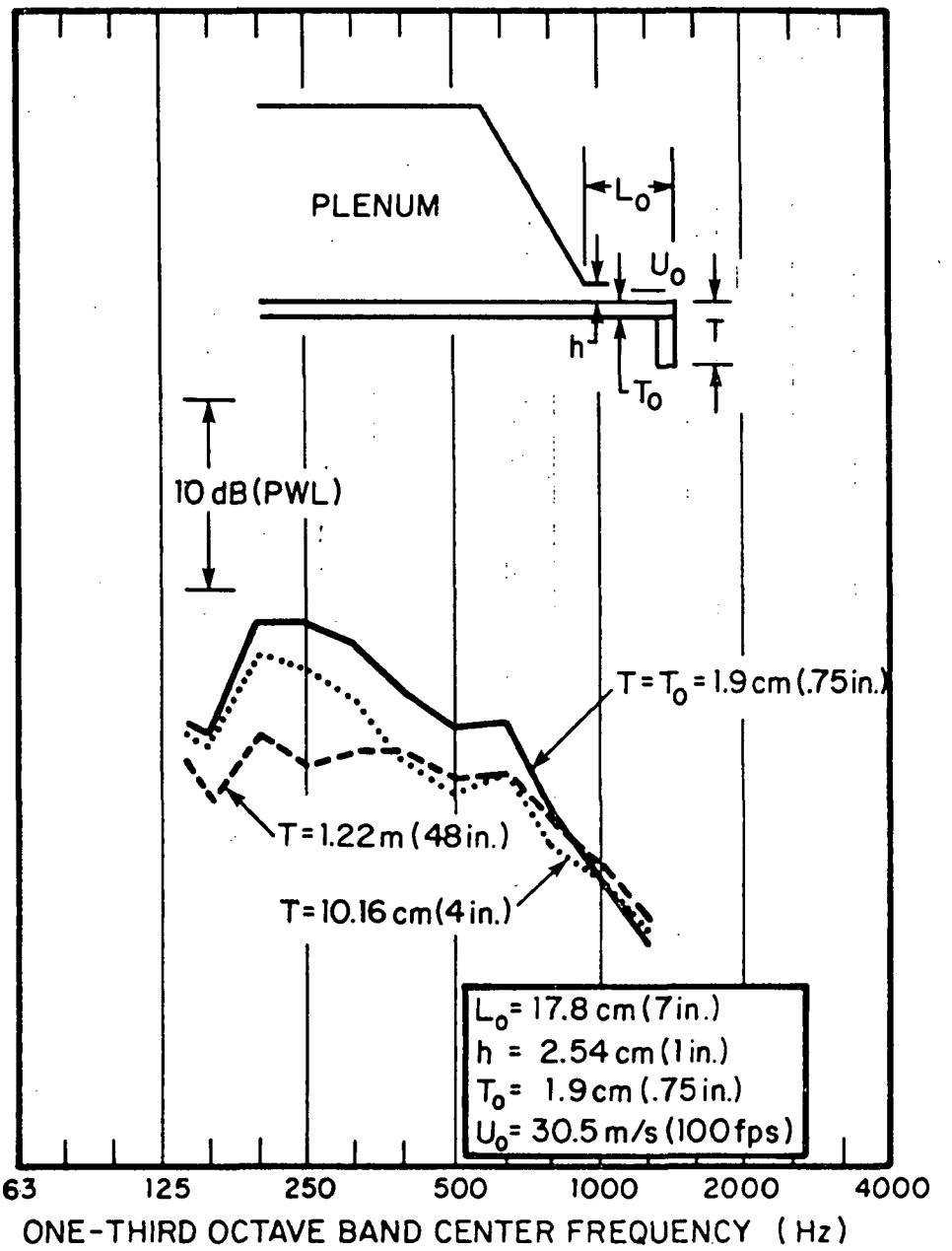

FIG. 21. RELATIVE REDUCTION OF TRAILING EDGE NOISE SOUND POWER DUE TO EDGE THICKNESS.

The cross covariance, measured in frequency bands, is shown in Fig. 22. Relatively high values of $C_{AB}(0)$ are seen at low frequencies, falling off toward higher frequencies. The cross covariance coefficient becomes strongly negative around 1000 Hz, which corresponds to a suspected vortex shedding from the 0.25 inch thick plate. The positive values of C_{AB} at low frequencies which decay toward higher frequencies is indicative of the large eddy scale frequencies, which do not cancel one another across the edge.

This data, combined with the considerations presented in Sec. 2.5, suggests that the far field sound spectra should reflect the variation in partial coherence of the independent source regions. Figure 23 compares the sound radiated by a trailing edge with flow over one side with the same edge having the identical flow on both sides. At low frequencies the two-sided flow actually generates less sound than the single sided flow. Around 1 kHz, the vortex shedding and the negative cross covariance of the two-sided flow is in evidence, as the sound radiated increases above the level of the one-sided flow. At higher frequencies, the edges appear to radiate independently (i.e., total SPL increases ~3 dB), as would be indicated by the cross covariance.

Thus, it is shown that the *differential pressure* across an edge is the important parameter controlling the unsteady acceleration of the medium near the edge. The data presented above tend to provide further evidence in support of the applicability of the model proposed in Sec. 2.

4.2 Leading Edge Experiments

The leading edge sound source becomes important when one airfoil or other surface is exposed to turbulent inflow. Some experiments and numerous analyses have been conducted on airfoils in turbulent inflow, but in these cases, it is difficult to isolate leading-edge-generated sound from the lift response of the entire airfoil, and possible trailing edge sources, although the previously described method of relating surface flow field parameters to far field sound would enable such isolation of sources.

To develop a data base on the leading edge source without the complexities of using correlation methods to isolate the source, an experimental configuration was devised which would ensure that sound measured was generated by flow impingement on a leading edge. This apparatus, shown in Fig. 24, utilized

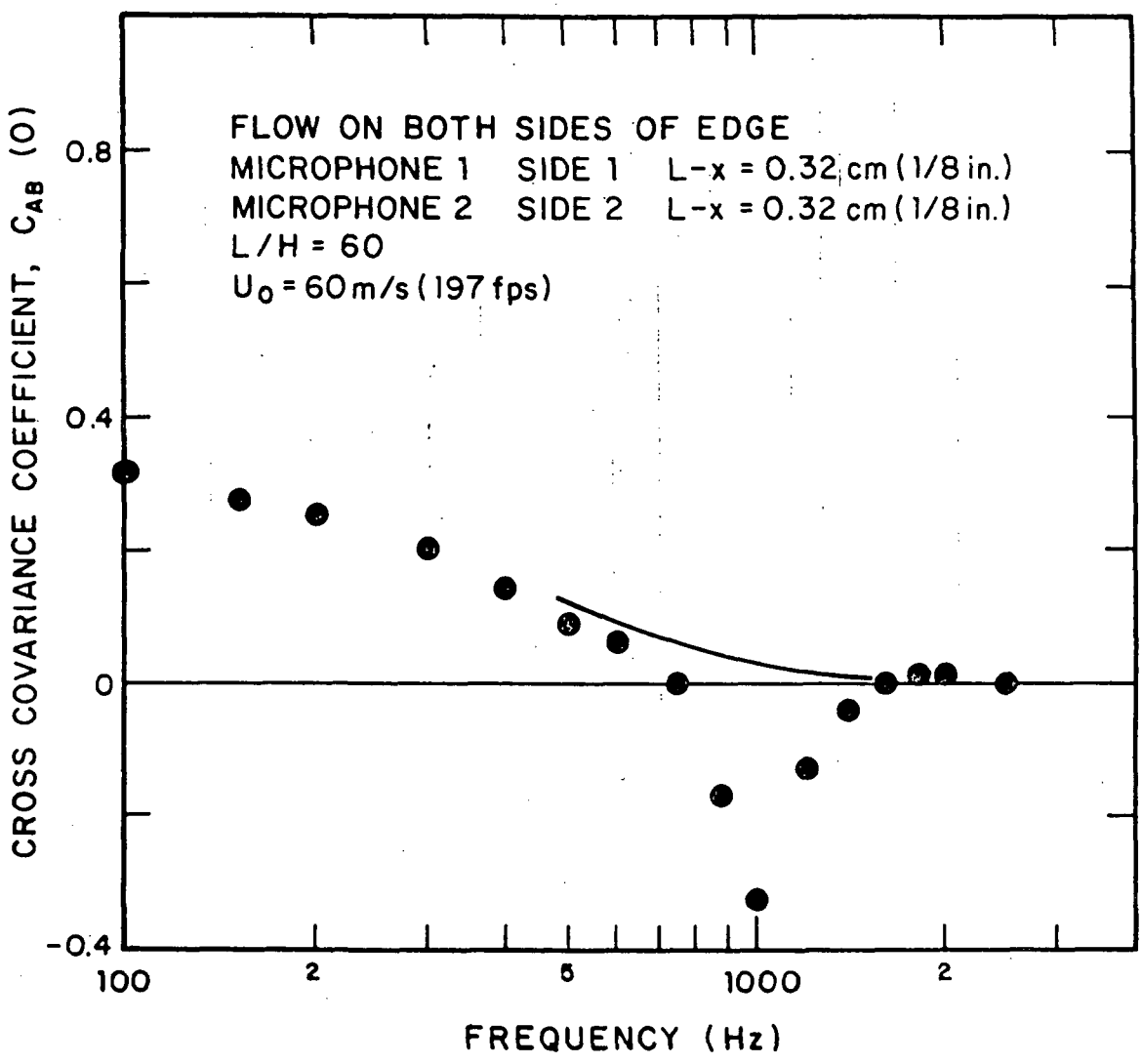

FIG. 22. CROSS-CORRELATION BETWEEN SURFACE PRESSURES OPPOSITE SIDES OF A TRAILING EDGE — FLOW ON BOTH SIDES.

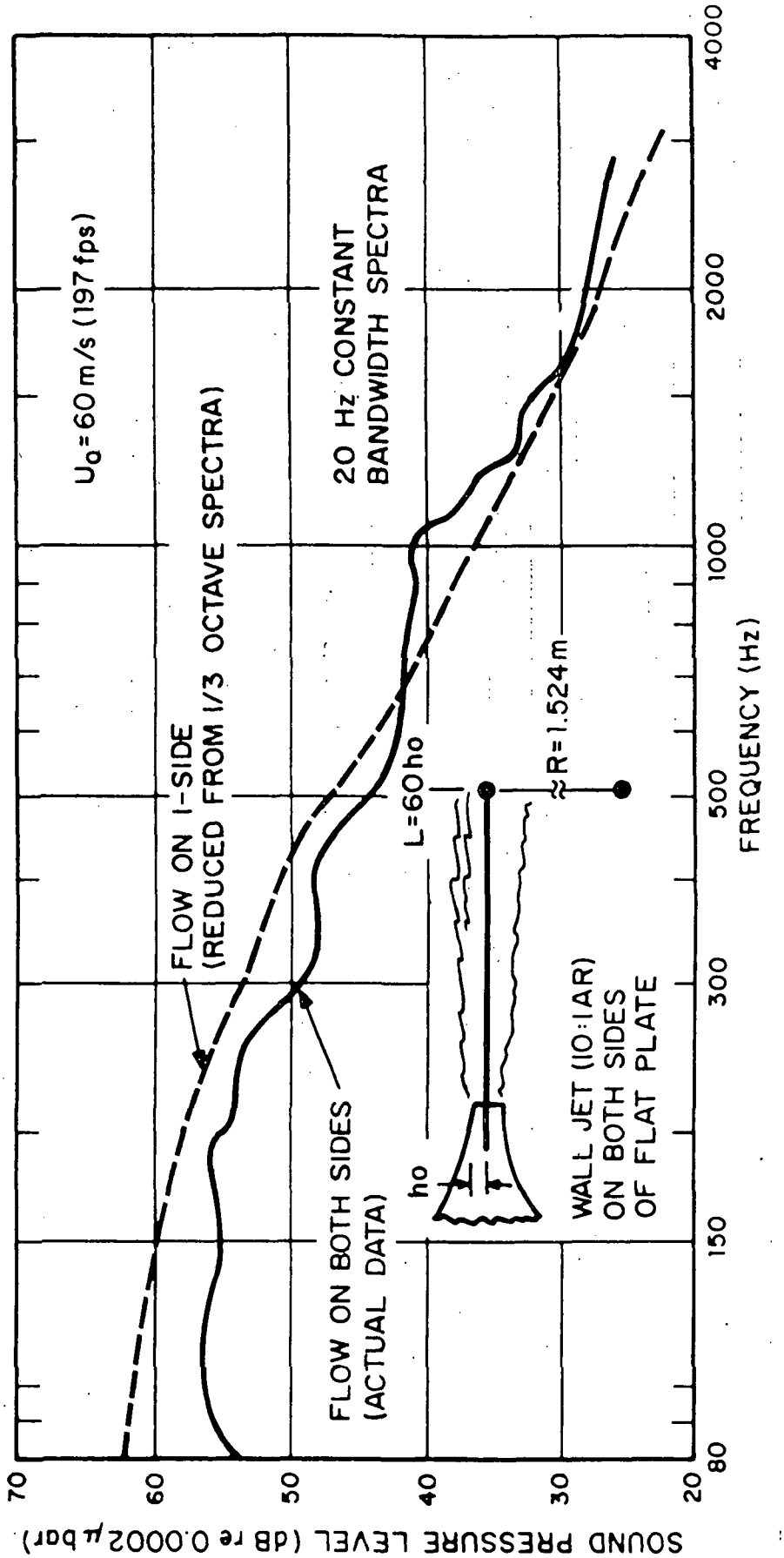

FIG. 23. COMPARISON OF SOUND PRESSURE SPECTRA RADIATED FROM WALL JET FLOW ON ONE AND BOTH SIDES OF A TRAILING EDGE.

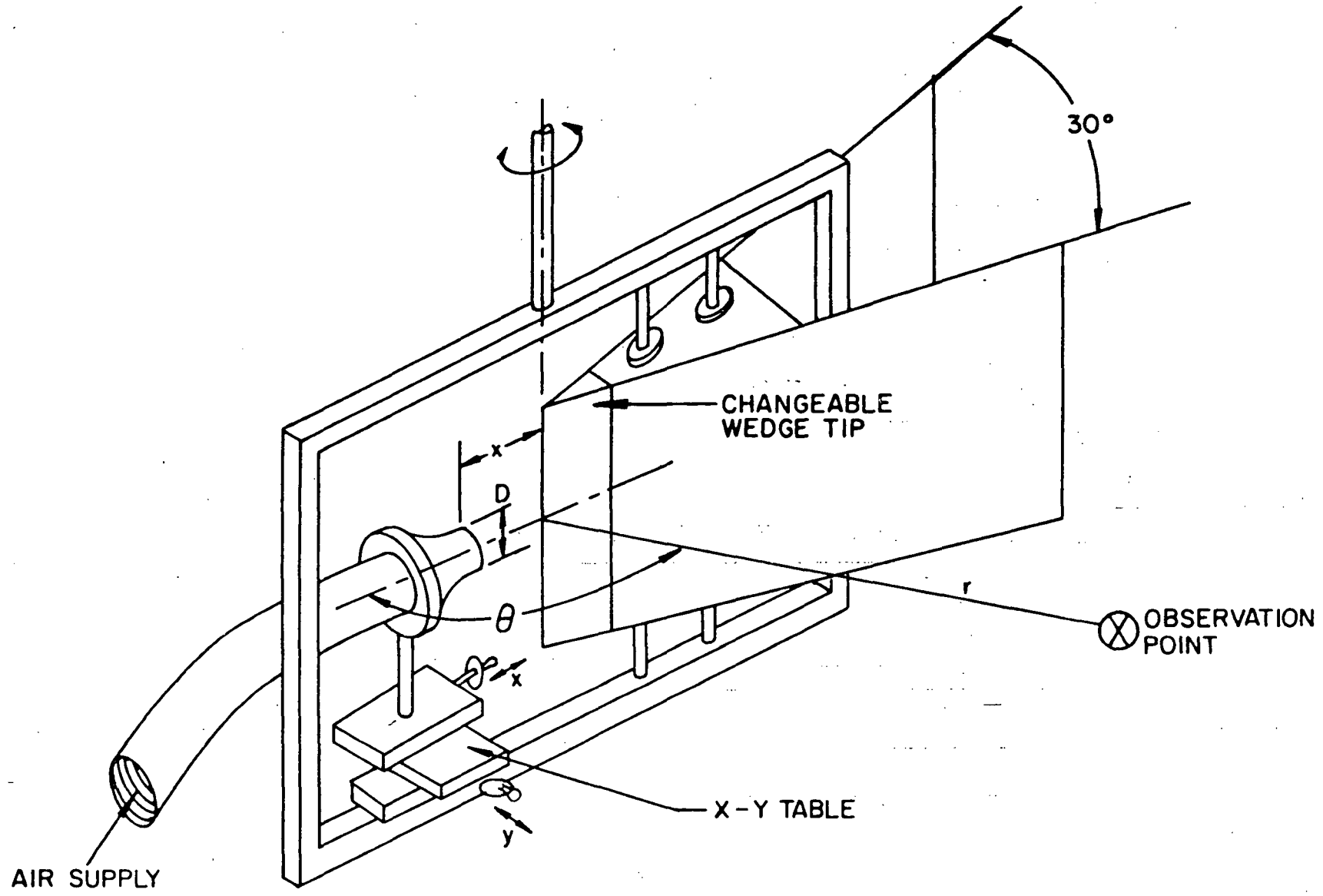

FIG. 24. EXPERIMENTAL ARRANGEMENT AND COORDINATE SYSTEM FOR LEADING EDGE NOISE STUDY.

a free jet (diameter 1.27 cm) blowing on a "semi-infinite" wedge (30° wedge angle). The jet position relative to the wedge could be varied using an x-y table. The tip of the wedge was instrumented with surface pressure sensors, and could also be replaced with tips of varying leading edge radius, and of other materials. All measurements were conducted in an anechoic room.

4.2.1 Velocity dependence of leading edge radiated sound

The effect of mean velocity on the spectrum level of leading edge noise was examined. Typical spectra are shown in Fig. 25. The velocity range extends to about $M_o = 0.8$, which could produce some deviations from the low Mach number M^6 velocity law derived in Sec. 2.

The data are then scaled to the highest velocity (262 m/s) using a U_o^6 law, with frequencies shifted linearly with velocity. The result is shown in Fig. 26. It is evident that below the spectral peak, an M^6 law is applicable, but above the spectral peak, some deviation toward a lower power occurs. In Sec. 5, the effect of the Mach number correction will be computed, and it will be shown that the velocity scaling laws predicted in Sec. 2 account for the differences at high frequencies shown in Fig. 26.

4.2.2 Directivity of leading edge source

Figure 27 presents spectra taken at various azimuths in a plane normal to the jet centerline and the wedge-surface. The spectra are seen to increase quite uniformly going toward the surface until the microphone is just off the surface. The increase beyond $\theta = 90°$ provides support for the cardiod-shaped directivity pattern expected for an edge dipole. At about $\theta = 120°$ and above, the high frequency levels decrease below those expected from a simple directivity pattern. This dropping off is believed to be due to refraction of the high frequency - originally directed along the surface - by the shear flow which attached to the wedge. The low frequency peak at 150° in Fig. 27 is believed to be due to flow impingement on the microphone.

The directivity can be visualized more clearly by replotting selected bands on polar plots as is done in Fig. 28 (a-c). The cardioid shape is evident in all bands. In the high frequency bands ($fD/U_o = 1.5$), a typical flow-refracted directivity shape is evident near the wedge surface.

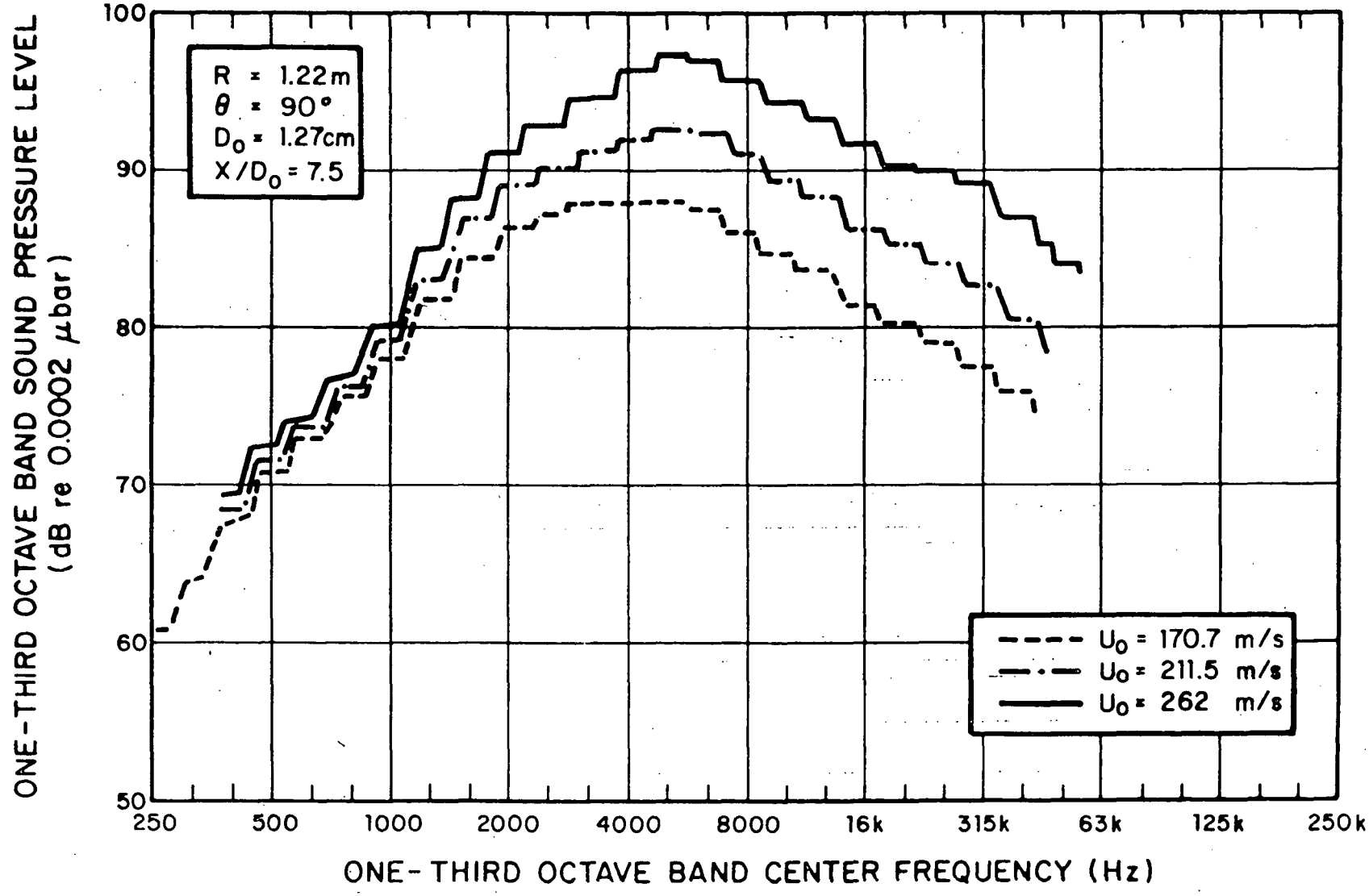

FIG. 25. LEADING EDGE SPECTRA FOR VARIOUS VELOCITIES.

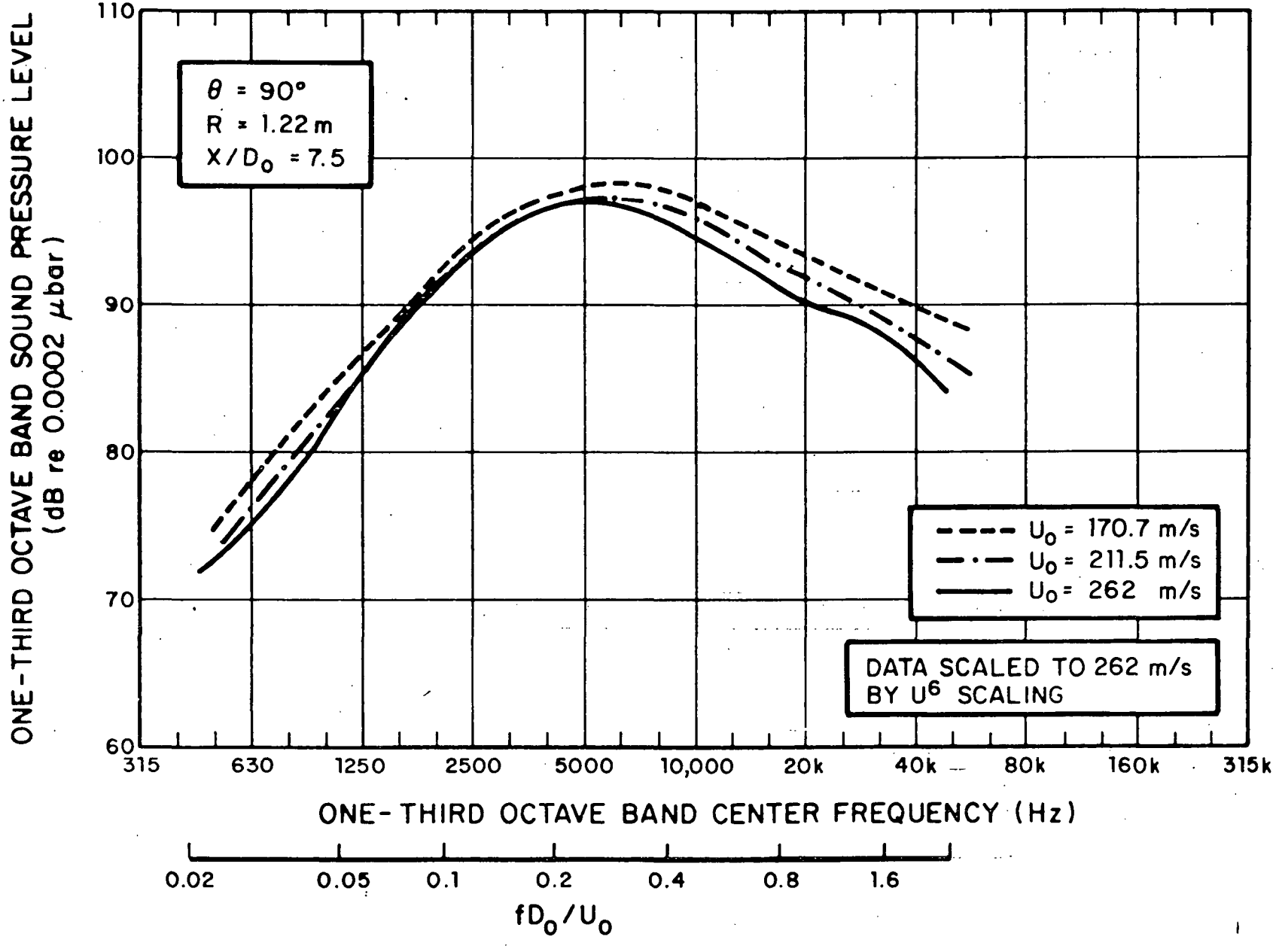

FIG. 26. LEADING EDGE SPECTRA SCALED BY U_0^6 to U_0 = 262 m/s.

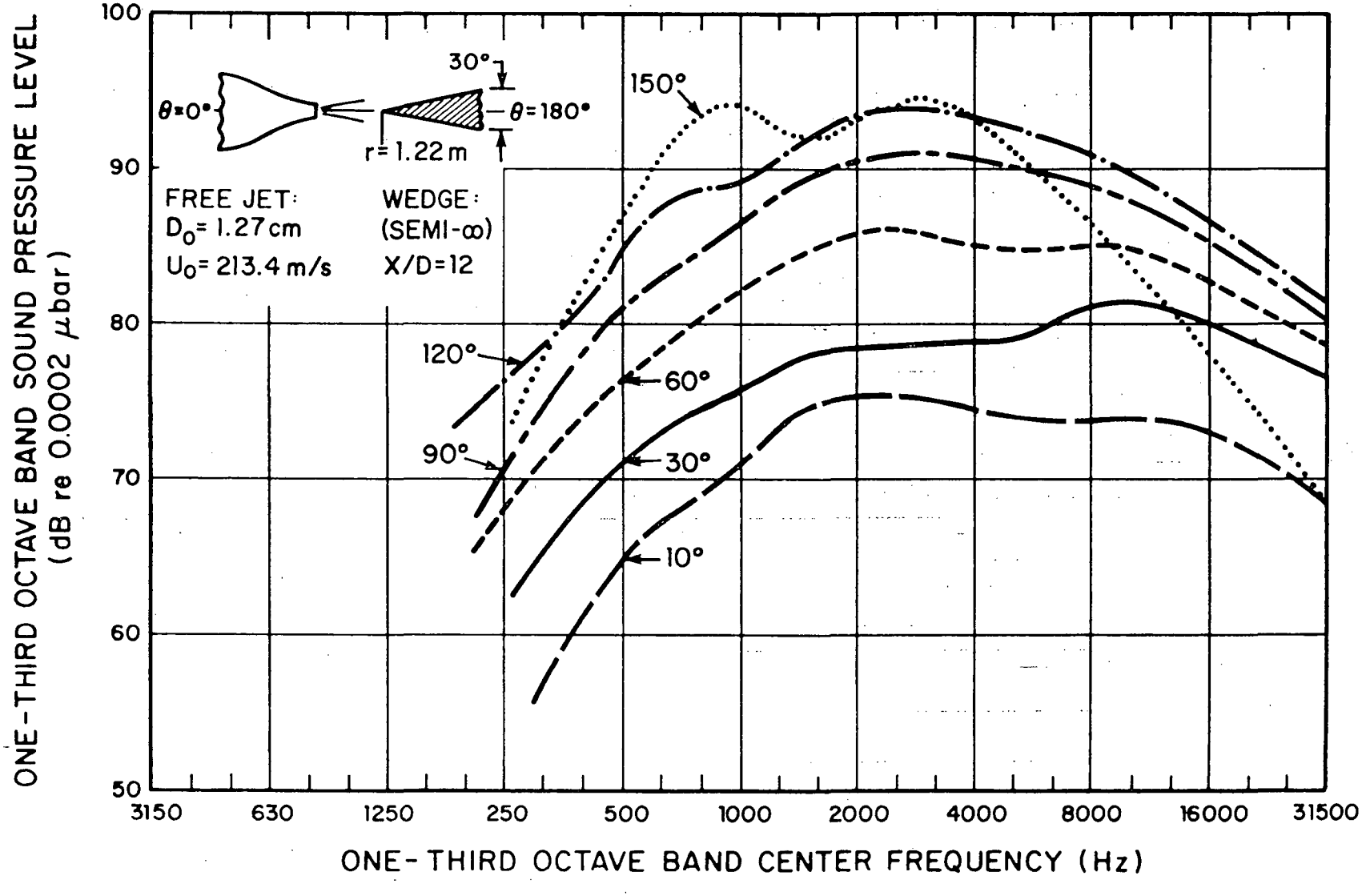

FIG. 27. SURVEY OF LEADING EDGE SPECTRA AT VARIOUS AZIMUTHS IN PLANE NORMAL TO JET CENTERLINE AND WEDGE SURFACE.

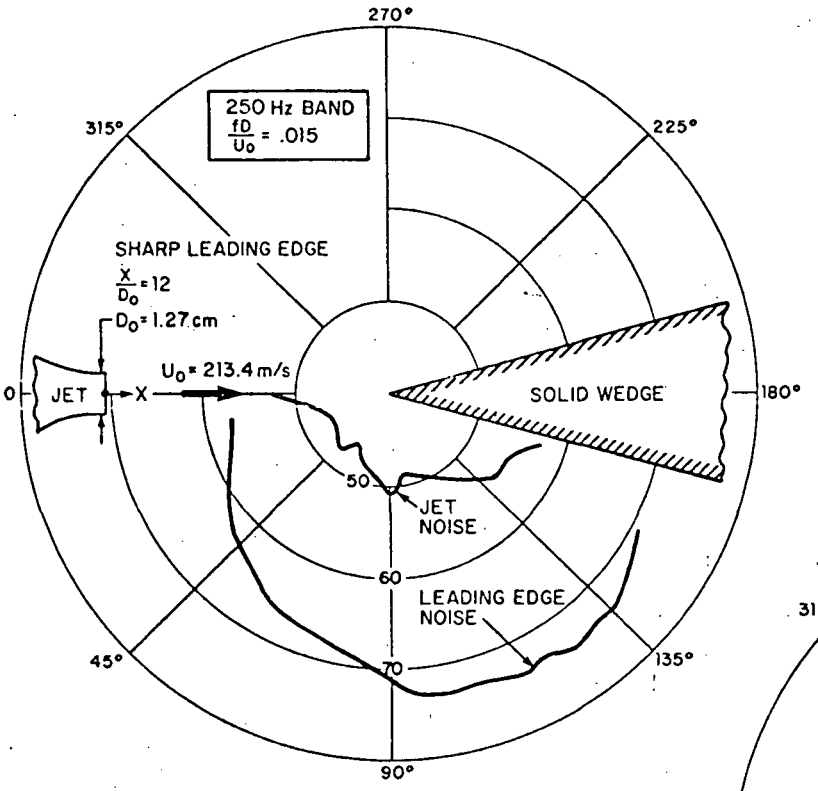

FIG. 28a. LEADING EDGE DIRECTIVITY (fD/U_o = .015).

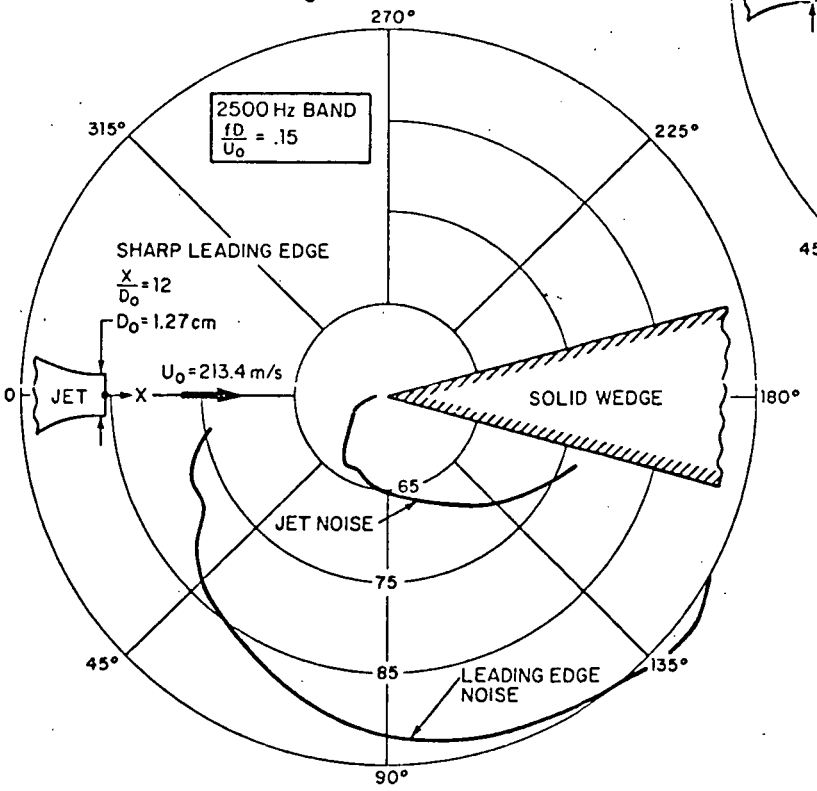

FIG. 28b. LEADING EDGE DIRECTIVITY (fD/U_o = 0.15).

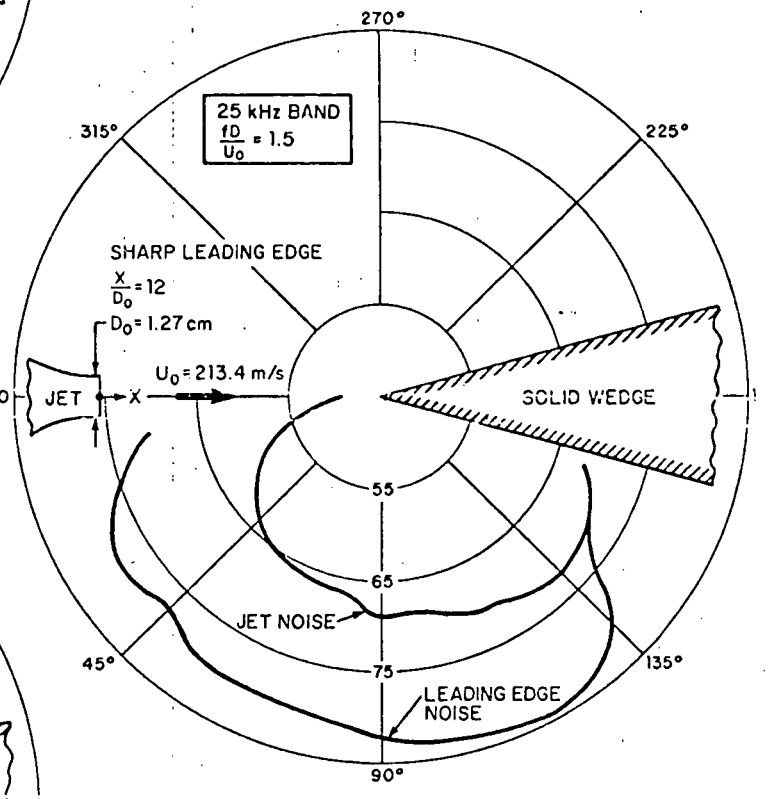

FIG. 28c. LEADING EDGE DIRECTIVITY (fD/U_o = 1.5).

Another set of directivity measurements was made on the same apparatus using a flat plate instead of the wedge. The purpose of these measurements was to verify the entire $\sin^2\theta \cos^2\psi/2$ pattern which is predicted by the edge dipole model. The results shown in Fig. 29 (a-c) strongly support the model, as can be seen by comparing with Fig. 6.

The directivity measurements of the leading edge source thus provide evidence that the edge dipole is an appropriate model for turbulent flow impingement on a leading edge.

4.2.3 Effect of distance of edge from nozzle exit on radiated noise

The effect of distance between a jet exit and leading edge of a flap, or other surface, is a case of practical interest. The experimental setup discussed above readily allowed a survey of this effect. The results are shown in Fig. 30, and indicate an increasing level and decreasing peak frequency. As the edge is moved away from the jet with the levels peaking at $x/D = 7.5$, which is slightly downstream of the end of the potential core. This trend reflects the essentially constant maximum velocity over the range $x/D = 0$ to $x/D \approx 6$ and the axially increasing wetted area of turbulence and the increasing scale of turbulence with increased downstream distance. The constant velocity and increasing length scales with distances up to $x/D \approx 6$ account for the decreasing peak frequency while the increasing span exposed to turbulence, and the constant peak velocity account for the increased levels.

Beyond $x/D = 6$, the peak velocity falls off with distance while the length scales continue to increase, as does the width of the jet. The scale effects and the reduced mean velocity account for the lowering of the peak frequency, while the reduced velocity effect apparently dominates the increasing wetted span thus accounting for the reduced levels.

4.2.4 Leading edge radius

The leading edge of the wedge was changed to allow examination of the effect of increasing radius on sound generation. Radii up to 0.635 cm (.25 in) were examined. The results, shown in Fig. 31, indicate a significant effect when the edge radius becomes on the order of typical turbulence length scales. No diagnosis of the effect was made. However, in view of the dipole model, some effect on the rate of acceleration of the turbulence encountering the edge, or in the cross covariance from upper to lower surface would be predicted *a posteriori*.

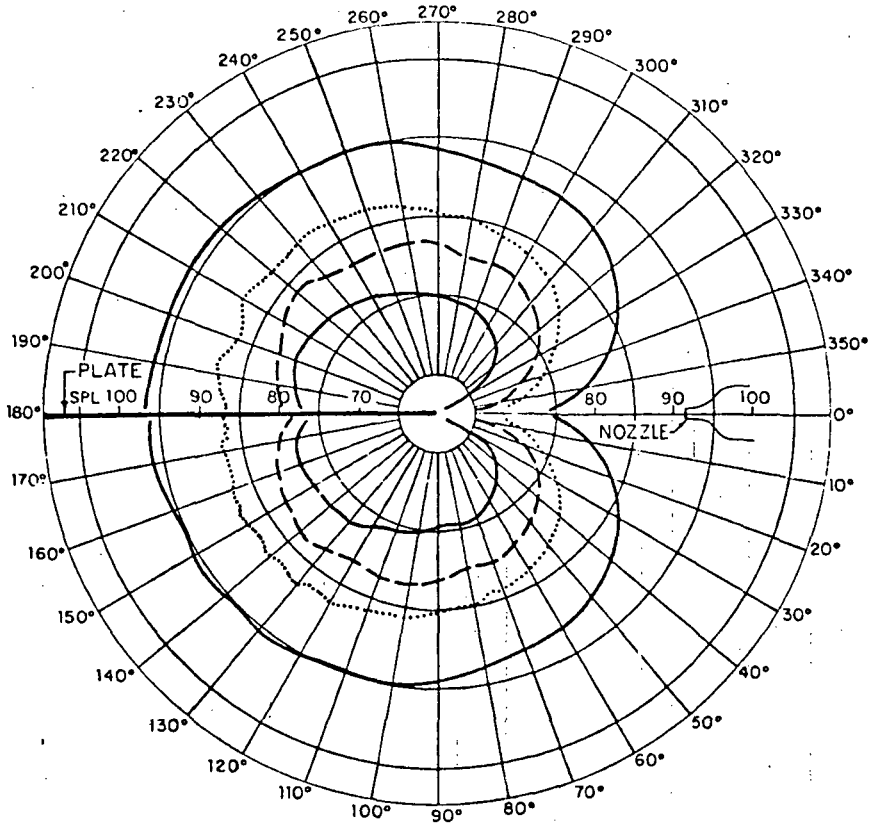

FIG. 29a. MEASURED DIRECTIVITY OF LEADING EDGE SOURCE IN PLANE NORMAL TO SURFACE PASSING THROUGH JET AXIS.

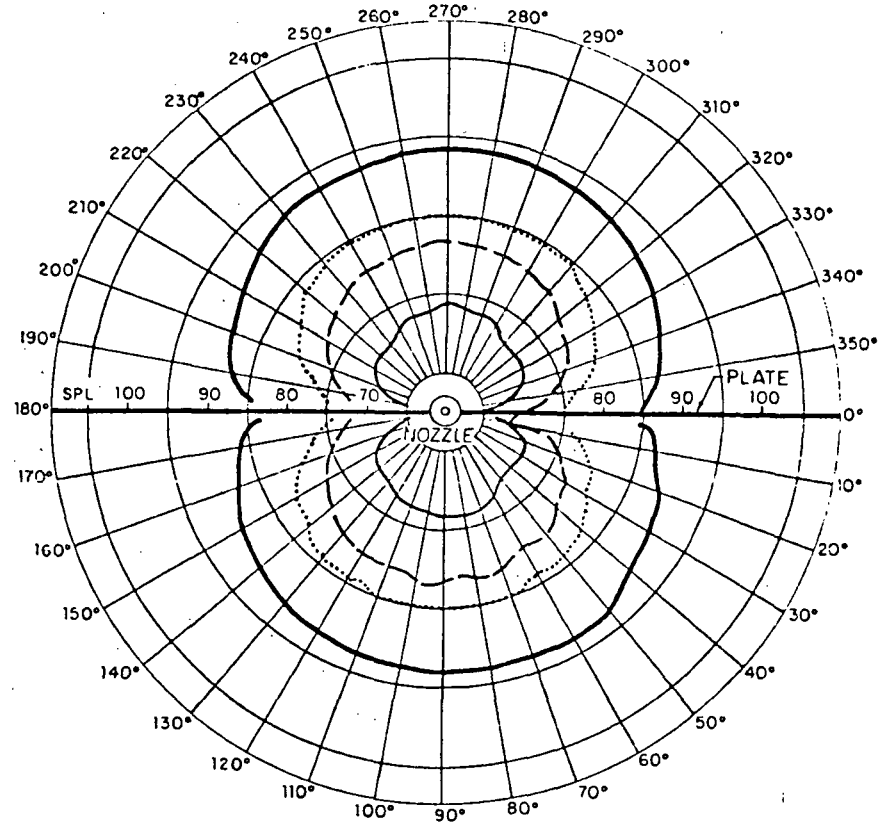

FIG. 29b. MEASURED DIRECTIVITY OF LEADING EDGE SOURCE IN PLANE NORMAL TO EDGE AND JET AXIS.

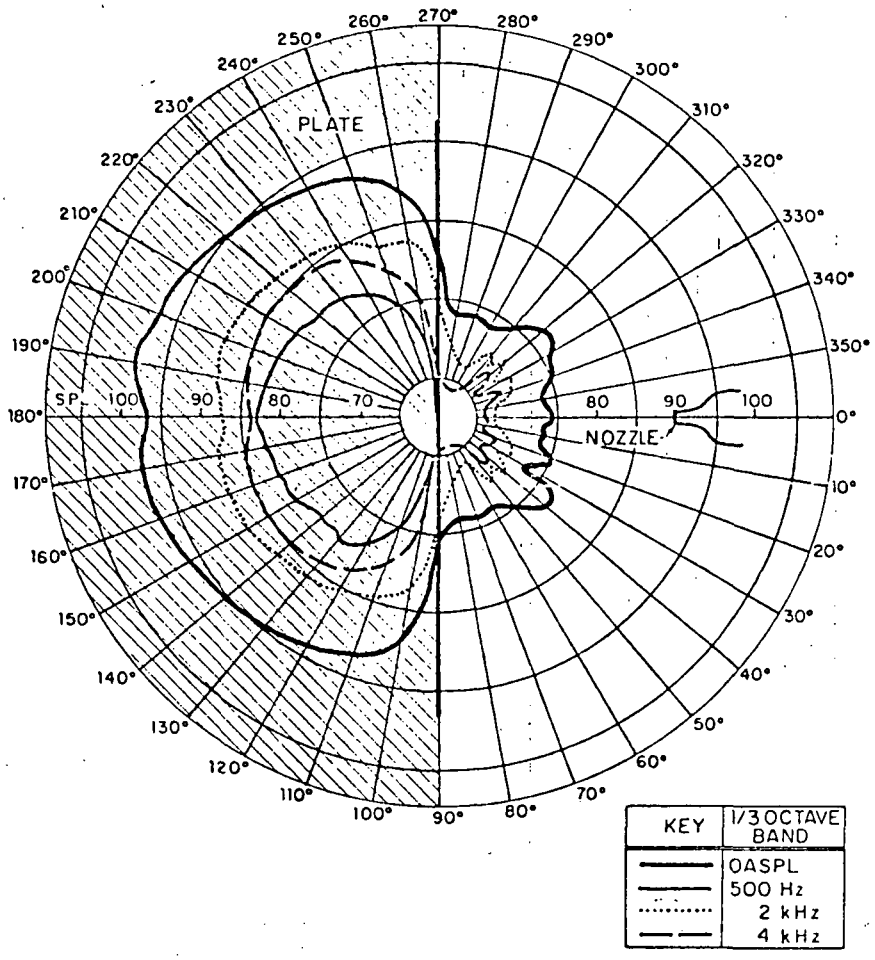

FIG. 29c. MEASURED DIRECTIVITY IN PLANE OF SURFACE.

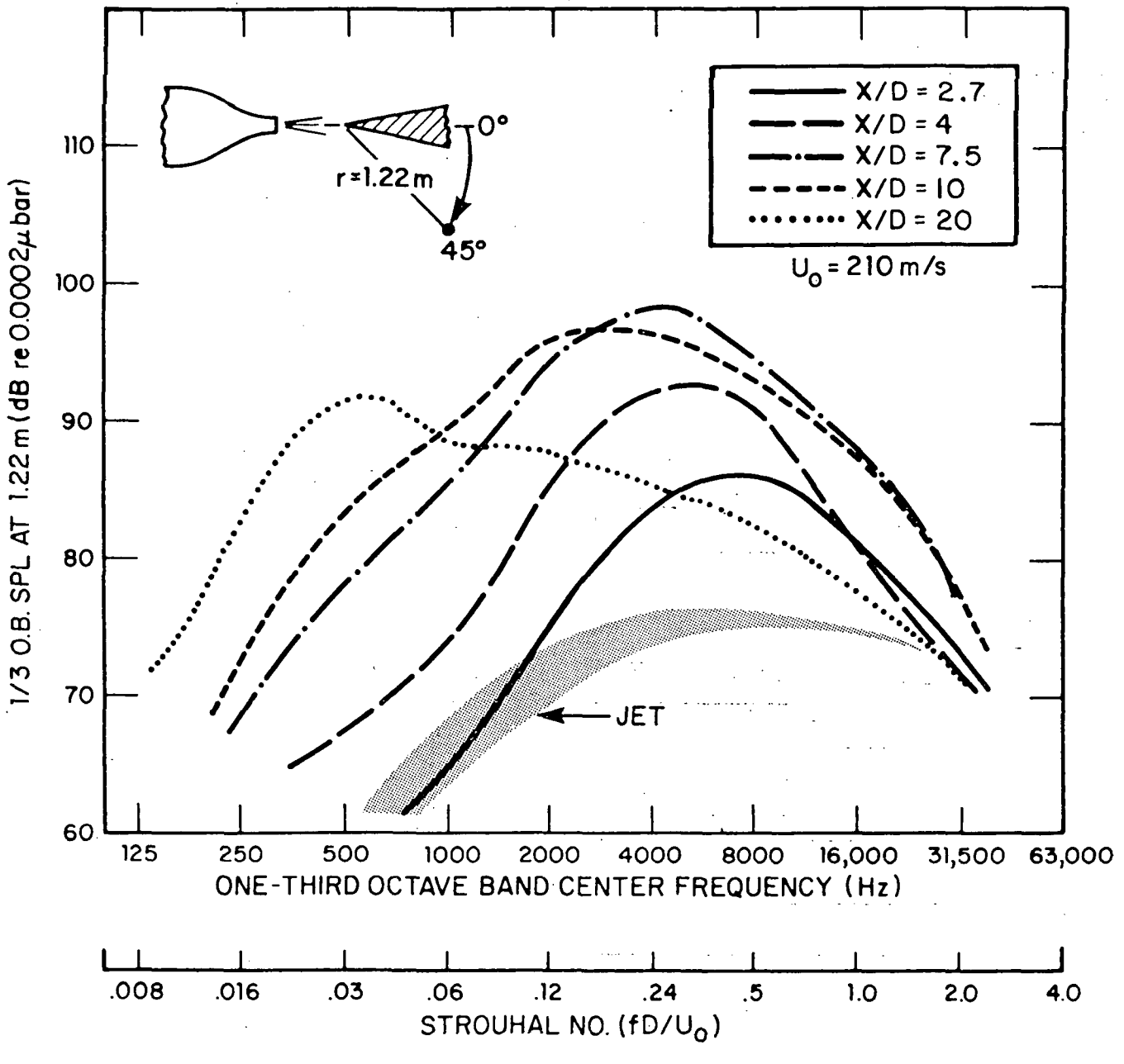

FIG. 30. EFFECT OF EDGE DISTANCE FROM ORIGIN OF A FREE JET ON RADIATED SOUND.

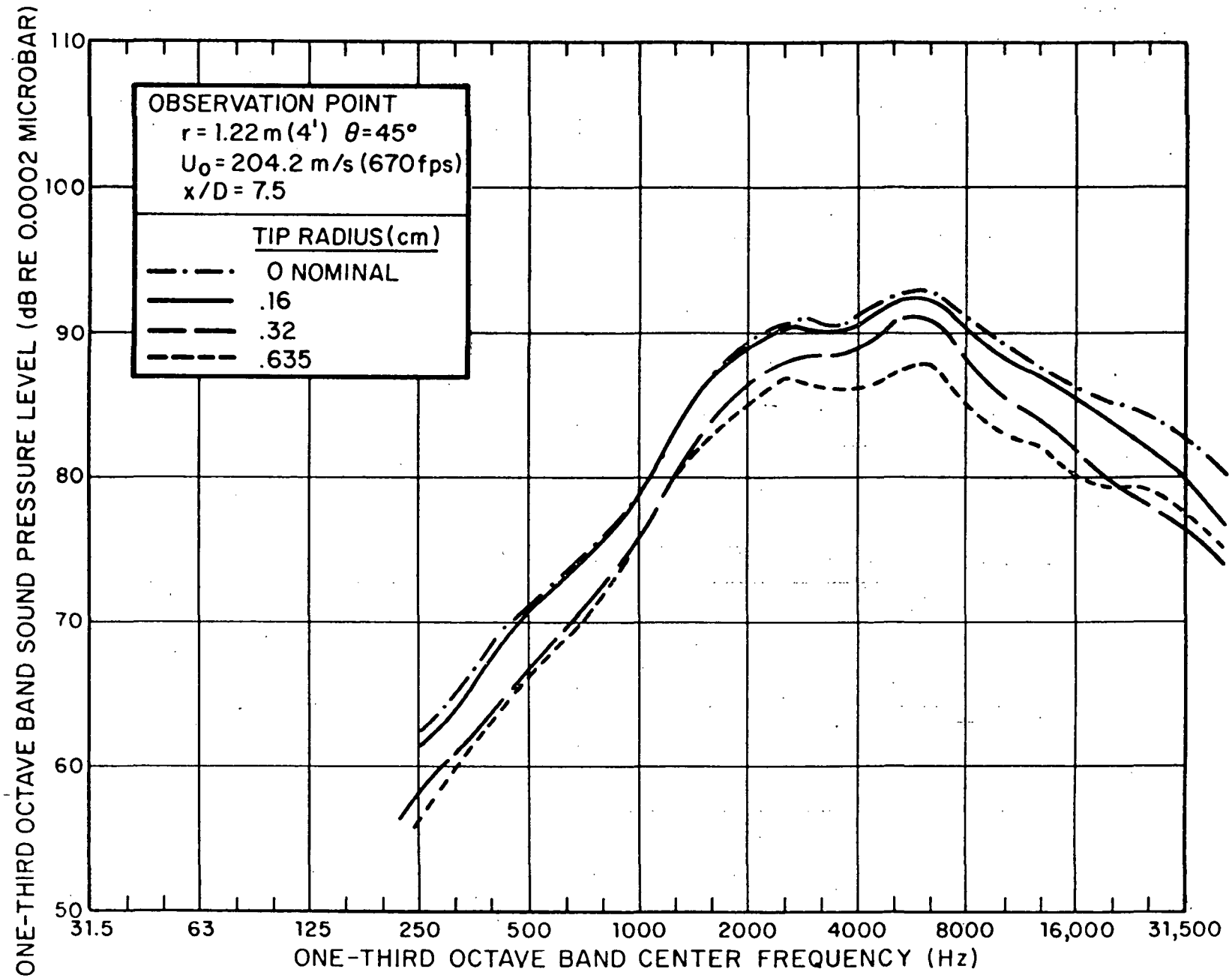

FIG. 31. EFFECT OF LEADING EDGE RADIUS ON SOUND GENERATION.

SECTION 5

COMPARISON OF EXPERIMENTAL DATA WITH PREDICTION OF EDGE DIPOLE MODEL

The theoretical model developed in Sec. 2 for edge dipole radiation requires knowledge of a number of physical parameters having to do with the unsteady flow field in order to arrive at a detailed calculation of the radiated sound spectra.

These parameters (given, for example, in Eqs. 2.14 and 2.15) are the convection Mach number M_c, length scales ℓ_x, ℓ_y, ℓ_z, axial separation between eddies (γ), spanwise separation between eddies (ξ), and the intensity of the unsteady flow as represented by the surface pressure fluctuations ($\overline{p/q_0}$). All these parameters vary with frequency for a given flow speed, and all may be influenced by Mach number and Reynolds number.

In view of the recent development of the model which requires all these parameters, it is not surprising that available experimental data typically do not provide both these flow field parameters and radiated sound spectra at the same time. Fortunately, there are at least two experiments in which sufficient detailed specification of the flow field was made, which will be used for comparison of predicted sound radiation with measured sound from the same configuration. Neither case is an idealized flow field or geometry, but both are of practical significance, and both involve convective Mach numbers in the range where the deviation from the low Mach number limit might be expected.

5.1 Trailing Edge Noise

The configuration chosen for a calculation of trailing edge noise is a large scale upper surface blown flap which was tested at NASA Lewis Research Center (Heidelberg, *et al.*, 1975; Hayden, Galaitsis and Alakel, 1975). The tests of Hayden, *et al.*, were designed to diagnose the noise sources on the flap and included far field sound measurements, surface pressure spectrum measurements ($\overline{p/q_0}$), surface-to-far field correlations, and limited length scale measurements of the surface pressure field.

The geometry of the test apparatus is shown in Figs. 32 and 33. The flap was set at a nominal deflection angle of 60° and had a constant radius of curvature of 1.94m (76.5 inches).

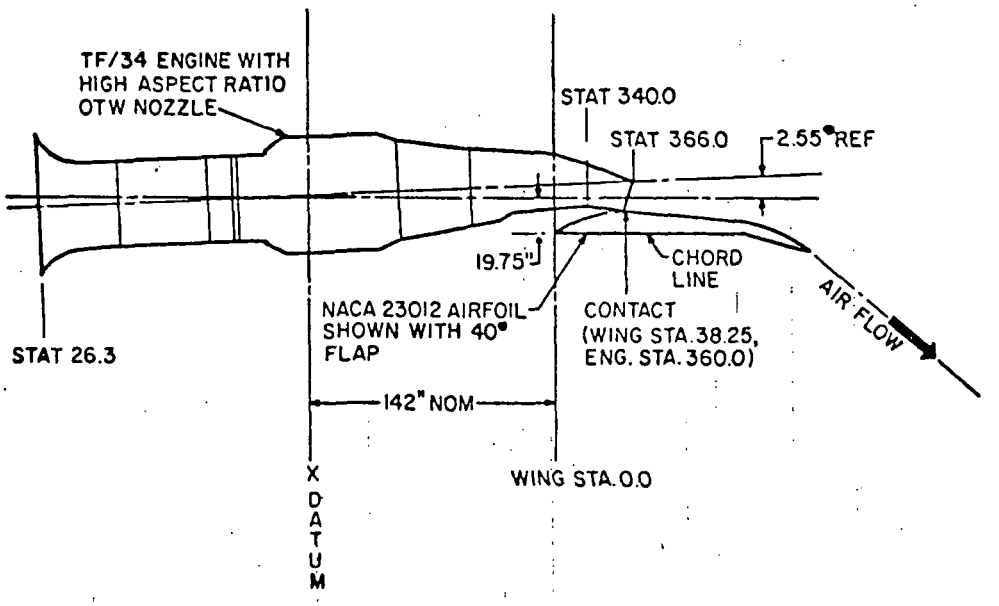

FIG. 32. SECTIONAL VIEW OF TF-34 TEST BED.

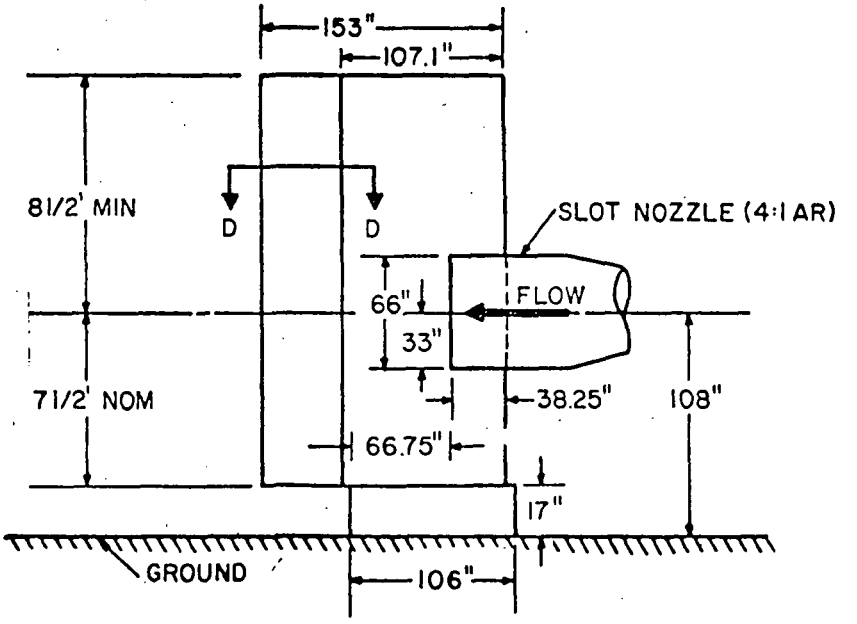

FIG. 33. ELEVATION OF WING SEGMENT LOOKING DOWN ON WING SURFACE.

Since no ℓ_z measurements were made in the actual experiment, it is assumed that $\ell_z \approx \ell_y$. The calculation of the far field levels is made from Eq. 2.15, which is modified by the above assumption to be

$$\frac{\overline{p_a^2}(r,\theta,\psi)}{\overline{p_s^2}} = \left(\frac{W}{\xi \ell_y}\right)\left(\frac{U_c}{U_o}\right)^4 \left(\frac{U_c}{\gamma \ell_x}\right)^2 \left(\overline{\ell_x \ell_y^2}\right)^{4/3} \frac{\pi \sin^2\theta}{2r^2 c_o^2} \qquad (5.1)$$

neglecting the "large surface" effects on directivity for now.

Alternatively,

$$\overline{p_a^2}(r,\theta,\psi) = (\overline{p_s^2}) \; f^2 \left(\frac{W}{\xi \ell_y}\right) \left(\frac{U_c}{U_o}\right)^4 \left(\overline{\ell_x \ell_y^2}\right)^{4/3} \left[\frac{\pi \sin^2\theta}{2r^2 c_o^2}\right] \qquad (5.2)$$

where $U_c/\gamma\ell_x$ has been replaced by frequency, f. The last term is equal to 3.1×10^{-10} for the particular case which is computed. A position of $\psi = 60°$ relative to the trailing edge was chosen; and $\theta = 90°$, and $r = 30.5$m (100 ft). The far field measurements were made on a rigid ground plane and were converted to an equivalent free field condition. Figure 34 gives the flow field parameters derived from the length scale measurements in various frequency bands. Note that ℓ_x and ℓ_y decrease with frequency, but not in a simple monotonic fashion as is often assumed. It is also surprising that for the USB flow field, the spanwise length scale ℓ_y is actually larger than ℓ_x in certain frequency bands — a trend that may be related to the effects of the convex surface. The relative convection speed was assumed to be 0.7 at all frequencies, since only a single broadband measurement was taken. Note in Fig. 34 that two flow field zones are identified on the flap — Zone I which is under the outer shear layers, and Zone II which is under the attached flow along the centerline of the flap. The length scale data given in Fig. 34 is from measurements in Zone II. However, some variations in turbulence parameters, especially the intensity spectrum $(\overline{p/q_0})$ and convection speed U_c/U_o would be expected in Zone I, due to the highly three-dimensional nature of the flow field.

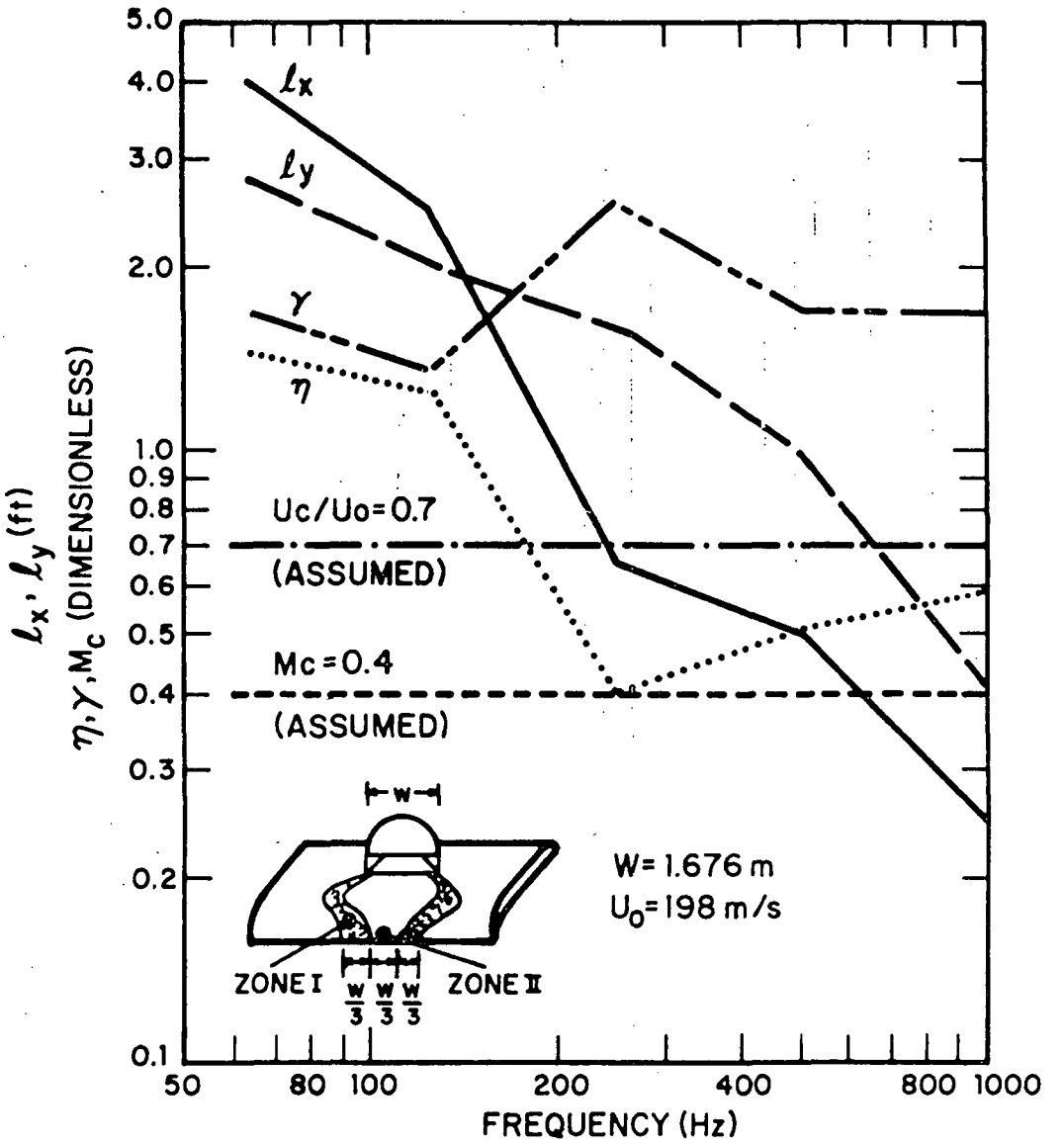

FIG. 34. FLOW FIELD PARAMETERS USED IN USB TRAILING EDGE NOISE CALCULATION.

Figure 35 shows measured surface pressure spectra in Zones I and II, and the measured far field spectra, as well as predicted far field spectra using Eq. (5.2) and the parameters given in Figs. 34 and 35. The spectra were predicted for each zone and added incoherently to arrive at the total far field spectrum. The curve labeled "Predicted SPL from Zone I" in Fig. 35 is that predicted from one side shear layer increased by 3 dB at all frequencies to account for the contribution from the other shear layer.

The agreement between prediction and measurement is good at high frequencies. However, the low frequency peak is over-predicted. A possible explanation for the over-prediction at low frequencies may be that the actual convection velocity in Zone II is lower than the assumed value of 0.7 U_o in the low frequency bands. Also, the directivity effects of the large surface are not taken into account in the analytical model.

5.2 Leading Edge

The previously-described leading edge noise apparatus (Sec. 4) provided some surface pressure and far field noise data, which was supplemented by flow parameter data measured by investigators of free jet turbulence structure. The combination of these data allows a calculation of noise from an isolated leading edge noise source which uses the model developed in Sec. 2, with no change in directivity or velocity exponent from the point model.

5.2.1 Leading edge of a wedge in a free jet at $x/D_o = 5$

The location of the leading edge at $x/D_o = 5$ was chosen for a calculation since data was available from the literature on length scales in the axial and radial direction in various frequency (Strouhal number) bands, and convection speed data was also taken in different bands, for a round subsonic jet in the same Reynolds number range (Scharton and White, 1972).

The measured flow parameters at $x/D_o = 5$ for an exit velocity of 210 m/s are shown in Fig. 36. The axial length scale is seen to decrease nearly monotonically with frequency, while the radial length scale, ℓ_y, is a complicated function of frequency. The convection velocity has an asymptote of $U_c/U_o \approx 0.6$ at low frequencies (Strouhal numbers <.1) and increases slowly to an upper bound of $U_c/U_o \approx 1$ at Strouhal numbers above 1.0. Referring to the equations developed for predicting dipole edge noise (such

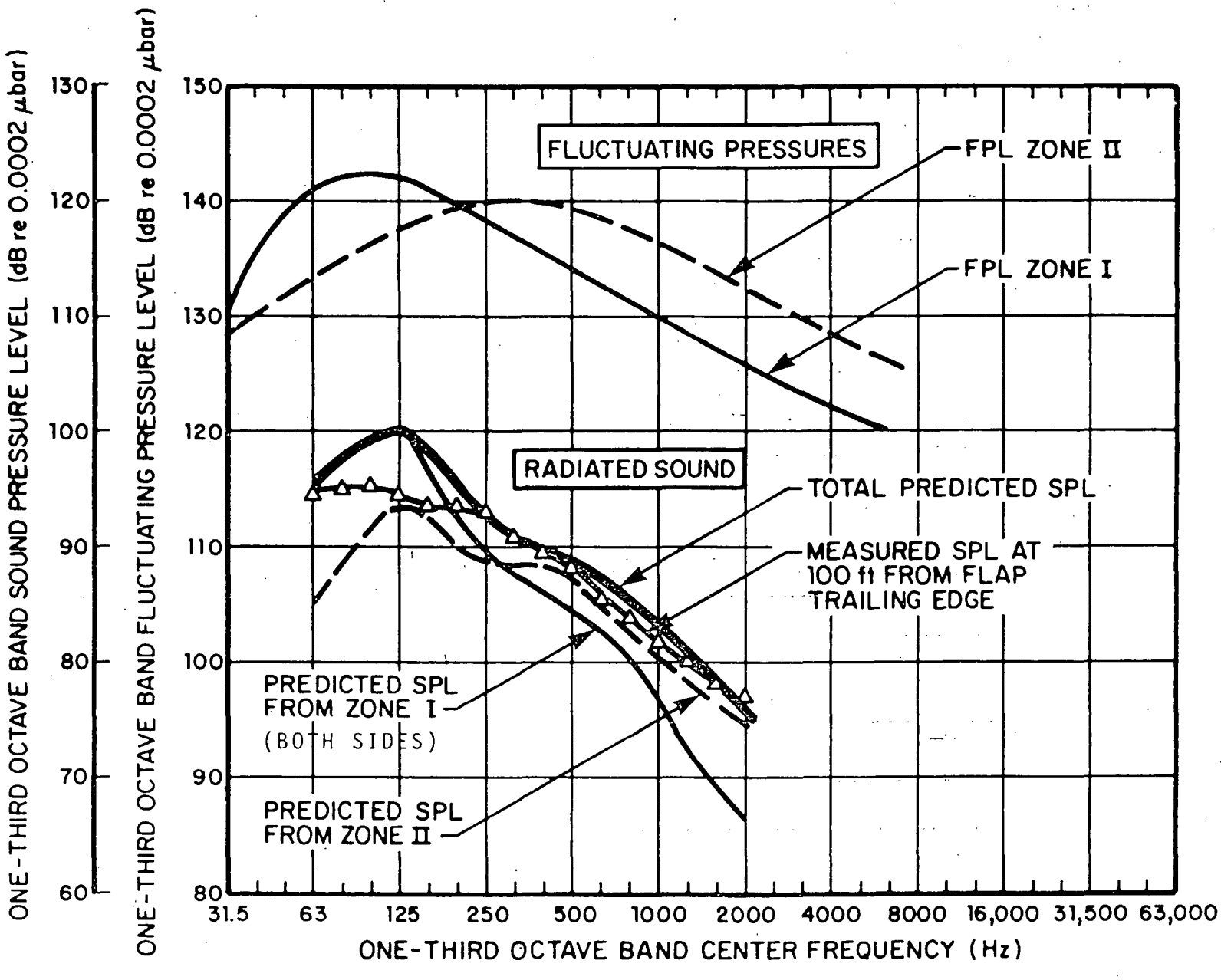

FIG. 35. SURFACE AND FAR FIELD PRESSURE LEVELS: MEASURED AND PREDICTED.

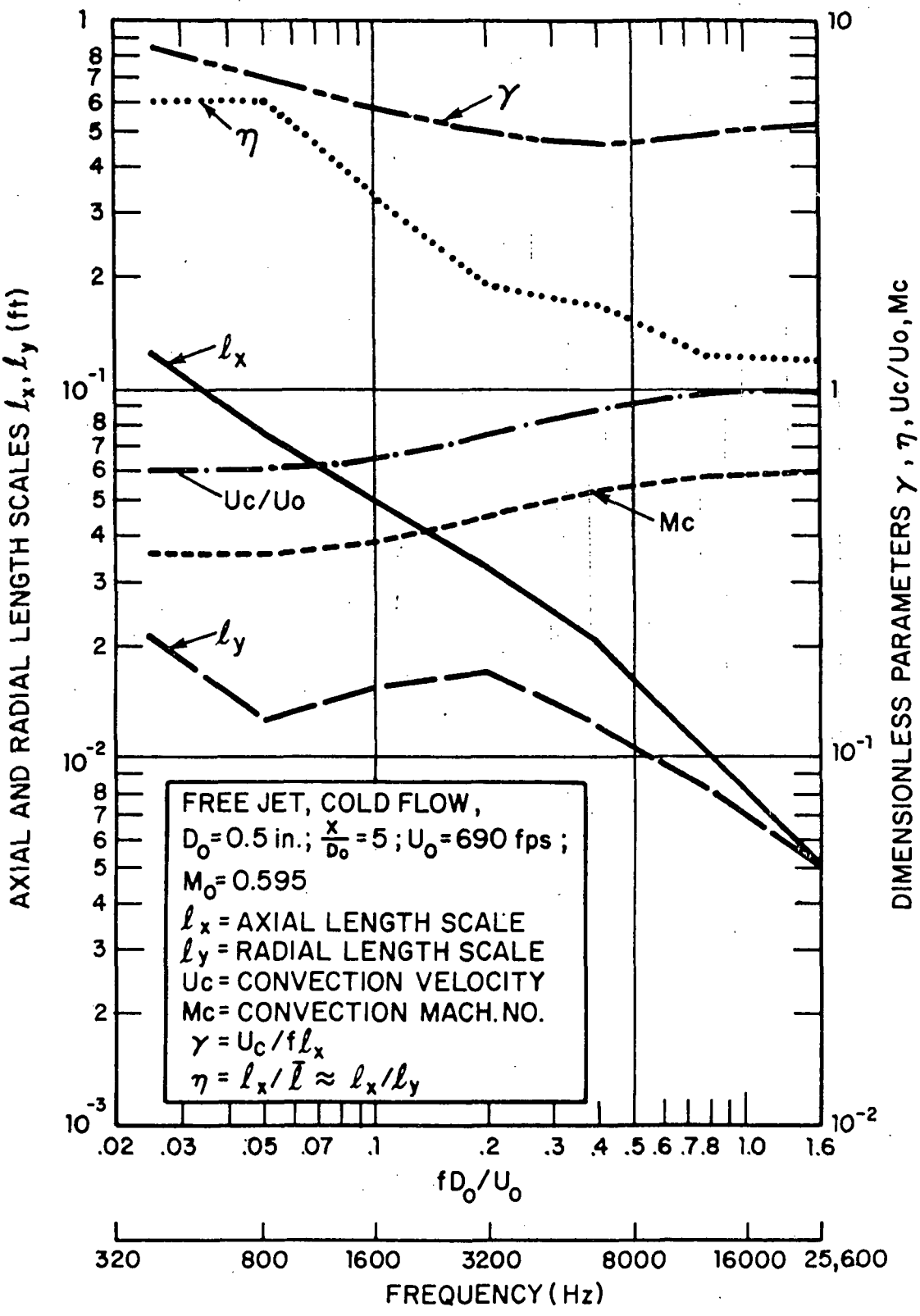

FIG. 36. FLOW FIELD PARAMETERS FOR ROUND SUBSONIC JET AT x/D_o = 5.

as Eqs. (2.14) (2.15), (5.1) and (5.2), it is evident that this variation in convective Mach number will have a significant effect on the spectrum level. It is also evident that the convective Mach number is high enough in this particular case to possibly cause a variation from the M_c^6 law of sound pressure level (or power level) generated from the edge source. The $\gamma\eta$ product varies from about 50 at low Strouhal numbers to about 6 at high Strouhal numbers. Figure 36 shows the radiated SPL spectrum from the leading edge of the wedge, and the measured surface pressure spectrum on the leading edge of the wedge when $x/D_o = 5$.

The calculation procedure chosen is the computation of the ratio between the spectrum of far field sound pressure $[\overline{p^2(r,\theta)}]$ and surface pressure $(\overline{p_s^2})$, which is also given in a logarithmic convention as "SPL - FPL." Equation (5.1) is used in this computation, and is, of course, fully equivalent to Eqs. (5.2) and (2.11). The measured parameters shown in Fig. 36 are used in Eq. (5.1) in various frequency bands; the effective wetted span, W, was taken to be D_o, the nozzle exit diameter, and the normalized spanwise separation between eddies of scale ℓ_y, ξ, was taken to be 1.

The results are plotted in Fig. 37 for two cases: first, using the low Mach number limit (which is indeed represented by Eqs. (5.1) and (5.2), and secondly using the deviations from the low Mach number limit which are given by Eq. (2.11), and plotted in Figs. 4 and 5. The effect of the high M_c correction becomes significant above about 15 kHz ($fD_o/U_o \gtrsim .9$) for the particular case computed. When compared with the measured SPL - FPL, the shape of the predicted curve agrees well with that measured at all frequencies when the high Mach number correction is applied. The level of the predicted SPL - FPL is about 3 dB below the measurements at all frequencies. This discrepancy would be reduced is the assumed W were $W > D_o$ (e.g., if W were taken as 2D, the curves would be essentially in agreement).

The results of this calculation are highly encouraging in that the importance of using actual length scale parameters at all frequencies has been demonstrated, and the high M_c effect predicted by the dipole model of edge noise has been demonstrated for actual $\xi\eta$ values. The close agreement between prediction and measurement strongly supports the applicability and detail of the model developed in Sec. 2.

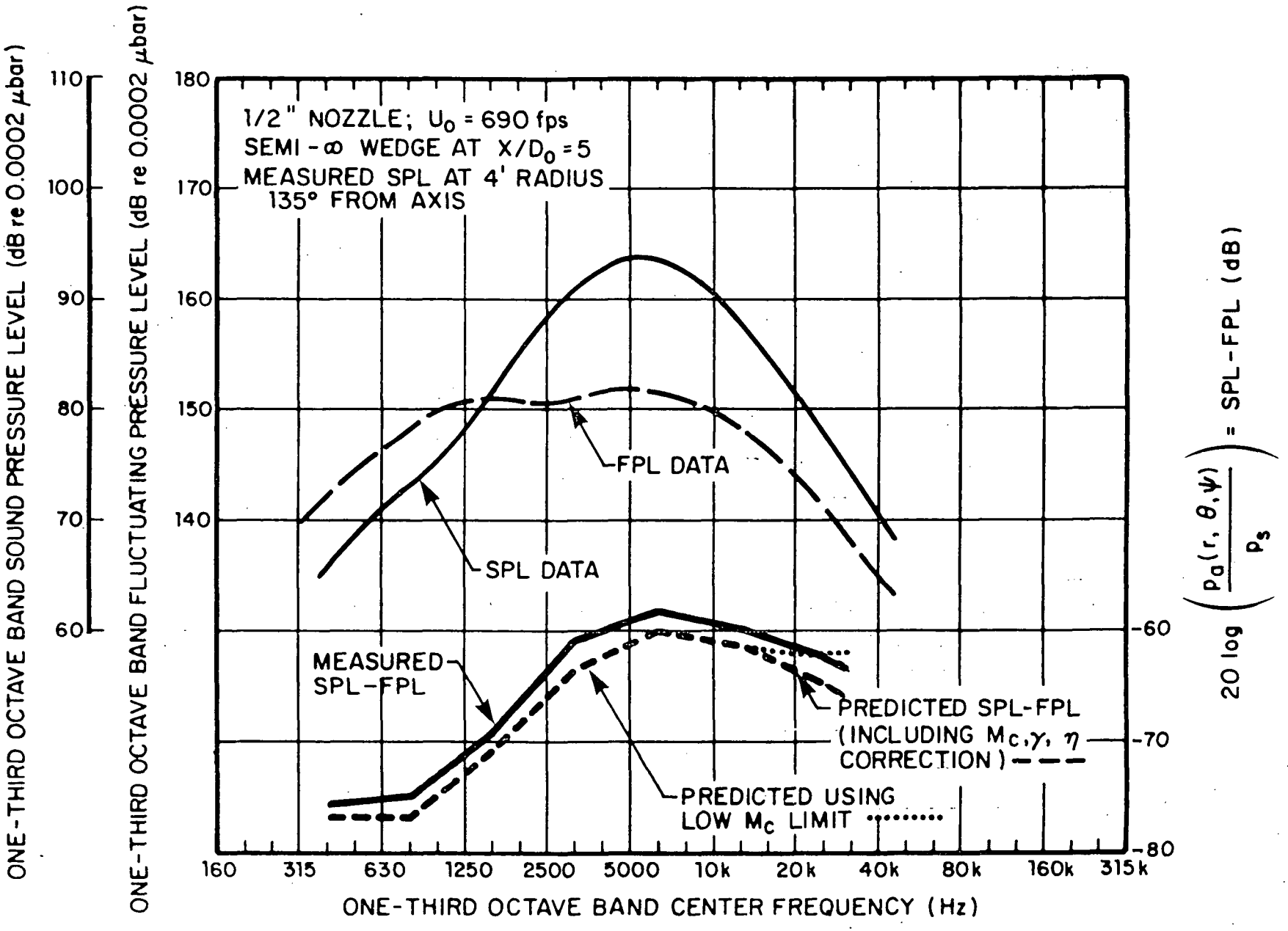

FIG. 37. MEASURED SPL AND FPL FROM WEDGE IN JET AT x/D_0 = 5, AND COMPARISON WITH PREDICTED SPL-FPL.

5.2.2 Leading edge of a wedge in a free jet at $x/D_o = 10$

As discussed in Sec. 4, the experiments performed on the leading edge of a semi-infinite wedge included a number of axial separations between the nozzle and leading edge. A calculation of the radiated sound at $x/D_o = 10$ is now performed using measured SPL and FPL spectra, but without the benefit of actual measured values of ℓ_x, ℓ_y, U_c/U_o in frequency bands at such an x/D position. These parameters were extrapolated from the detailed data taken at $x/D_o = 5$ by Scharton and White (1972) by (1) assuming that length scales increase linearly with distance from the end of the potential core (i.e., ℓ_x, ℓ_y at $x/D_o = 10$ are twice the values at $x/D_o = 5$ and γ, η are the same for both x/D positions), (2) using the maximum local velocity U_{Lmax} at $x/D_o = 10$ as $0.75\ U_o$, a commonly-measured value for round subsonic jets, (3) assuming that U_c/U_{Lmax} at $x/D_o = 10$, is similar to that at $x/D_o = 5$, and (4) using $W = 2D_o$ as the effective wetted span at $x/D_o = 10$ to reflect the radial growth of the jet at that distance.

The measured SPL and FPL spectra are shown in Fig. 38, along with the results of the calculation of SPL - FPL. The computed SPL - FPL agrees well with experimental data at low frequencies (up to the Strouhal peak), but is considerably lower than the measured values for the next two octaves. The two values converge at high Strouhal numbers, but perhaps artificially since the high M_c correction was not applied.

The discrepancy between prediction and measurement at high Strouhal numbers probably indicates that the extrapolation of turbulence and convection speed data as described above was too crude. However, the fact that the spectrum shape is predicted quite well is supportive of the model developed in Sec. 2.

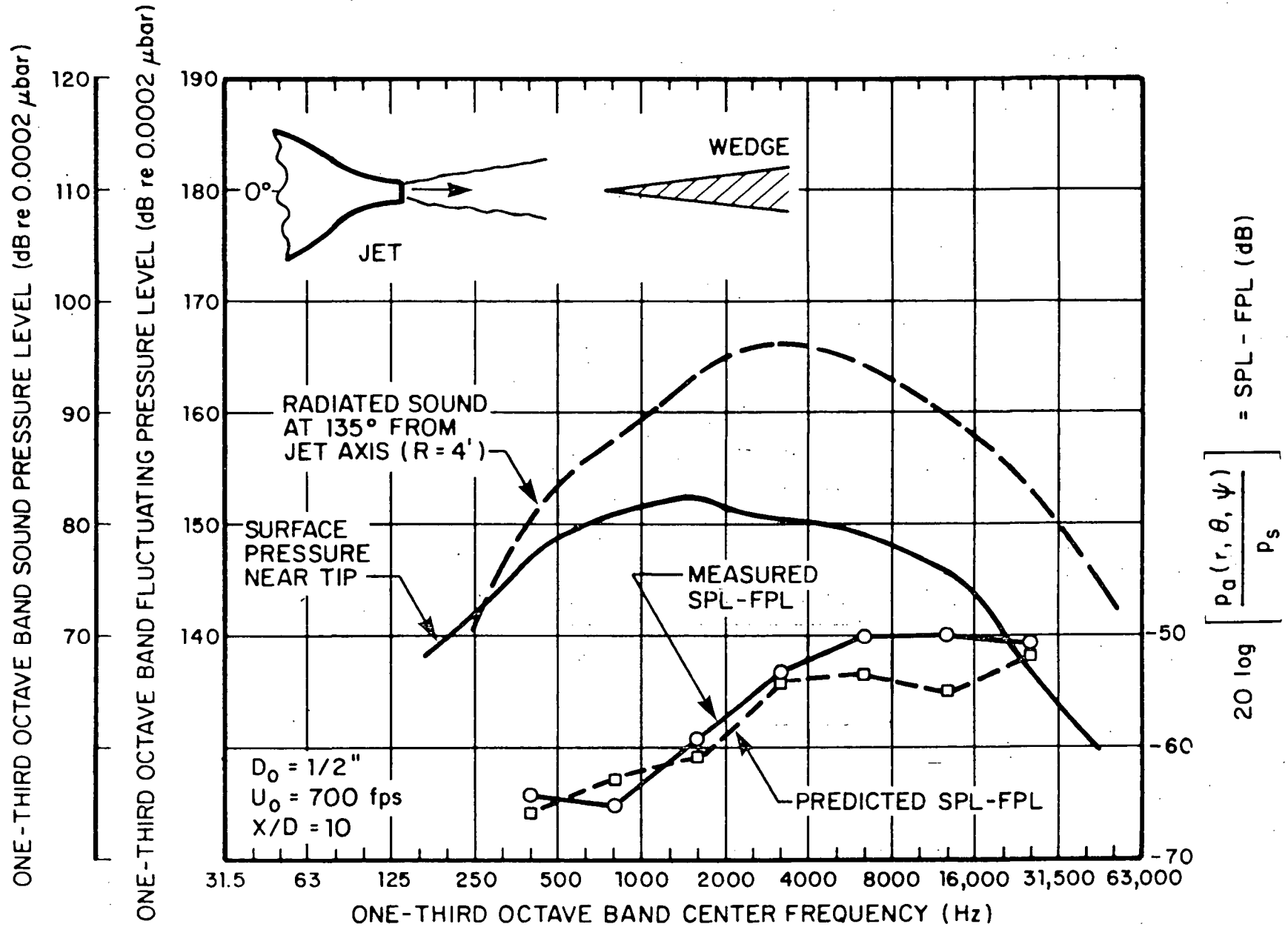

FIG. 38. MEASURED SPL AND FPL FROM WEDGE IN JET AT x/D = 10, AND COMPARISON WITH PREDICTED SPL-FPL.

SECTION 6

SUMMARY AND CONCLUSIONS

This study has dealt with identifying and characterizing factors which influence sound generation by, and radiation from, the edges of surfaces which are exposed to unsteady flow. Edges of such surfaces have been shown to cause both strictly acoustic effects (i.e., scattering of evanescent pressure fields from turbulent flow, as shown by Ffowcs-Williams and Hall (1970), Chase (1972), Goldstein (1974), and Chandiramani (1974), and diffraction of sound generated in the vicinity of the edge), and hydrodynamic effects in the form of generation of new hydrodynamic sources (turbulent eddies released from an unstable shear layer) in the immediate vicinity of the edge. The latter aspect was treated in detail in the development of an analytical model which describes the radiation of edge-generated sound in terms of detailed descriptions of the turbulent and mean flow parameters.

The hydrodynamic dipole model of edge noise shows that the predominant physical effect which takes place at an edge is an almost discontinuous acceleration of the medium, in a direction normal to the plane of the surface, caused by the abrupt change in boundary conditions encountered by turbulent eddies, and that this process takes place essentially within one scale length of the edge, thus making the source acoustically compact in the streamwise direction.

The model explicitly develops the role of the velocity and Mach number of the eddy convection past the edge, and the importance of relative scale lengths of the turbulence, as well as the relative intensity of pressure fluctuations.

The Mach number (velocity) effects show that the important parameter is the convection Mach number, M_c, of the eddies; the radiated power from the edge of an acoustically "small" surface varies as M_c^6 at low M_c, to lower powers of M_c as M_c approaches unity — the departure from the familiar M^6 law depending upon the isotropy of the turbulence (i.e., ℓ_x/ℓ), and the axial (flow-wise separation (γ) between eddies of axial scale ℓ_x. Thus, the effects of turbulence scale lengths (ℓ_x, ℓ_y, ℓ_z), the ratio between axial scale and mean scale length (η), and spatial density (separation) of scales (γ and ξ) are shown to be very important in determining the level and spectrum shape of edge sound radiated. For semi-infinite surfaces, the low Mach number limit on velocity exponent is predicted to be M_c^5 for the edge dipole mechanism, the deviation to lower powers at $M_c \gtrsim 0.3\text{-}0.5$ occurring just as in the case of the acoustically-compact surface.

Based on the contribution of diffraction from the non-source edges of *finite* surfaces, it is expected that the velocity exponent on radiated power will tend toward M_c^6 (low M_c limit) when the observer is in the geometric far field, even though the surface may be very large with respect to a wavelength.

Experimental data presented for large finite surfaces tend to show a definite although not completely unambiguous trend toward the M_c^6 limit. Future analyses and experiments should be made with an objective of determining at what ratio of surface size (chord) to acoustic wavelength the behavior changes from a compact-surface-type behavior to a semi-infinite surface-type behavior. The experimental data reviewed herein suggest that this transition occurs at a surface dimension many times an acoustic wavelength.

The effects of coherence between independent source regions was shown analytically (and experimentally) to be an important effect, although, in practice, a weaker effect than relative and absolute eddy scale lengths and Mach number. However, the coherence between source regions is also related to eddy scale, and Mach number, since it is a function of frequency, which is in turn determined by the convection velocity and axial scale separation of the turbulence. Coherence between source regions across an edge can increase dipole sound power levels by up to 6 dB, or can decrease dipole sound and cause degeneration to higher order sources (which will have velocity scaling laws with exponents greater than 6, and directivity patterns different than the edge dipole source).

The directivity of dipole sources located near an edge has been shown by analysis and experiment to deviate from a free field dipole. For surfaces much larger than an acoustic wavelength (approaching semi-infinite), the directivity of edge dipoles approaches the half-plane limit of $(\sin^2\theta\cos^2\psi/2)$, a cardioid shape in a plane normal to the surface passing through the dipole axis. For surfaces which do not approach the semi-infinite limit, the far field sound intensity pattern becomes modified by diffraction at the edges of the surface (which are not involved in the generation of the particular source), the exact effects being a function of surface geometry.

Experimental data was presented which provides support for the dipole edge noise model in terms of Mach number (velocity) scaling, parametric dependence on flow field parameter, directivity, and edge diffraction effects. Additional empirical data indicates that the source level of both leading and trailing

edge/edge sources are affected by edge thickness and/or radius of curvature. One limitation of the present study was the lack of experimental data in which both the flow parameters needed to calculate the radiated sound spectra, and the radiated sound spectra themselves were measured.

The modelling approach developed in this study allows the radiated field to be viewed as a ratio to the surface pressure field, along the lines proposed by Chase (1972). The ratio

$$\frac{\overline{p_a^2(r,\theta,\psi,\omega)}}{\overline{p_s^2(\omega)}}$$

is set equal to a complicated function of flow parameters, and physical parameters of distance, surface dimensions, and physical properties of the medium. The right hand side may thus be viewed as a "transform" or "transfer function" between surface pressure spectrum and far field spectrum. This transform has been shown to be non-unique, i.e., it will vary from one flow field to another and, as a function of Mach number for a particular flow field. Nevertheless, the concept has practical significance if the base of experimental data can be expanded to include:

(1) the distance, in axial length scales, from an edge at which to measure $\overline{p_s^2(\omega)}$, and

(2) a catalog of length scale and convection speed data for various flow fields as a function of Strouhal number.

Given this additional data, one could make surface pressure spectrum measurements near the edges airfoils on flying aircraft, wind tunnel models, rotors, etc., and make a reasonably accurate estimate of the far field sound spectrum, given the knowledge of mean flow and geometric parameters, and resolution of the aforementioned question of how many wavelengths long a surface must be to begin exhibiting "semi-infinite" behavior.

Nevertheless, the apparent simplicity of the transform concept does not mitigate the need and desirability of making surface pressure field measurements with multiple sensor arrays, with time-domain effects preserved to assess convection speed and length scale parameters for each case of interest.

Finally, the model developed in this study does not explicitly account for diffraction effects, or moving medium effects, both of which could readily be added as an effective directivity term.

APPENDIX A

SIMPLIFIED MODEL OF DIFFRACTION OF TRAILING EDGE SOUND BY A LEADING EDGE

The preceding sections have shown that the primary source of trailing edge radiated sound is a distribution of dipoles along the trailing edge. However, the total sound field consists of, not only direct radiation from this distribution, but also the scattered field from the leading edge of the plate over which the flow passes. An experiment was designed to emphasize this effect by replacing the large rectangular plates used for studying the trailing edge noise mechanism by a semicircular plate. The plate was large enough so that the source, provided by a small wall jet, would be concentrated near the geometric origin of the semicircular plate. Thus, because of the symmetry of the semicircular plate with respect to the source (and observation point which was along the z-axis), the diffraction sources are all equidistant from the observation point and hence, are likely to produce a stronger in-phase diffracted field than leading and side edge scattering from the rectangular counter parts. The experiment data does indicate peaks at discrete frequencies for a semicircular plate, and hence constitute quantitative support for the assumption that the sound source is localized at the trailing edge. In the following section, we have provided a simplified analysis of the sound field produced by these sources.

Analysis of Diffracted Field from Leading Edge of a Rigid Semicircular Planform Plate with a Localized Trailing Edge Source at the Origin

Consider a point dipole which is oriented in the z-direction and locate at the origin of a spherical coordinate system. The rigid plate is in the r-ψ plane, and the assumed directivity of the dipole, which is cardioid in shape is shown in Fig. A.1. The acoustic velocity is opposite in sign on the upper surface with respect to the lower surface. The strength of the direct radiated point dipole field falls off like $1/r^2$ from the source. Since there is a point of inflexion on the surface, it is out of the near field that the scattered field from the surface cancels out, when integrated over the entire surface. Hence, we are left with the source dipole at the origin and a weaker "image" dipole all along the boundary of the plate.

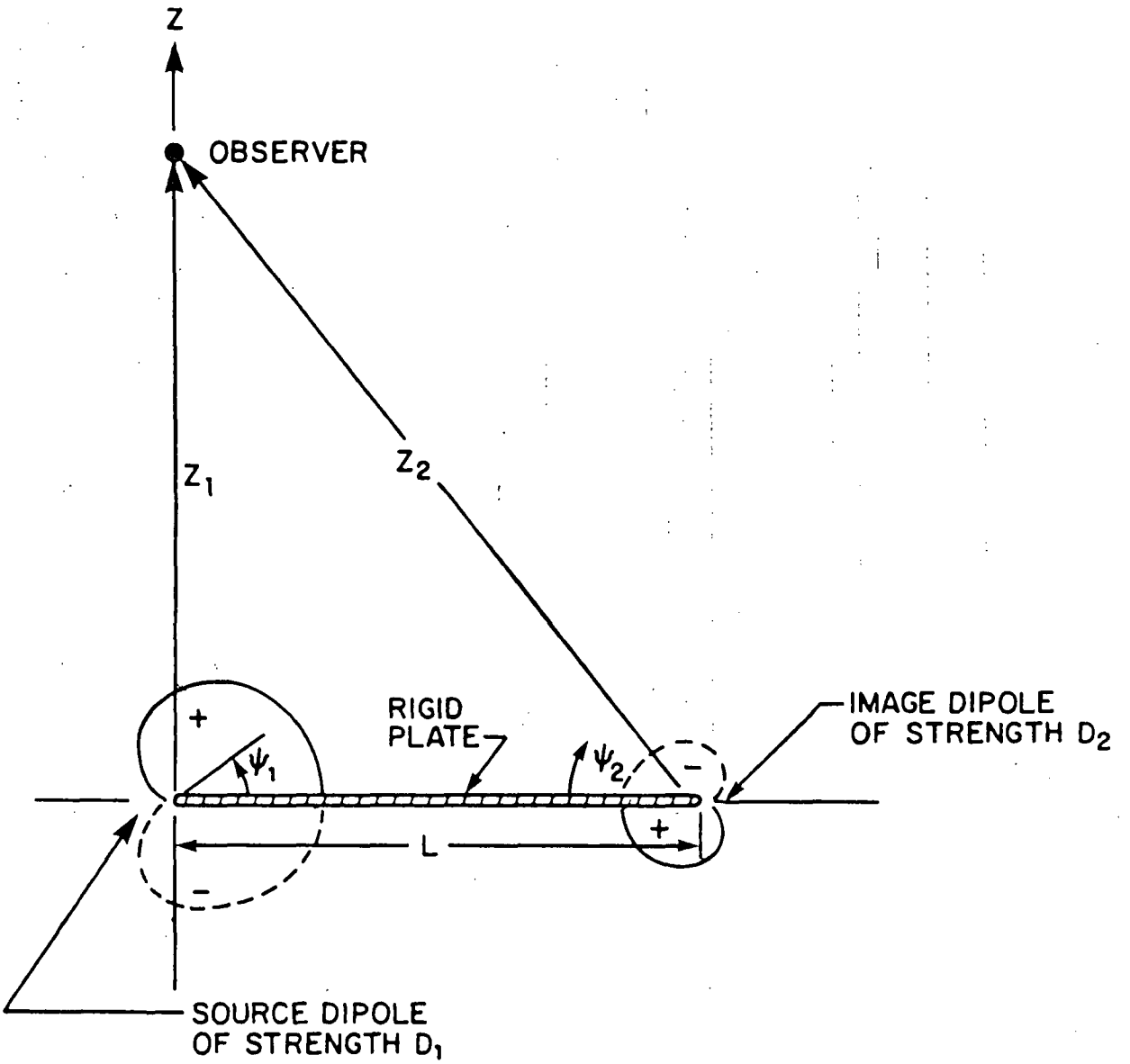

FIG. A.1. SCHEMATIC SOURCE AND SCATTERER GEOMETRY.

The following analysis is restricted to the convenient geometry of the semicircular plate and an observer along the source dipole axis, which happens to correspond to a measured case. Let the observation point, O, be at a distance z_1 from the origin, along z-axis. Let distance from the image dipole to the observation point by z_2. Let D_1 and D_2 be the strengths of the dipoles at unit distances, respectively. Then the total field at O is given by:

$$p_1 = - \frac{k^2 D_1 \rho c}{4\pi z_1} \cos^2 \frac{\psi_1}{2} \left[1 + \frac{i}{kz_1} \right] e^{ikz_1} \qquad (A.1)$$

where ψ_1 is the angle between the axis and the observation point (Fig. A.1). The field due to the image source over a sector $Ld\theta$

$$p_2 = - \frac{k^2 D_2 \rho c}{4\pi z_2} \cos^2 \frac{\psi_2}{2} \left[1 + \frac{i}{kz_2} \right] e^{ikz_2} \, Ld\theta \, D(\theta)$$

where $D(\theta)$ is the directivity of the source at the origin. Ignoring the effect of directivity and integrating in the θ plane leads to

$$p_2 = \frac{-k^2 (D_2 L) \rho c}{4\pi z_2} \cos^2 \frac{\psi_2}{2} \left[1 + \frac{i}{kz_2} \right] e^{i(kz_2 + \pi)} \qquad (A.2)$$

where $(D_2 L)$ denotes the total strength of the image dipole. Since the total strength of the dipole field varies as $1/r^2$, we have

$$(D_2 L) = \frac{D_1 \, e^{ikL}}{(L^2)} \qquad (A.3)$$

and the total field, which is the sum of Eqs. (A.1) and (A.2) is

$$p = -\frac{k^2\rho c}{4\pi}\ \frac{D_1}{z_1}\ \cos^2\frac{\psi_1}{2}\left[\left(1+\frac{i}{kz_1}\right)\ e^{ikz_1}\right.$$

$$\left.+\frac{\pi z_1}{L_2 z_2}\ \frac{\cos^2\psi_2/2}{\cos^2\psi_1/2}\ e^{i(kz_2+kL+\pi)}\ \left(1+\frac{i}{kz_2}\right)\right] \quad (A.4)$$

The mean square pressure is given by

$$(p\cdot p^*) = \frac{k^4\rho^2c^2}{16\pi^2}\ \frac{D_1^2}{z_1^2}\ \cos^4\frac{\psi_1}{2}\left[\left(1+\frac{1}{k^2z_1^2}\right)+C_0^2\left(1+\frac{1}{k^2z_2^2}\right)\right.$$

$$-2C_0\left\{\left(\cos k(z_2+L)+\frac{\sin k(z_2+L)}{kz_2}\right)\ \left(\cos kz_1-\frac{\sin kz_1}{kz_1}\right)\right.$$

$$\left.\left.+\left(\frac{\cos kz_1}{kz_1}+\sin kz_1\right)\ \left(\frac{\cos k(z_2+L)}{kz_2}+\sin k(z_2+L)\right)\right\}\right] \quad (A.5)$$

where

$$C_0 = \frac{\pi z_1}{L^2 z_2}\ \frac{\cos^2\psi_2/2}{\cos^2\psi_1/2} \quad (A.6)$$

The fluctuating part of the field is given by the terms in square brackets, which has been computed for various frequencies.

$$\Delta p(f) = \left(1 + \frac{1}{(kz_1)^2}\right) + C_0^2 \left(1 + \frac{1}{k^2 z_2^2}\right)$$

$$- 2C_0 \left\{ \left(\cos k(z_2+L) + \frac{\sin k(z_2+L)}{kz_2}\right) \left(\cos kz_1 - \frac{\sin kz_1}{kz_1}\right) \right.$$

$$\left. + \left(\frac{\cos kz_1}{kz_1} + \sin kz_1\right) \left(\frac{\cos k(z_2+L)}{kz_2} + \sin k(z_2+L)\right) \right\} \qquad (A.7)$$

As we increase frequency, the asymptotic limit for the fluctuating pressure will be, (as $kz_1, kz_2 \to \infty$)

$$\Delta p(f) = (1+C_0^2) - 2C_0 \leftarrow \cos\ k(z_2-z_1+L) \qquad (A.8)$$

Hence, the fluctuating part has a frequency of

$$f_p = \frac{c_0}{(z_2+L-z_1)} \qquad (A.9)$$

and amplitude $C_0 \sim 1/L^2\ z_1/z_2$, where c_0 is local speed of sound and essentially is due to the finiteness of the scatterer. If the scatterer dimension were to be infinite, the frequency as well as the amplitude would tend to zero, hence, no measurable fluctuations in the pressure are found.

APPENDIX B

EXPERIMENTAL DATA FROM WALL JET/TRAILING EDGE NOISE TESTS

In this appendix, the raw laboratory data taken by Hayden (1969) is presented. The configuration tested was a flat plate of varying lengths and width of 24 inches in an anechoic room, with a single 0.5 in × 5.0 in rectangular wall jet blowing on one side of the plate as the flow field. The configuration is shown in Fig. 13. (Section 4 of main part of text.) Exit velocities were varied up to about 300 fps.

The data shown in Fig. B.1 is from the flow regime which is just beyond the end of the potential core of a 10:1 AR wall jet; this regime is sometimes called the characteristic decay regime. The microphone was positioned normal to the trailing edge at a distance of 60 inches (5.0 ft) on the side opposite that to which the nozzle was attached. The ambient temperature in the room was about 100°F.

Figure B.2 shows similar data for a larger plate (30 inches) which has the trailing edge located in the so-called radial decay region of the wall jet. The microphone was again positioned normal to the trailing edge, on the side opposite that to which the nozzle was attached, at a distance of 30 inches (2.5 ft).

The purpose of these tests was to examine the effect of mean velocity on the spectrum and level of trailing edge radiated sound. In both Figs. B.1 and B.2, data below the 63 Hz band should be ignored due to background noise in the room, and due to the size of the anechoic room. In Fig. B.1a, the levels at frequencies below the 125 Hz band are thought to contain background noise contributions.

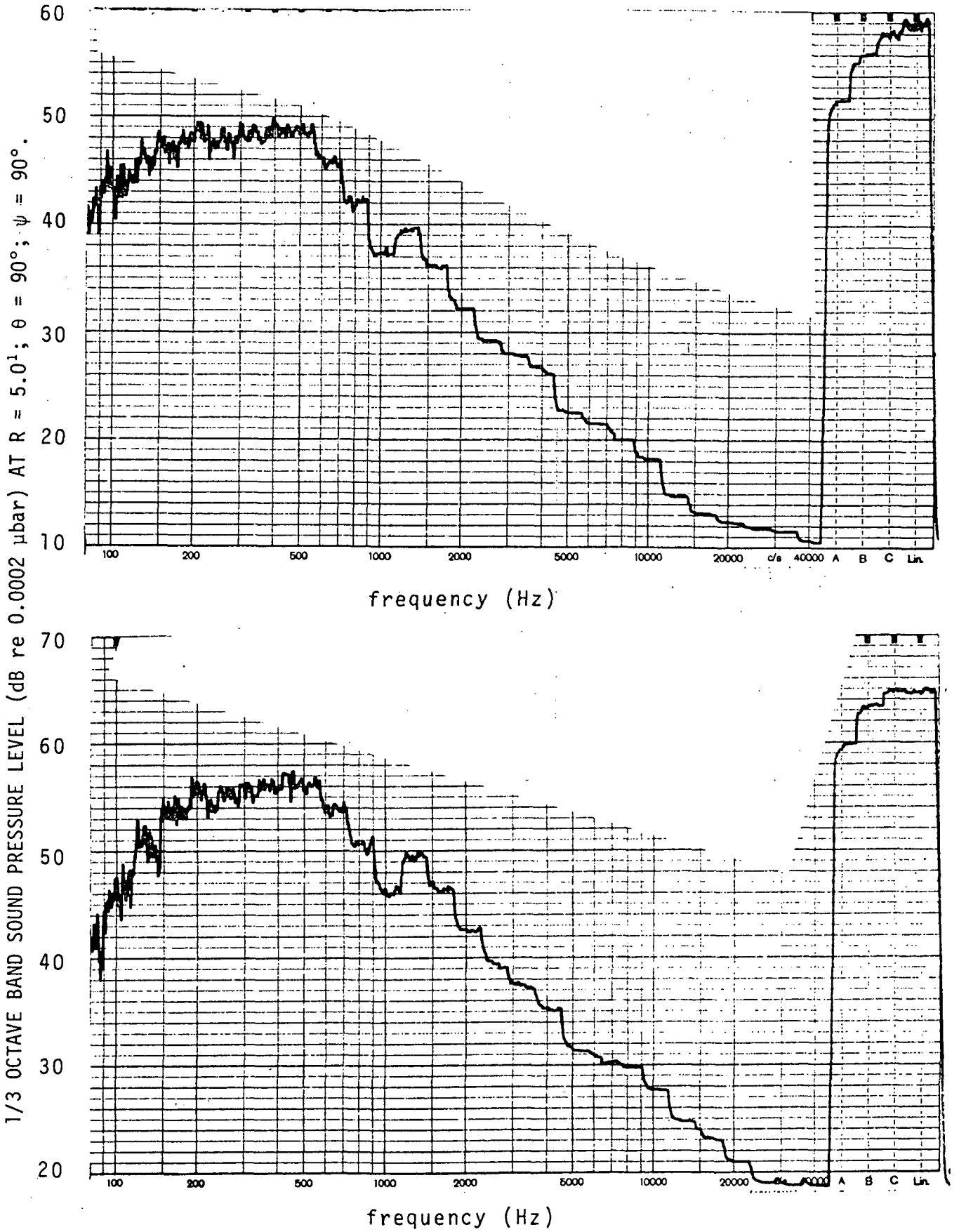

FIG. B.1. TRAILING EDGE NOISE DATA FROM 0.5 in × 5 in (10:1 AR) WALL JET BLOWING OVER FLAT PLATE OF L/H = 16: (a) U_o = 93 fps, (b) U_o = 125 fps.

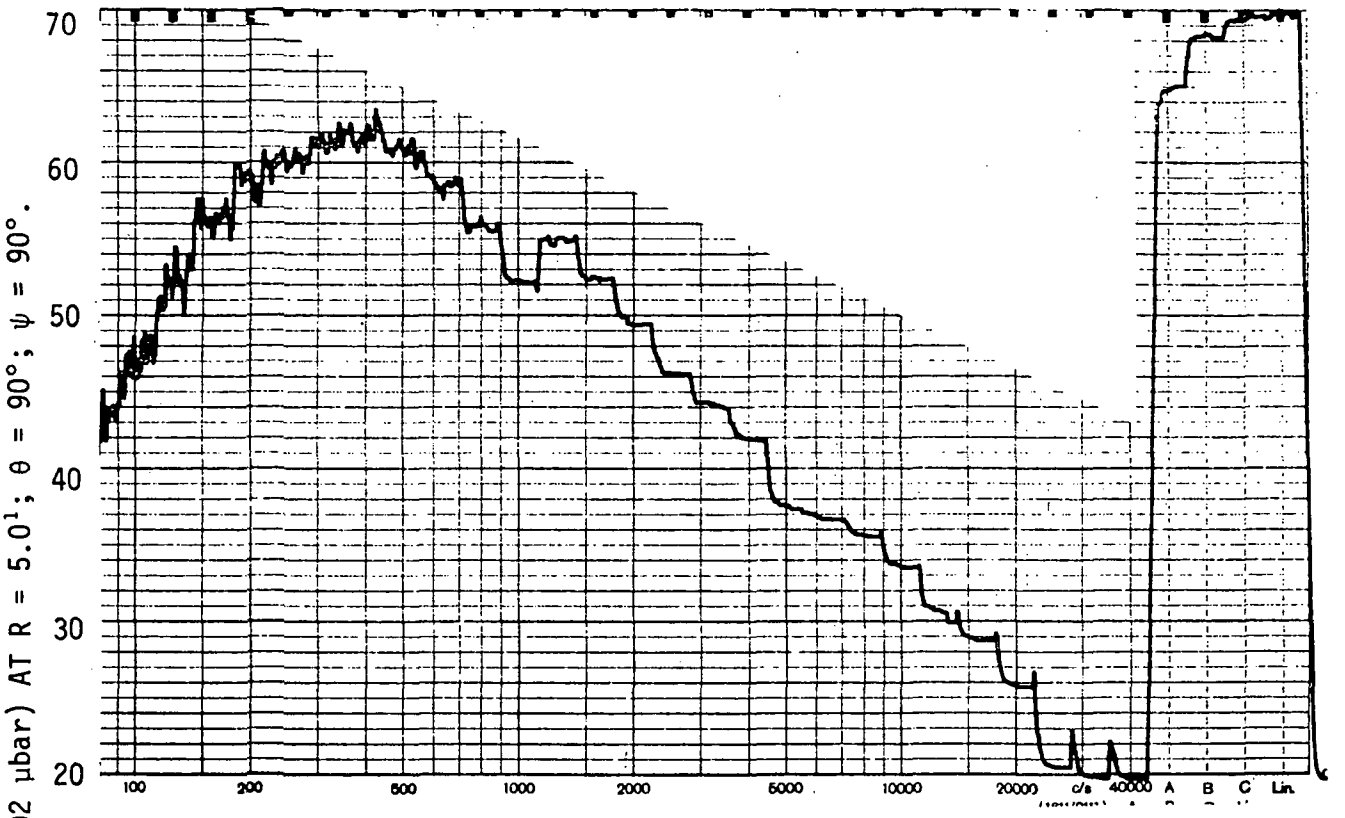

(c)

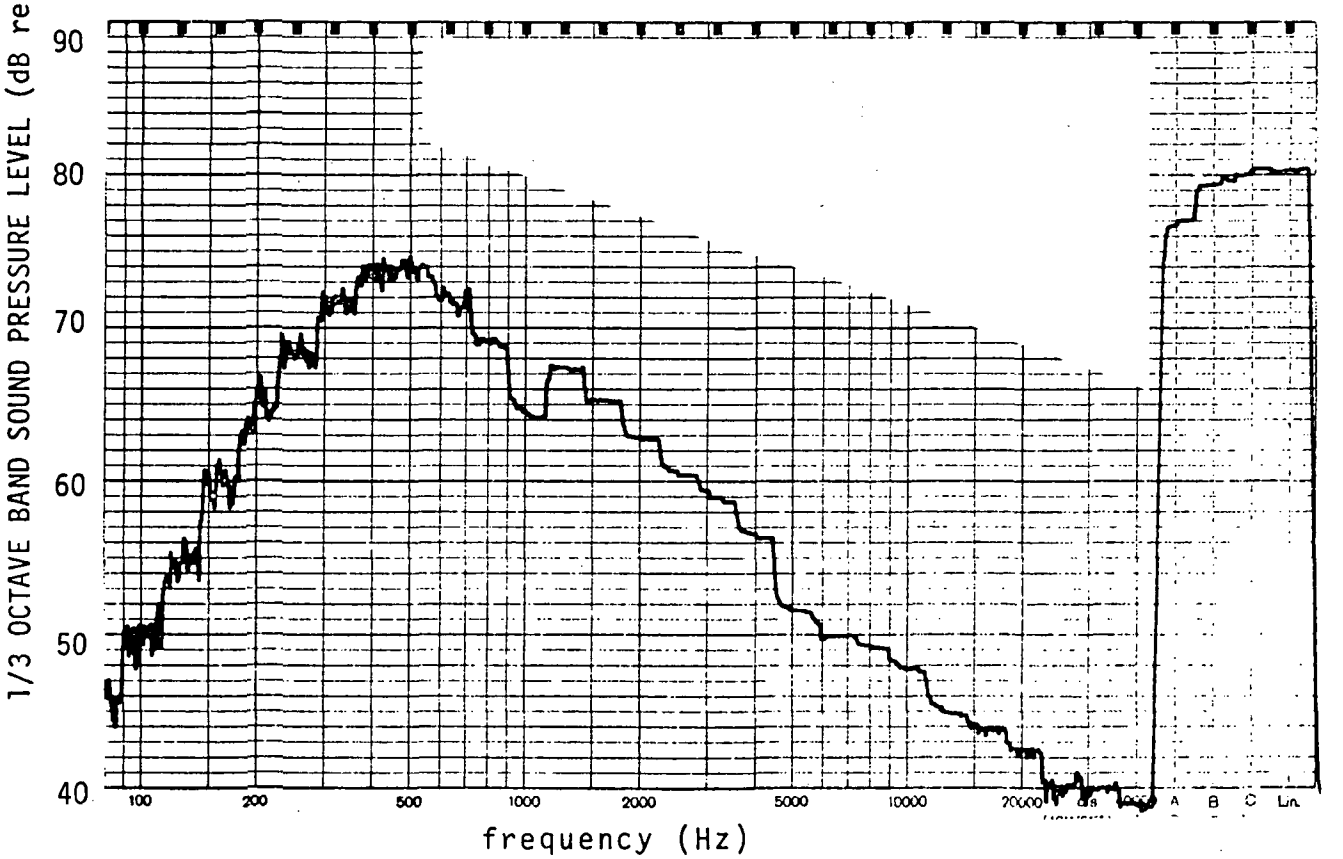

(d)

FIG. B.1 (Continued). (c) U_o = 146 fps, (d) U_o = 225 fps.

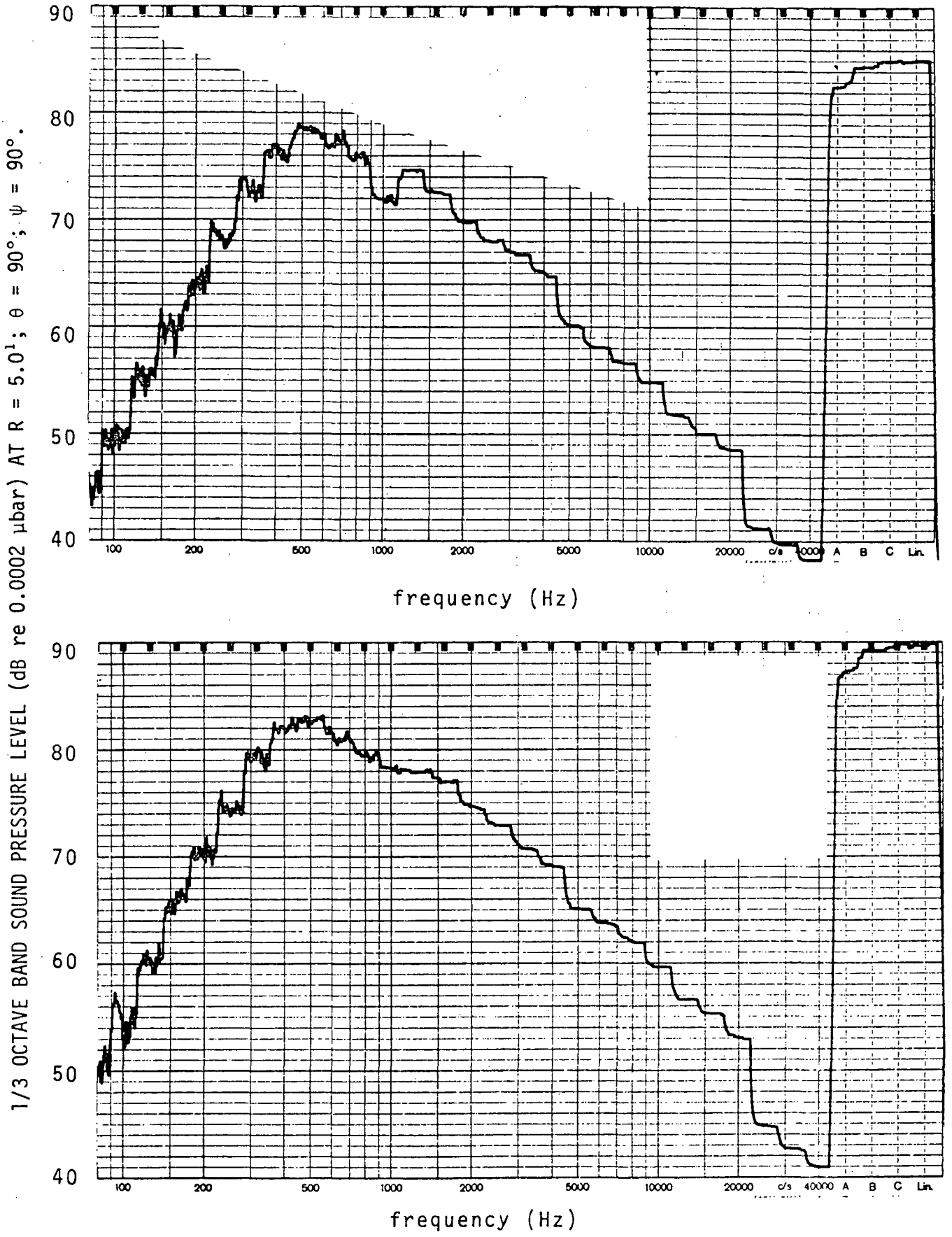

FIG. B.1 (Continued). (e) U_o = 277 fps, (f) U_o = 296 fps.

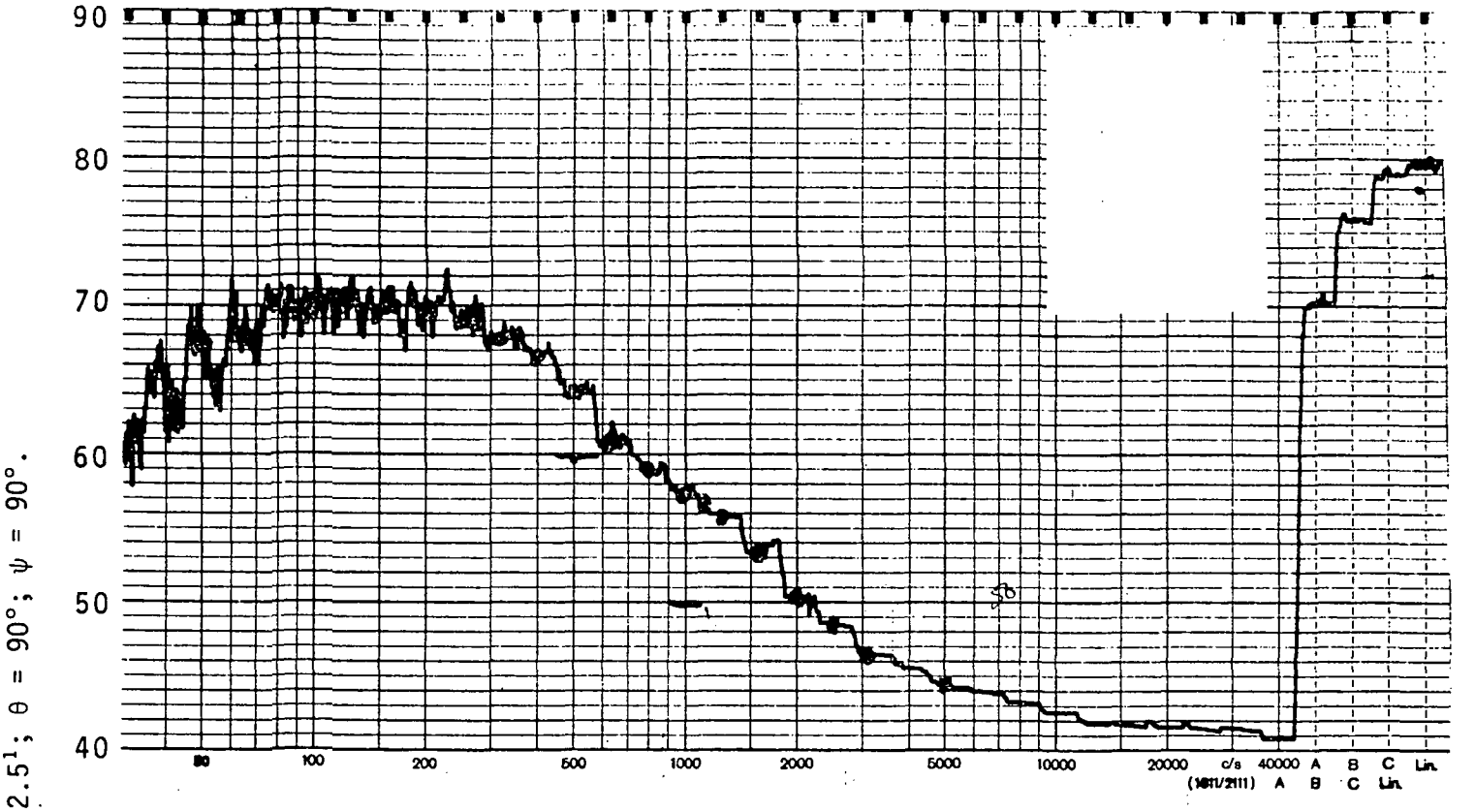

frequency (Hz)

(a) U_o = 208 fps

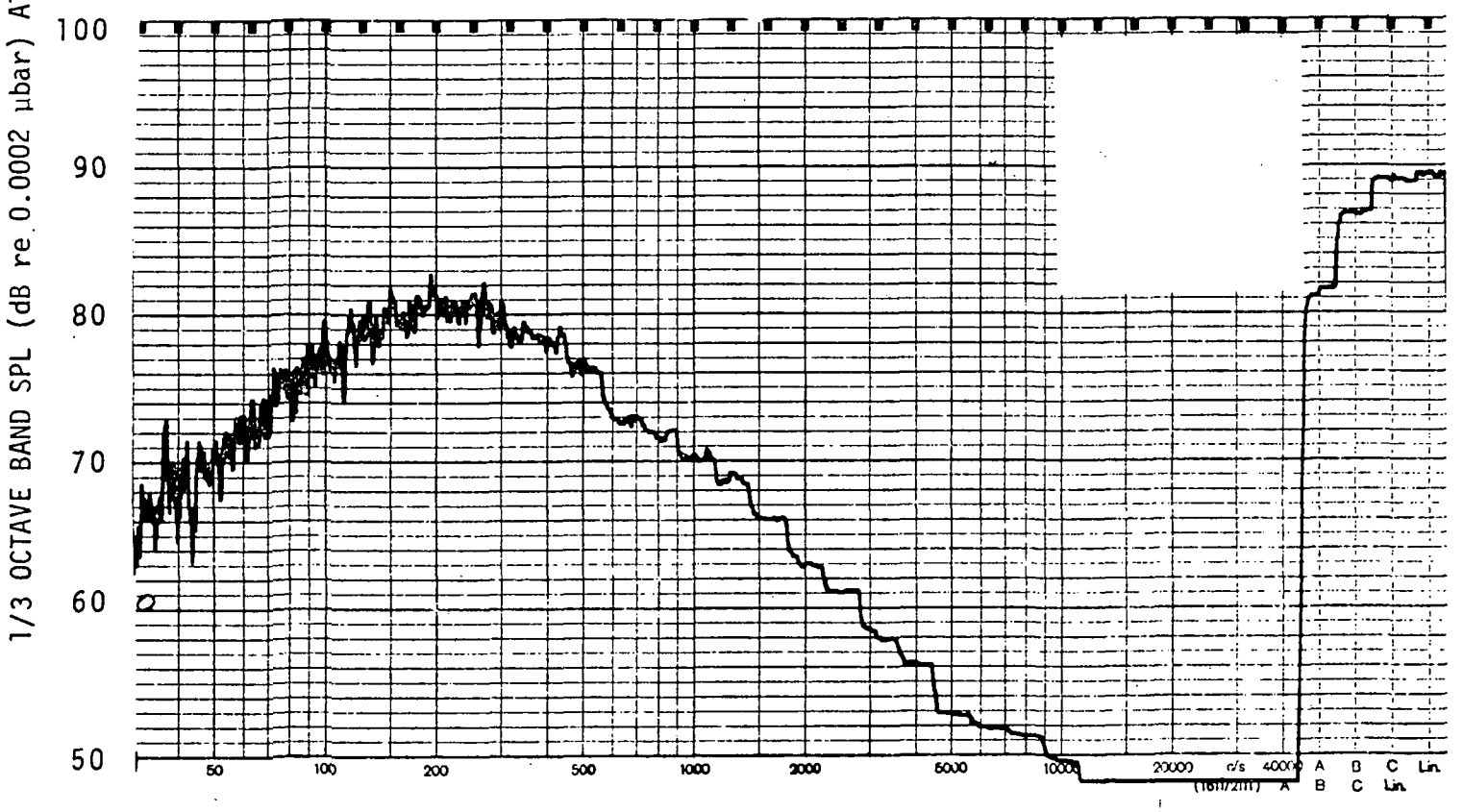

1/3 OCTAVE BAND SPL (dB re 0.0002 μbar) AT R_o = 2.5'; θ = 90°; ψ = 90°.

frequency (Hz)

(b) U_o =]90 fps

FIG. B.2. TRAILING EDGE NOISE DATA FROM 0.5 × 5 in (10:1 AR) WALL JET BLOWING OVER FLAT PLATE OF L/H = 60.

REFERENCES

Bender, E.K., Hayden, R.E., and Heller, H.H., "Analysis of Potential Noise Sources of the Tracked Air Cushion Vehicle," BBN Report 2178, also DOT-TSC-194-1, (July 1971).

Bowman, J.J., Senior, T.B.A., and Uslenghi, P.L.E., "Electromagnetic and Acoustic Scattering by Simple Shapes," North-Holland Publishing Company – Amsterdam, (1969).

Chanaud, R.C. and Hayden, R.E., "Edge Sound Produced by Two Turbulent Wall Jets," Paper FF-11, Spring Meeting of the Acoustical Society of America (1970).

Chandiramani, K., "Diffraction of Evanescent Waves with Applications to Aerodynamically Scattered Sound and Radiation from Baffled Plates," *J. Acoust. Soc. Amer.*, 55, pp. 19-29 (Jan. 1974).

Chase, D.M., "Sound Radiation by Turbulent Flow off a Rigid Half Plane as Obtained from a Wavevector Spectrum of Hydrodynamic Pressure," *J. Acoust. Soc. Amer.*, 52, No. 3 (Part 2)(1972).

Crighton, D.G., "Scattering and Diffraction of Sound by Moving Bodies," *J. Fluid Mech.*, Vol. 72, Part 2, (1975).

Curle, N., "The Influence of Solid Boundaries on Aerodynamic Sound," Proc. R. Soc. (1955).

Curle, N., "General Theory of Aerodynamic SOund," Chapter 5 in Richards, E.J. and Mead, D.J., *Noise and Acoustic Fatigue in Aeronautics,* John Wiley and Sons Ltd., (1968).

Fink, M.R., "Experimental Evaluation of Trailing Edge and Incidence Fluctuation Noise Theories," AIAA 13th Aerospace Sciences Meeting (January 1975).

Ffowcs Williams, J.E. and Hall, L.H., "Aerodynamic Sound Generation by Turbulent Flow in the Vicinity of a Scattering Half Plane," *J. Fluid Mech.* 40,(Part 4) (1970).

Goldstein, M., "Unified Approach to Aerodynamic Sound Generation in the Presence of Solid Boundaries," *J. Acoust. Soc. Amer.* 56, (2) (1974).

Hayden, R.E., "Sound Generation by Turbulent Wall Jet Flow Over a Trailing Edge," M.S. Thesis, Purdue University, (1969).

REFERENCES (*Continued*)

Hayden, R.E., "Noise from Interaction of Flow with Rigid Surfaces: A Review of Current Status of Prediction Techniques," BBN Report No. 2276, also NASA CR-2126, (October, 1972).

Hayden, R.E., Galaitsis, A.G., and Alakel, M.N., "Diagnosis of Flap Noise Sources on a Full Scale Upper Surface Blown Flap System," BBN Report No. 2998 (1975).

Hayden, R.E., "Fundamental Aspects of Noise Reduction from Powered-Lift Devices," SAE Paper 730376, also in SAE Proceedings (1973).

Heidelberg, L.J., Homyak, L., and Jones, W.L., "Full-Scale Upper-Surface-Blown Flap Noise," NASA TM X-71708 (1965).

Lighthill, M.J., "On Sound Generated Aerodynamically: I-General Theory," Proc. R. Soc. (1952).

Morse, Philip M. and Ingard, K. Uno, *Theoretical Acoustics*, McGraw-Hill, Inc., (1968).

Powell, A.O., "On the Aerodynamic Noise of a Rigid Flat Plate Moving at Zero Incidence," *J. Acoust. Soc. Amer.*, 31, No. 12, pp. 1649-1653, (Dec. 1959).

Scharton, T.D. and White, P.H., "Simple Pressure Source Model of Jet Noise," *J. Acoust. Soc. Amer.* 52, (1) (1972).

Yildiz, M. and Mawardi, O.K., "On the Diffraction of Multipole Fields by a Semi-Infinite Wedge", *J. Acoust. Soc. Amer.*, 32, 12, (1960).